GEORGIA INSTITUTE OF TECHNOLOGY
OFFICE OF RESEARCH ADMINISTRATION

RESEARCH PROJECT INITIATION

Date: January 6, 1975

Project Title: Combustion Dynamics of External Burning Phenomena

Project No: E-16-655

Principal Investigator Dr. W. C. Strahle/Dr. J. E. Hubbart

Sponsor: Air Force Office of Scientific Research; Arlington, Virginia

Agreement Period: From 2/1/75 Until 1/31/76

Type Agreement: Grant No. AFOSR-75-2794

Amount: $29,999 AFOSR Funds (E-16-655)
5,018 GIT Contrib. (E-16-348)
$35,017 Total

Reports Required:
Final Scientific Report; Interim (Annual) Report if project extended beyond one year.

Sponsor Contact Person (s):

Technical Matters
~~Mr. Bernard T. Wolfson~~ ← Maj. Thomas J. Meier
Program Manager
AFOSR (NAR)
~~1400 Wilson Boulevard~~
~~Arlington, Virginia 22209~~
Bolling AFB, DC 20332

Contractual Matters
(Thru ORA)
Ms. Joan O. Marshall
Buyer
AFOSR (PMD)
1400 Wilson Boulevard
Arlington, Virginia 22209

Assigned to: Aerospace Engineering

COPIES TO:

Principal Investigator	Library
School Director	Rich Electronic Computer Center
Dean of the College	Photographic Laboratory
Director, Research Administration	Project File
Director, Financial Affairs (2)	
Security-Reports-Property Office	
Patent Coordinator	Other

RA-3 (6-71)

GEORGIA INSTITUTE OF TECHNOLOGY
OFFICE OF CONTRACT ADMINISTRATION

SPONSORED PROJECT TERMINATION

Date: 10/31/77

Project Title: "Combustion Dynamics of External Burning Phenomena".

Project No: E-16-655

Project Director: W. C. Strahle and J. E. Hubbartt

Sponsor: Air Force Office of Scientific Research

Effective Termination Date: 9/30/77

Clearance of Accounting Charges: 9/30/77

Grant/Contract Closeout Actions Remaining:

_ Final Invoice and Closing Documents
X Final Fiscal Report
_ Final Report of Inventions
_ Govt. Property Inventory & Related Certificate
_ Classified Material Certificate
_ Other _____

Assigned to: Aerospace Engineering (School/Laboratory)

COPIES TO:

Project Director
Division Chief (EES)
School/Laboratory Director
Dean/Director—EES
Accounting Office
Procurement Office
Security Coordinator (OCA)
Reports Coordinator (OCA)
Library, Technical Reports Section
Office of Computing Services
Director, Physical Plant
EES Information Office
Project File (OCA)
Project Code (GTRI)
Other _____

CA—4 (3/76)

E-16 655

1 cy

GEORGIA INSTITUTE OF TECHNOLOGY
ATLANTA, GEORGIA 30332

OFFICE OF
THE DIRECTOR OF
FINANCIAL AFFAIRS

April 5, 1977

Ms. Joan Marshall
AFOSR/PM
Building 410
Bolling AFB, D. C. 20332

Dear Ms. Marshall:

Enclosed in duplicate is the interim Grant Fiscal Report for grant number AFOSR-75-2794 covering the period February 1, 1975 through January 31, 1977.

If you have questions or desire additional information, please let us know.

Sincerely yours,

Evan Crosby
Associate Director of
Financial Affairs

EC/bs
enclosures:
cc: Dr. J. E. Hubbartt
Mr. E. E. Renfro
Mr. A. H. Becker
File E-16-655

E-16-655

AIR FORCE OFFICE OF SCIENTIFIC RESEARCH
GRANT FISCAL REPORT

Submit in duplicate. Interim reports are required each year for grants of more than one year's duration. Submit final report as soon as possible but not more than 90 days after the end of the grant period.

FROM:	TO:	REPORT DATE	GRANT NO.
Georgia Institute of Technology Atlanta, Georgia 30332	AFOSR/PM 1400 Wilson Blvd Arlington VA 22209	2/23/77	AFOSR- 75-2794

TYPE OF REPORT	REPORT PERIOD
[ ] FINAL [X] INTERIM	FROM: INCEPTION TO: 1/31/77

TOTAL PROJECT COST NEGOTIATED	TOTAL GRANT AMOUNT	AGREED PERCENT OF TOTAL PROJECT COST REPRESENTED BY GRANT AMOUNT
$ 69,880.	$ 59,999.	86 %

DIRECT COSTS	[2]GRANT FUNDS EXPENDED
[1]SALARIES AND WAGES	
PRINCIPAL INVESTIGATOR	$ 8,581.98
SENIOR SCIENTIFIC	
OTHER	22,923.44
PERMANENT EQUIPMENT	
EXPENDABLE SUPPLIES AND MATERIALS	2,903.19
TRAVEL	955.10
PUBLICATION COSTS	
COMPUTER COSTS	776.02
EMPLOYEE BENEFITS	2,495.44
OTHER *(Specify)*	
TOTAL DIRECT COSTS	38,635.17
INDIRECT COSTS: 65 % OF S & W	20,478.52
TOTAL GRANT FUNDS EXPENDED	$ 59,113.69
I CERTIFY THAT THE PRINCIPAL INVESTIGATOR(S) HAS *(HAVE)* DEVOTED APPROXIMATELY_____% OF HIS *(THEIR)* TIME TO PERFORMANCE OF THE RESEARCH UNDER THE GRANT. I FURTHER CERTIFY THAT THIS FISCAL REPORT IS CORRECT; THAT ALL EXPENDITURES REPORTED WERE FOR APPROPRIATE PURPOSES; AND THAT THE GRANTEE HAS EXPENDED FROM NON-FEDERAL FUNDS IN THE COST CATEGORIES LISTED ABOVE, IN PERFORMANCE OF THE RESEARCH UNDER THIS GRANT, THE AMOUNT OF	10,037.35
TOTAL ACTUAL PROJECT COST FOR REPORT PERIOD	69,151.04
IN FINAL FISCAL REPORT ONLY: IF ACTUAL TOTAL PROJECT COST IS LESS THAN NEGOTIATED TOTAL PROJECT COST, MULTIPLY THE ACTUAL TOTAL PROJECT COST BY THE AGREED PERCENTAGE REPRESENTED BY THE GRANT AMOUNT AND ENTER RESULT HERE. *(NOTE: Regardless of the above computation, any unexpended or uncommitted grant funds must be returned to AFOSR in accordance with the paragraph of the Grants Brochure "Unexpended Funds and Earned Interest")*	
DEDUCT THIS AMOUNT FROM TOTAL GRANT AMOUNT	
ADD INTEREST EARNED	
REFUND DUE *(return this amount with the final report by check made payable to the Treasurer of the United States)*	

SIGNED	TITLE
J. E. Hubbartt	Professor
Evan Crosby	Associate Director of Financial Affairs

If the actual cost in this category varies more than 10% from the estimate, provide an explanation of the variance on the reverse of this form. Firm outstanding commitments are considered as costs.

AFOSR FORM MAR 75 2

AFSC—Andrews AFB Md 1975

AFOSR Interim Scientific Report

AFOSR-TR-76-

Experiments and Analysis Related to External Burning for Propulsion

Prepared for

Air Force Office of Scientific Research
Aerospace Sciences Directorate
Bolling Air Force Base, D. C.

by

James E. Hubbartt
Warren C. Strahle
Douglas H. Neale
Walter W. Wilson

School of Aerospace Engineering
Georgia Institute of Technology
Atlanta, Georgia 30332

Approved for public release; distribution unlimited
Grant No. AFOSR 75-2794 March 1976

AFOSR Interim Scientific Report

AFOSR-TR-76-

Experiments and Analysis Related to External Burning for Propulsion

Prepared for

Air Force Office of Scientific Research
Aerospace Sciences Directorate
Bolling Air Force Base, D. C.

by

James E. Hubbartt
Warren C. Strahle
Douglas H. Neale
Walter W. Wilson

School of Aerospace Engineering
Georgia Institute of Technology
Atlanta, Georgia 30332

Approved for public release; distribution unlimited
Grant No. AFOSR 75-2794 March 1976

REPORT DOCUMENTATION PAGE

READ INSTRUCTIONS BEFORE COMPLETING FORM

1. REPORT NUMBER: AFOSR-TR-76
2. GOVT ACCESSION NO.:
3. RECIPIENT'S CATALOG NUMBER:

4. TITLE (and Subtitle): Experiments and Analysis Related to External Burning for Propulsion

5. TYPE OF REPORT & PERIOD COVERED: INTERIM, Feb. 1975 - Jan. 1976

6. PERFORMING ORG. REPORT NUMBER:

7. AUTHOR(s): J. E. Hubbartt, W. C. Strahle, D. H. Neale, Walter W. Wilson

8. CONTRACT OR GRANT NUMBER(s): AFOSR-75-2794

9. PERFORMING ORGANIZATION NAME AND ADDRESS: Georgia Institute of Technology, School of Aerospace Engineering, Atlanta, Georgia 30332

10. PROGRAM ELEMENT, PROJECT, TASK AREA & WORK UNIT NUMBERS:

11. CONTROLLING OFFICE NAME AND ADDRESS: Air Force Office of Scientific Research/NA, Bolling Air Force Base, D. C. 20332

12. REPORT DATE: March 1976

13. NUMBER OF PAGES: 57

14. MONITORING AGENCY NAME & ADDRESS (if different from Controlling Office):

15. SECURITY CLASS. (of this report): Unclassified

15a. DECLASSIFICATION/DOWNGRADING SCHEDULE:

16. DISTRIBUTION STATEMENT (of this Report): Approved for public release; distribution unlimited

17. DISTRIBUTION STATEMENT (of the abstract entered in Block 20, if different from Report):

18. SUPPLEMENTARY NOTES:

19. KEY WORDS (Continue on reverse side if necessary and identify by block number):
External burning propulsion
Base flow
Supersonic flow
Wind tunnel

20. ABSTRACT (Continue on reverse side if necessary and identify by block number):
The results of first year's efforts on an experimental base flow program are reported. The design and checkout for a Mach 3.0 axisymmetric wind tunnel with a model base diameter of 2.25 inches is described, as well as the automated data requisition system. Experiments are reported on detailed static pressures for the diffuser wall, model wall and base and near wake. Temperature measurements are presented to establish a near adiabatic wall condition. The relationship between the experimental program and propulsive external burning is discussed

Abstract

The results of first year's efforts on an experimental base flow program are reported. The design and checkout for a Mach 3.0 axisymmetric wind tunnel with a model base diameter of 2.25 inches is described, as well as the automated data requisition system. Experiments are reported on detailed static pressures for the diffuser wall, model wall and base and near wake. Temperature measurements are presented to establish a near adiabatic wall condition. The relationship between the experimental program and propulsive external burning is discussed.

TABLE OF CONTENTS

CHAPTER I

INTRODUCTION

There are a great number of potential air-to-air, air-to-ground, and ground-to-air weaponry missions that require either a sustain or mild acceleration phase of the missile trajectory or which could benefit from a substantial drag reduction during a portion of the trajectory. Furthermore, many of these missions require operation sufficiently low in the atmosphere that airbreathing propulsion, if it is competitive with the rocket, is attractive. Recent concepts of external burning for propulsion appear attractive for these missions because it is possible to make these systems extremely simple, essentially eliminating the requirement for an inlet, combustion chamber and nozzle, at an acceptable sacrifice of I_{sp} compared with usual airbreathing systems. At the present time, there is experimental proof that the concept will work, but the ability to scale and predict is not available with any precision. The experimental facility described herein is designed to provide experimental proof that an analytical model currently under development will actually predict the effects on base pressure of many processes which take place during external burning.

Historically, the concept of external burning for propulsion appears to have evolved through three phases, all subsequent to a firm understanding of supersonic flight, with the last phase dependent upon preliminary understanding of base flows. The three phases are tied to the three concepts shown in Figure 1. The initial attempts at the manipulation of the base flow operated upon base-bleed combustion, shown in Figure 1a. Combustion, confined to the

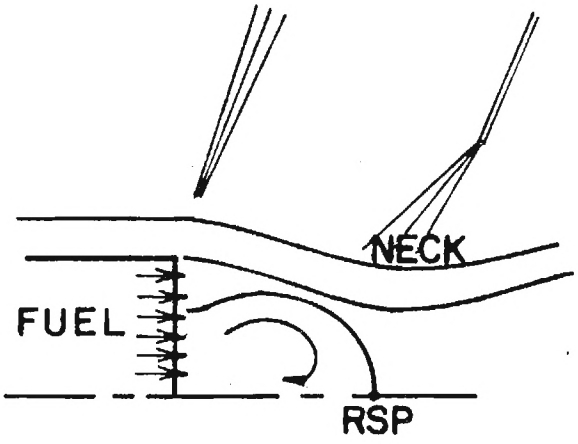

a. BASE BLEED COMBUSTION

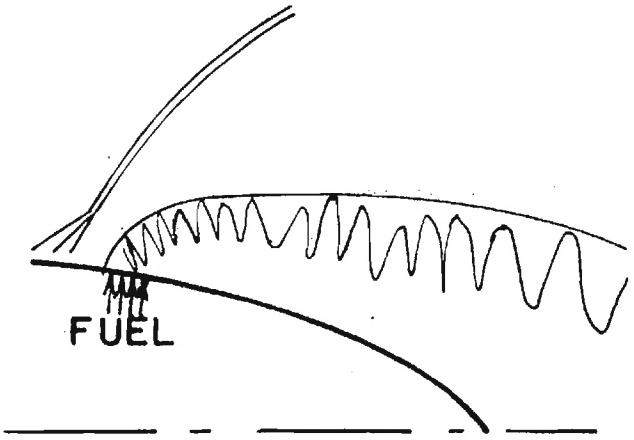

b. COMBUSTION ADJACENT TO AN AFTERBODY

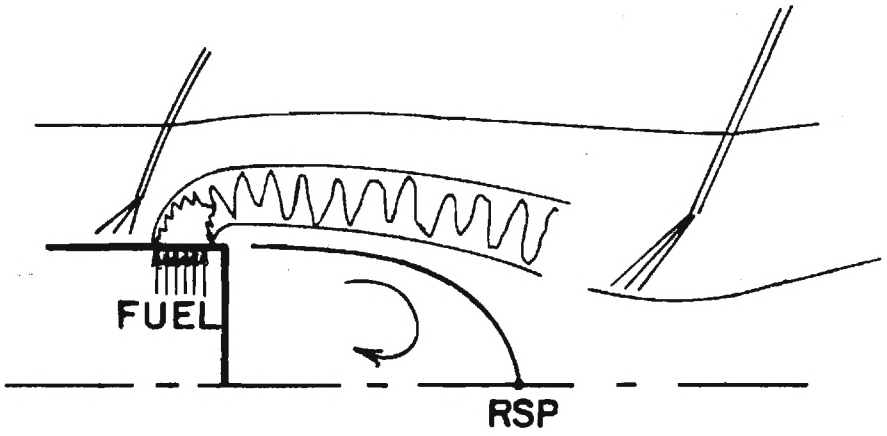

c. COMBUSTION ADJACENT TO THE NEAR WAKE

FIGURE I. CONCEPTS OF EXTERNAL COMBUSTION FOR PROPULSION.

recirculating flow field or in the shear layer between the inviscid flow-field and the recirculating flow, has its main action upon the total pressure of the flow in the shear layer. In all cases base pressure is determined by the downstream condition that the flow must pass into a far wake condition. Consequently, the flow in the shear layer above the stagnating stream must have sufficient momentum to negotiate the compression turn near the axis. Base-bleed combustion operates by increasing the static and total temperatures of the flow in the shear layer. Increasing the temperature increases the speed of sound. Since the velocity field is fairly well fixed by the exterior inviscid flow and the low velocity recirculating flow, the effect of combustion is to reduce the average Mach number in the shear layer. Since the static pressure is bounded by the free stream static pressure, the net effect of combustion is to decrease the total pressure of the shear layer and its ability to undergo a reattachment pressure rise. Consequently, the base pressure, which is the initial condition for the wake flow, cannot be small; it must rise toward the free stream static pressure as combustion raises the temperature.

This effect was indeed found in References (1) and (2). In the work of Baker et. al.[1] injection and spark ignition of H_2 in the base flow region was carried out at a free stream Mach number of 1.9 on a projectile with a 2.25 inch base diameter. The free stream static pressure was atmospheric, and, when burning occurred, the base pressure rise maximized around 6 psi, or to a level about 2 psi below atmospheric. Defining the specific impulse as the change in base-force level divided by the hydrogen mass-flow rate, the I_{sp} peaked at about 1000 sec. The thrust produced by the hydrogen jets themselves exhausting through ports in the base, was negligible compared to the thrust increase due to base burning.

In the work of Scanland and Hebrank,[2] 40-mm rounds were loaded with a pyrotechnic that exhausted through the base. Effects on drag were measured by observing the flight of a fired round. At $M_\infty = 1.65$, it was concluded that 65% of the base drag was eliminated by a flow rate of roughly 0.027 lb/sec, or an I_{sp} of roughly 180 sec was attained.

Work on this concept was renewed in the late 1960's, as given in References (3) and (4). Townsend and Reid[3] bled H_2 gas around the entire periphery, normal to the free stream, near the base of a 1.0-inch diameter projectile. The test conditions were $M_\infty = 2.16$ and $P_\infty = 3$ psi. Spark ignition was used and the maximum I_{sp} was approximately 3600 sec, but again, the base pressure rise was limited. It was found that the base pressure could only be raised slightly higher than the body static pressure foward of the injection ring. Experiments were run with and without a conical afterbody, but no essential difference in results was found, since the base flow was separated regardless of the afterbody presence. The theoretical work of Davis[4] showed clearly that the above-mentioned mechanism is responsible for the base pressure rise and theoretically explained the order of magnitude of the I_{sp} attainable with H_2. While the I_{sp} levels are attractive with base-bleed combustion, it is quite clear that these magnitudes can only be attained at low base pressure rises. Base injection may be thought of as a mass addition and heat generation in the near wake, and it is now quite clear what the gross effects should be.[5-7] These manipulations do not change the condition that the flow must ultimately reattach to a stream characterized by P_∞. They only change the ability to withstand a reattachment pressure rise within the constraint imposed by P_∞. The limitation on base pressure clearly becomes the free stream static pressure.

The second phase, augmented by the theoretical work of References (8-10), was initiated during the middle 1950's and is summarized in the unclassified literature in Reference (11). The concept of external burning adjacent to boattail afterbodies is shown in Figure 1b. Except for a combustion strength sufficient to cause massive separation, no limitation appears on the base pressure rise attainable with this method, presuming also that the flowfield does not become subsonic through the action of heat addition. A maximum thrust I_{sp} of 818 sec has been obtained on a 20^{o} half-angle wedge using triethaluminum (TEA) as a fuel at Mach 5.0. The majority of results were far lower than this value, however, due to combustion difficulties in the wind tunnel facilities available at the time. In any event, a primary drawback to the method, for many missions, is the requirement of an afterbody. Furthermore, extensive separation may be induced at large pressure rises, and this may be objectionable from a controls standpoint.

Concept b) of Figure 1 operates on the known principle of heat addition to a supersonic flow that streamlines diverge under the heating action. This in turn causes a pressure increase in supersonic flow. Not surprisingly, this method produces an I_{sp} of roughly $\frac{1}{2}$ that of a SCRAMJET at the same combustor conditions, because $\frac{1}{2}$ of the thrust surface is thrown away; that is, there is no outer wall containing the combustion. It is only through manipulation of the inviscid flowfield that large pressure rises may occur. Usually, mission requirements are such that only partial drag relief does not justify the incorporation of a propulsion system; consequently, large pressure rises are required by an external burning system.

It was Strahle[12] who first introduced the concept shown in Figure 1c,

which led into the third phase of investigation of external burning for propulsion. Strahle was the first to systematically explore the possibility of raising the base pressure behind bluff-base bodies by combustion in the exterior inviscid flow. An indication that this method is feasible was given by Serafini et. al.[13] Aluminum borohydride was injected at discrete points perpendicular to the flow at a station 10.5 inches from the nose of revolution 21 inches long. The Mach number was 2.47 at a pressure altitude of 55,000 feet. A net thrust condition was observed and the base specific impulse was roughly 200 sec. This result is open to question because of possible tunnel interference, but the nature of this interference was never explicitly shown.

The primary idea in this concept is that there is a base flow mechanism for transmission of high downstream pressures upstream to the base, because of the subsonic recirculation zone. Consequently, an afterbody is not required, and for many vehicles it is not desired anyway. Although it is an oversimplification, one way of viewing this concept is an entrapment of the subsonic region in a zone of high pressure caused by combustion. The actual mechanism is intimately involved with the reattachment process, however.

Several classified programs have followed the work of Reference (12) in an attempt to provide an experimental basis for the concept. While the results cannot be discussed in detail because of classification difficulties, it may be stated that it is not proved that the base pressure may be raised above the free stream static pressure and the I_{sp} values are substantially in excess of rocket engine values. A major improvement on the concept was added by the Atlantic Research Corporation. In Reference (12) it was tacitly

assumed that the fuel would be a pyrophoric liquid. Practically, this leads to difficulties at small size scales in obtaining an axisymmetric ring of fuel with large air capture. ARC introduced the concept of using a solid propellant gas generator as the fuel generator. Since the mass flow per unit area of a gas is lower than that of a liquid, larger injection ports may be used and the fuel better distributed about the body periphery. Furthermore, the usual advantages of solids over liquids are apparent.

The theory of Reference (12) was based upon a highly simplified picture of the process, using the two dimensional Crocco-Lees[12] theory of base flows and confining combustion to the inviscid flow. In practice, combustibles will become entrained in the shear layer and the concept will operate as a mixture of concepts a) and c) in Figure 1. No analysis exists capable of treating these phenomena. Given impetus by the field of wake observables, much has been done in recent years concerning analysis of near wakes.[6,15] Nevertheless, no analysis yet exists, except for a reasonably inaccurate older theory,[16] of the axisymmetric, turbulent base flow with a non-adiabatic condition on the shear layer.

For adiabatic shear layers with external combustion, recent theory and experiment have become available from the U.S. Naval Postgraduate School.[17-19] Experiments at Mach 2 have been carried out simulating external burning by compression waves generated by the nozzle wall contour. Base pressure was the single parameter measured and the theoretical treatment of the Crocco-Lees theory,[14] modified for axial symmetry, and using the method of characteristics in the inviscid stream. Cold gas injection through the base was investigated in conjunction with externally generated pressure waves. In this program it was found that a) net thrust could be expected to be produced by external burning, b) it was advantageous to locate the heat release

region so that compression waves impinged slightly forward of the base, c) the shorter the length of the effective heat release zone for a fixed heat release, the better and d) although cold gas injection through the base increases the base pressure, the effects of base injection and external compression are not additive.

A new base flow model, for the configuration of Figure 2, is now being developed by Strahle. This model is expected to yield more accurate structure of the base flow region than may be produced by the older Crocco-Lees theory. Furthermore, the model will be capable of treating the case of base injection and entropy layers adjacent to the near wake.

A major problem at the current time is the lack of data against which to test an analytical model. Even data on base pressure and pressure distribution is meager for an axisymmetric case in the absence of injection and burning. This report describes a facility which is designed to test base flow theory at Mach 3.0 so that confidence with which external burning effects can be predicted will be known. Results of preliminary flow evaluation tests and the first series of base flow measurements are also presented.

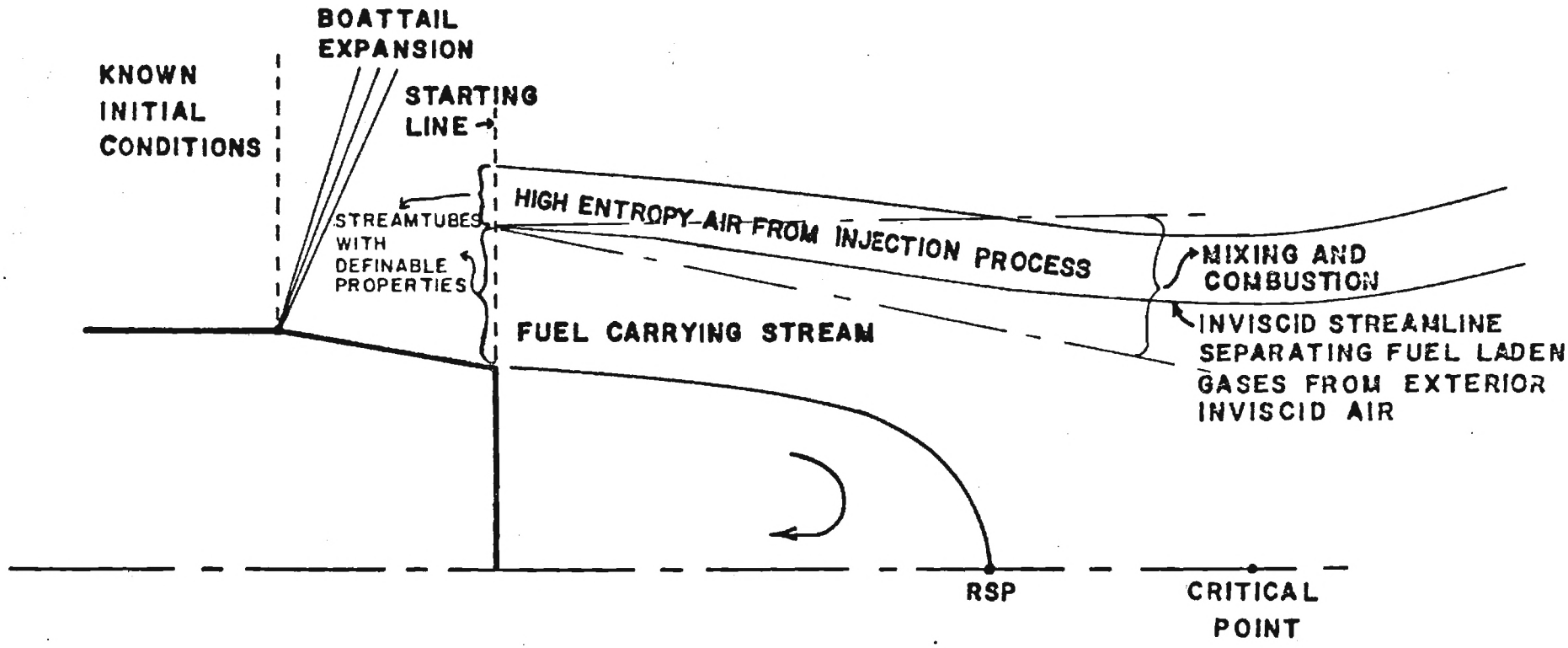

FIGURE 2. FLOW FIELD SCHEMATIC.

CHAPTER II

TEST FACILITY

The base flow test facility was designed to simulate the base flow for a projectile at Mach 3 with a fineness ratio of about 6 and Reynolds numbers, based on the diameter, in excess of 3.0×10^6. A relatively large base was selected in order to facilitate experimental accuracy and detailed flow measurements. Furthermore, the facility was designed for the versatility required to expose the base flow to disturbances that simulate those expected with external burning for propulsion. This includes disturbances due to a) axisymmetric pressure waves generated external to the near wake, b) cold gas injection, peripheral to the base in discrete jets, c) base bleed, and d) entropy layers adjacent to the near wake created by axisymmetric and discrete probes ahead of the base plane.

Details of this facility are presented and discussed in the following paragraphs.

Complete Assembly

A schematic of the complete flow system is shown in Figure 3. It is a blown-down system which uses air stored at a maximum pressure of 3000 psia in a cluster of tanks with a total capacity of 500 cu. ft. Air from the storage tanks is reduced to about 400 psia by three remotely controlled, high pressure regulators. The line from these regulators divides into the secondary air supply ducting, which will provide air for either base bleed or radial jets, and the primary tunnel ducting. Each of these ducts has an auxiliary pressure regulator which permits the fine control required for

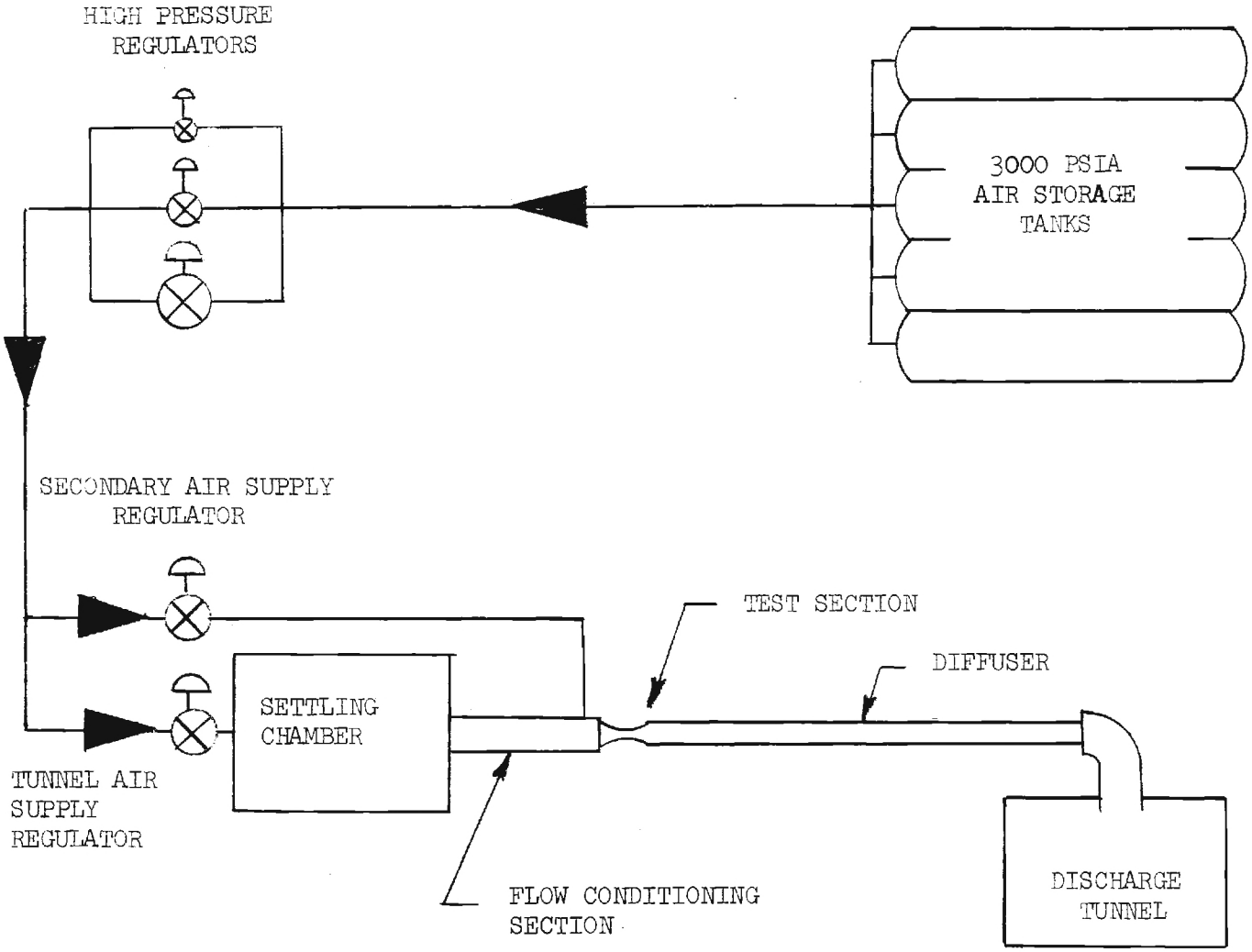

Figure 3. Schematic of the base flow facility flow system.

maintaining accurate test conditions. The combined flows finally dump into a large discharge tunnel. The total run time is from about 3 to in excess of 5 minutes, depending upon the stagnation pressure setting. Secondary air flow, for base bleed and radial jets, will be used later in the program. Therefore, this section of the ducting has not been installed to date.

A more detailed illustration of the test facility is presented in Figure 4. The primary tunnel flow first passes through a settling chamber, consisting of perforated tubes and baffles, which minimizes large scale fluctuations and nonuniformities produced by throttling through the auxiliary pressure regulator. The flow then passes through a final flow conditioning section, consisting of a series of screens and honeycomb, before entering the nozzle and test section. The supersonic flow in the test section is then decelerated in a constant area, shock diffuser before being dumped into the discharge tunnel.

Three spacers, each having an axial length of one base radius and located between the nozzle and external compression section, are illustrated in the schematic of Figure 4. Each of these may be removed to change the location of the external compression section relative to the base.

Photographs of the base-flow test facility are shown in Figure 5. These photographs show the existing configuration and identifies the components from the settling chamber to the diffuser. The probe actuator is remotely stepped radially in increments of 0.0001 inch by a stepping motor driving an accurate, no-backlash lead screw. It is manually moved horizontally on two sets of rigid guide rods.

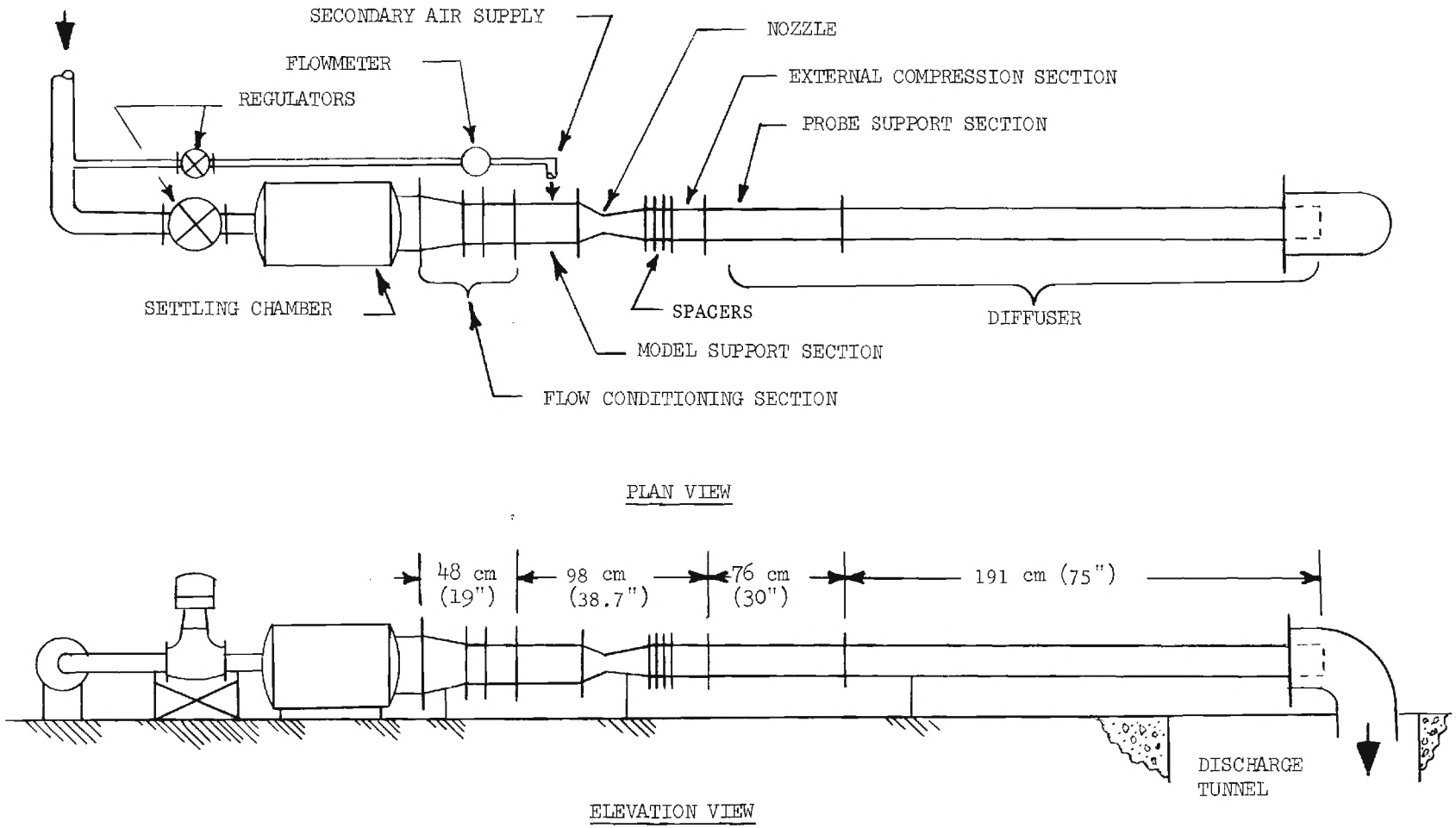

Figure 4. Schematic of the base flow test facility.

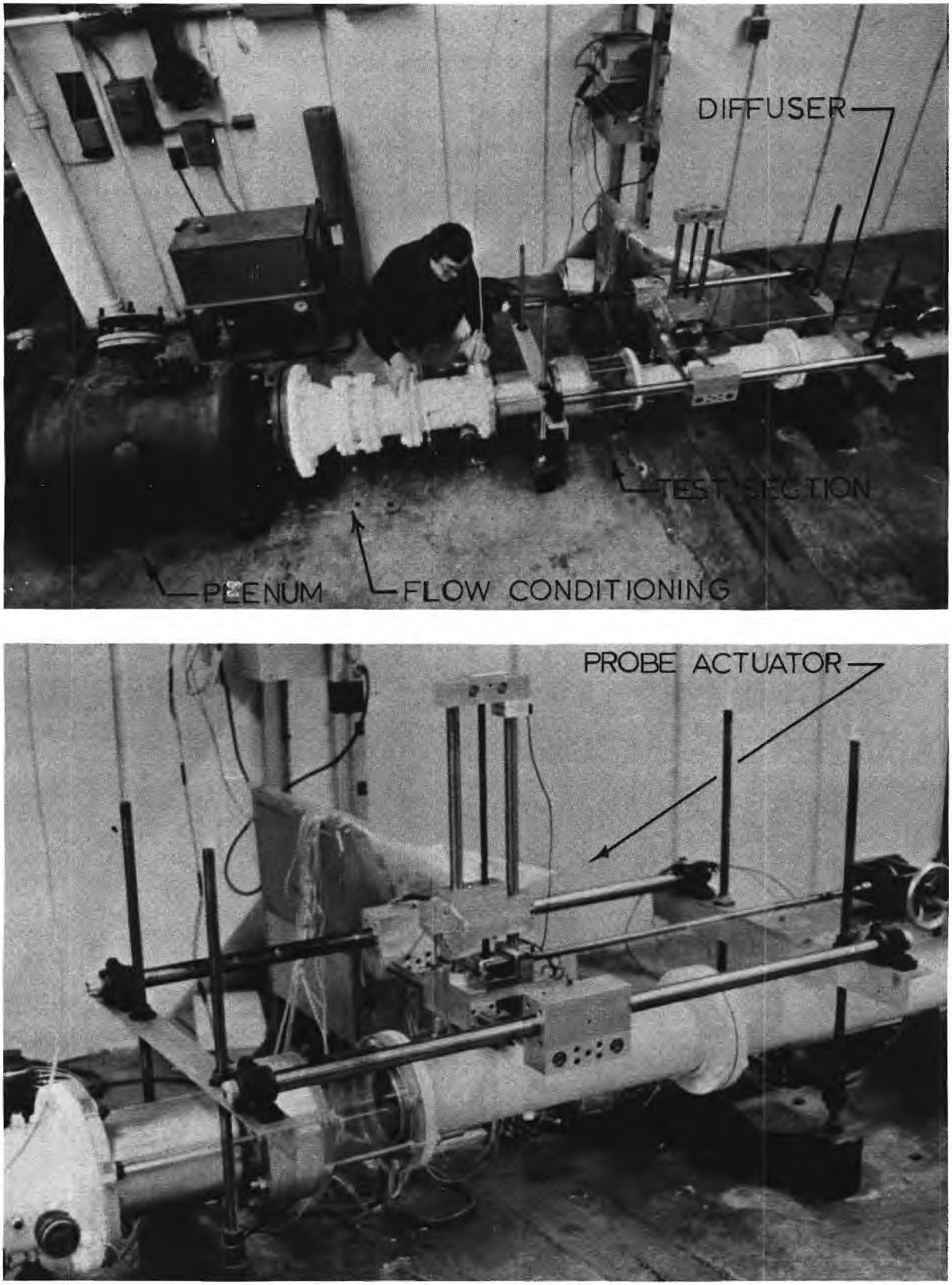

FIGURE 5 BASE FLOW TEST FACILITY

Flow Conditioning Section

Details of the flow conditioning section are shown in Figure 6. Flow from the settling chamber enters this section through a one-inch thick perforated plate with 1,627 drilled holes 0.07 inches in diameter. The flow through perforations is slightly subcritical and the stagnation pressure ratio across the plate is about 1.5. A one-inch deep honeycomb section, constructed of 0.002 inch thick aluminum with a 0.11 inch mesh, is located immediately downstream of the perforated plate to remove axial components of vorticity generated by unsymmetric coalescence of adjacent jets. The duct is then reduced to the 8-inch diameter employed upstream of the supersonic nozzle. Three 36-mesh stainless steel screens constructed of 0.0065 inch diameter wire are located between flanges in the 8-inch ducting. The screen open-area ratio of 0.59 is in the range of stable flow downstream of the screen.[20] The pressure drop coefficient for these three screens is adequate to eliminate significant turbulence and transverse gradients in the longitudinal velocities. An additional honeycomb is located between the last two screens to remove any remaining axial components of vorticity.

Test Section

The test section of the base-flow facility is shown on Figure 7. This schematic illustrates the model support section, the supersonic nozzle, the centerbody, and the external compression section. The nozzle is designed to expand the flow from a Mach number of 0.07 in the 8-inch-diameter model support section to 3.02 at the nozzle exit. The outer diameter at the nozzle exit was selected to mate with a standard 6-inch diameter pipe. A centerbody diameter of 2.25 inches, before boundary layer corrections, was then selected for the design. This is conservatively less than that for which

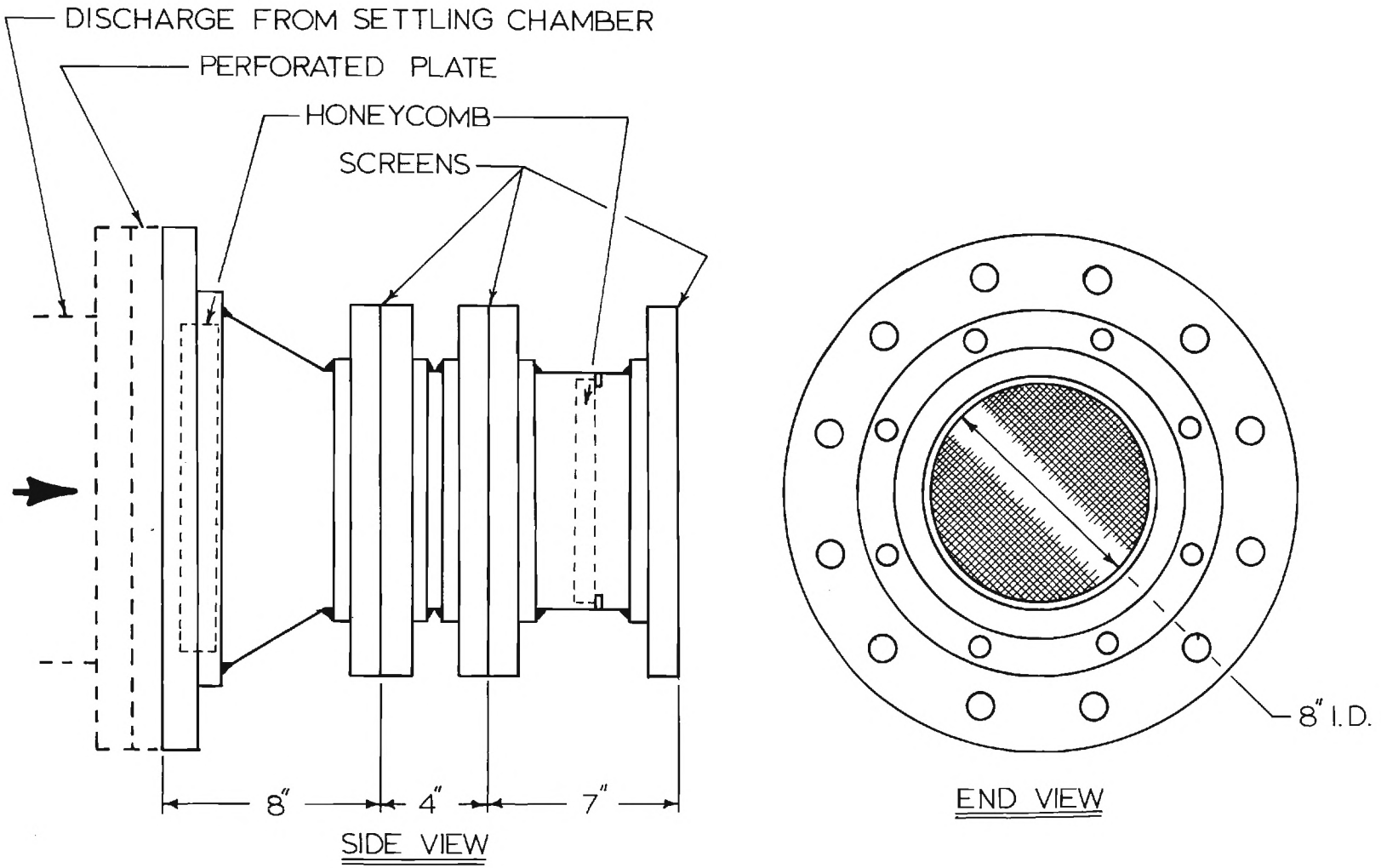

Figure 6. Flow Conditioning Section.

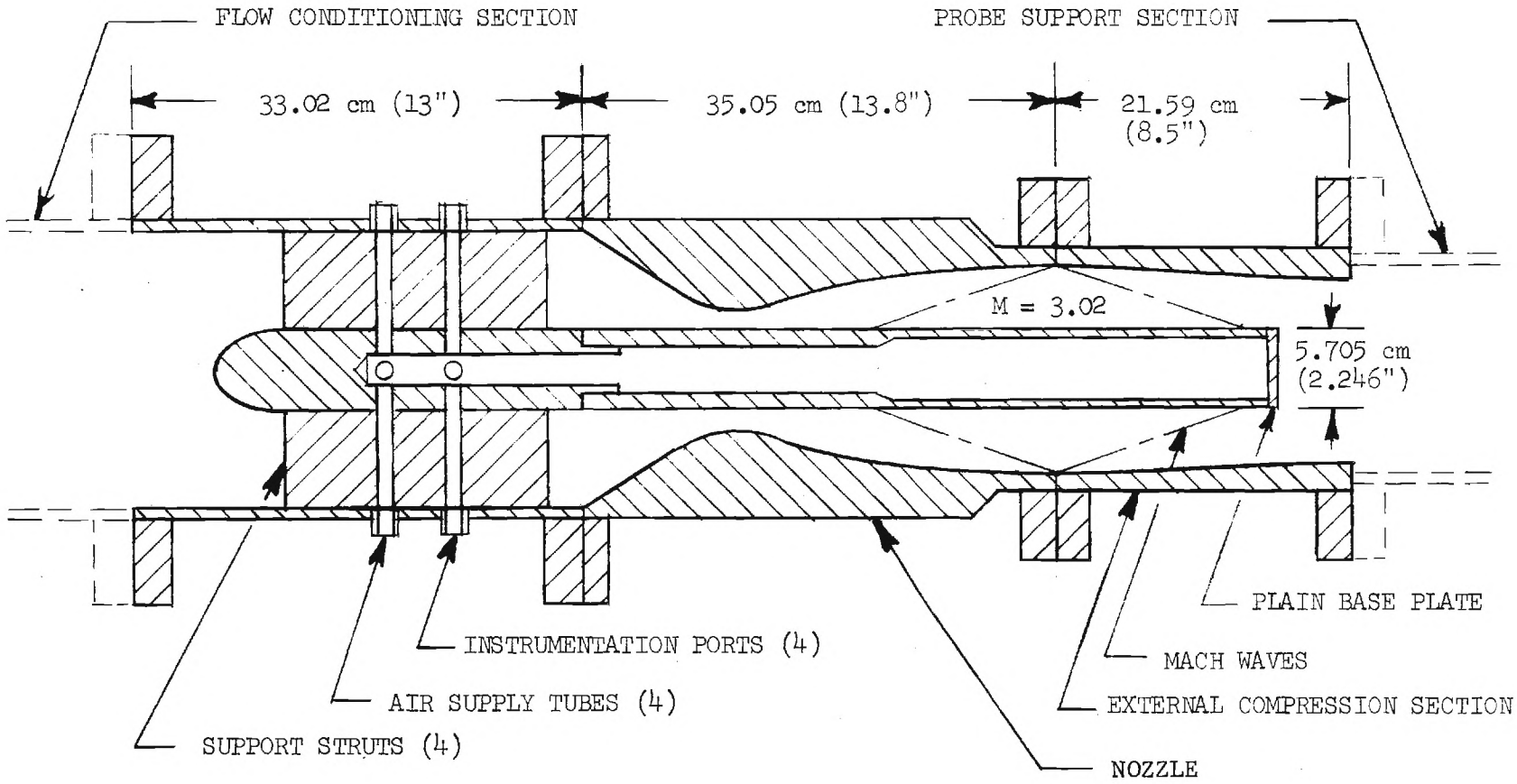

Figure 7. Schematic of the base flow test section.

base expansion waves would reflect from the outer ducting backs to the wake ahead of the critical condition.

The convergence half-angle for the subsonic region of the nozzle is 30^{o}. The throat radius of curvature is five times the throad height. The Mach number distribution in the transonic region was evaluated using an expansion in powers of the reciprocal of the throat radius of curvature following the method of Hall[21] modified to incorporate the boundary condition imposed by the constant diameter centerbody. This transonic solution included terms to third order.

The supersonic contour was evaluated using the theory of characteristics starting from the transonic solution at 0.2 throat-heights downstream of the point of minimum area. A very fine characteristic mesh, corresponding to about 125 points on the outer nozzle surface, was used. The outer nozzle contour and the centerbody diameter at the throat are corrected for the boundary layer displacement thickness. The boundary layer development was evaluated using the theory of Cebeci et. al.[22] (i.e., a numerical solution of the boundary-layer partial differential equations). Since it was considered to be desirable to maintain a constant diameter centerbody, the centerbody downstream of the throad was not corrected for the slight boundary-layer growth.

The centerbody is constructed in two sections as illustrated in Figure 7. Of particular importance, the long aft section shown in Figure 7 can be removed and replaced by a shorter aft section, thereby reducing the boundary layer thickness on the cylinder ahead of the base by about 60 percent. Only the long aft section has been fabricated to date.

The forward section of the centerbody is supported in the low-speed subsonic region by four streamline struts which provide access to instrumen-

tation in the base model and for the secondary-air supply to be used in later tests. The support section assembly, including the forward section of the centerbody, is shown in Figure 8a. The centerbody forward section is shown in Figure 8b. Each streamline strut contains one secondary-air supply duct and one instrumentation access duct. The mating surfaces of the support pipe, the struts, and the forward section of the centerbody are accurately machined to assure centering. Mating rings on the flanges of the support section and nozzle accurately locate the centerbody in the nozzle.

The external compression section shown in Figure 7 forces the flow to converge toward the axis, simulating the effects of axially symmetric external burning. This particular configuration is designed to approximately eliminate base drag. The design was generated using available experimental data to estimate the required wake convergence and axial pressure gradients and then calculating forward using the method of characteristics to establish the required compression-surface contour. The contour was then slightly adjusted such as to simulate a reasonable and smooth combustion, analytically modeled by one-dimensional, simple, heat addition centered above the wall. The compression surface, the simple heat addition zone, the surface Mach number distribution, and the ratio of the cumulative heat releases, qdx, to the initial enthalpy, h, are shown in Figure 9. The net heat addition is about three times the initial enthalpy. The external compression section terminates abruptly, forming a base which expands the flow back to the standard 6-inch pipe downstream. This augments the far wake acceleration by imposing an expansion along the wake downstream of the critical point.

The external disturbance section can be moved axially by locating the

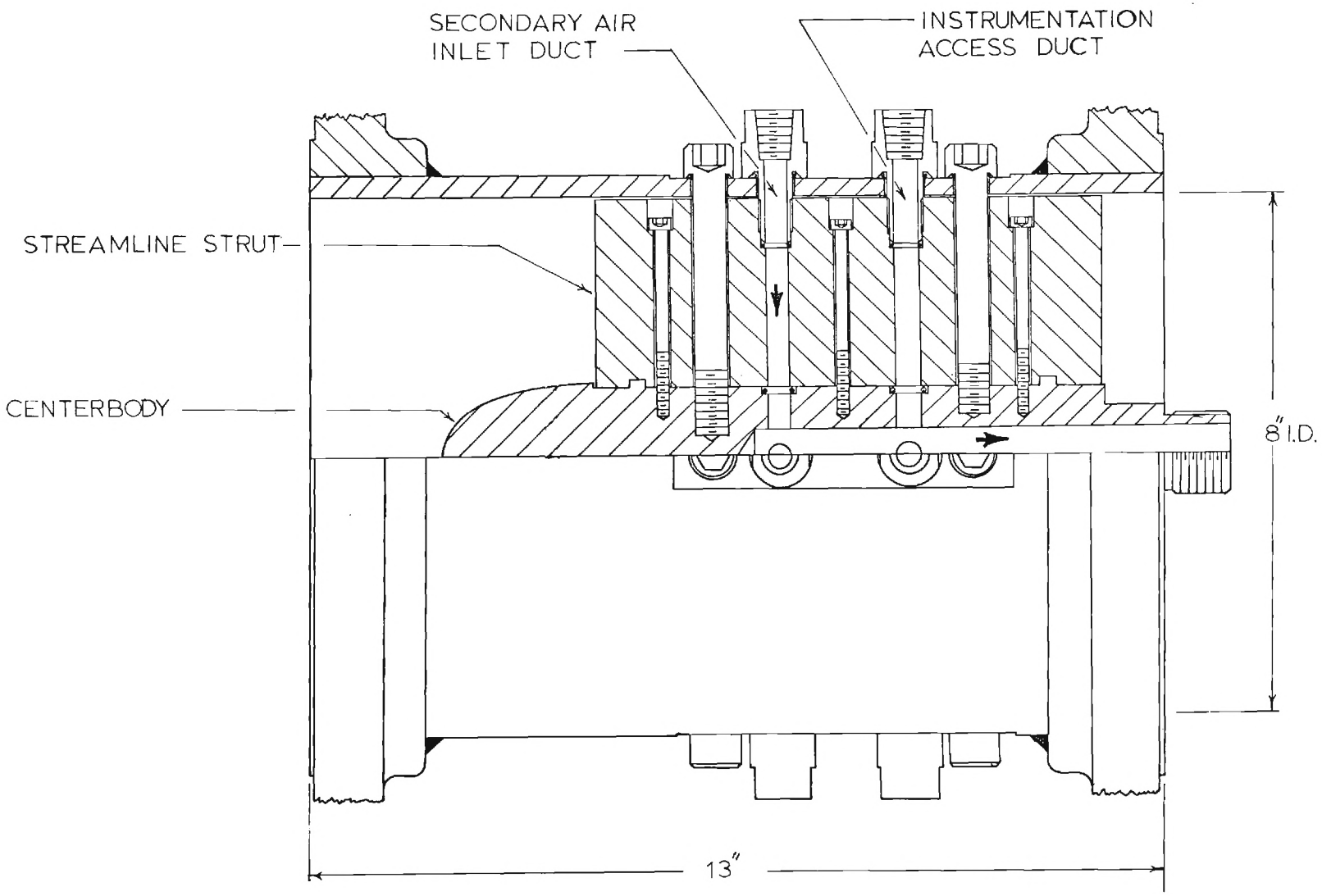

Figure 8a. Centerbody Support Section Assembly.

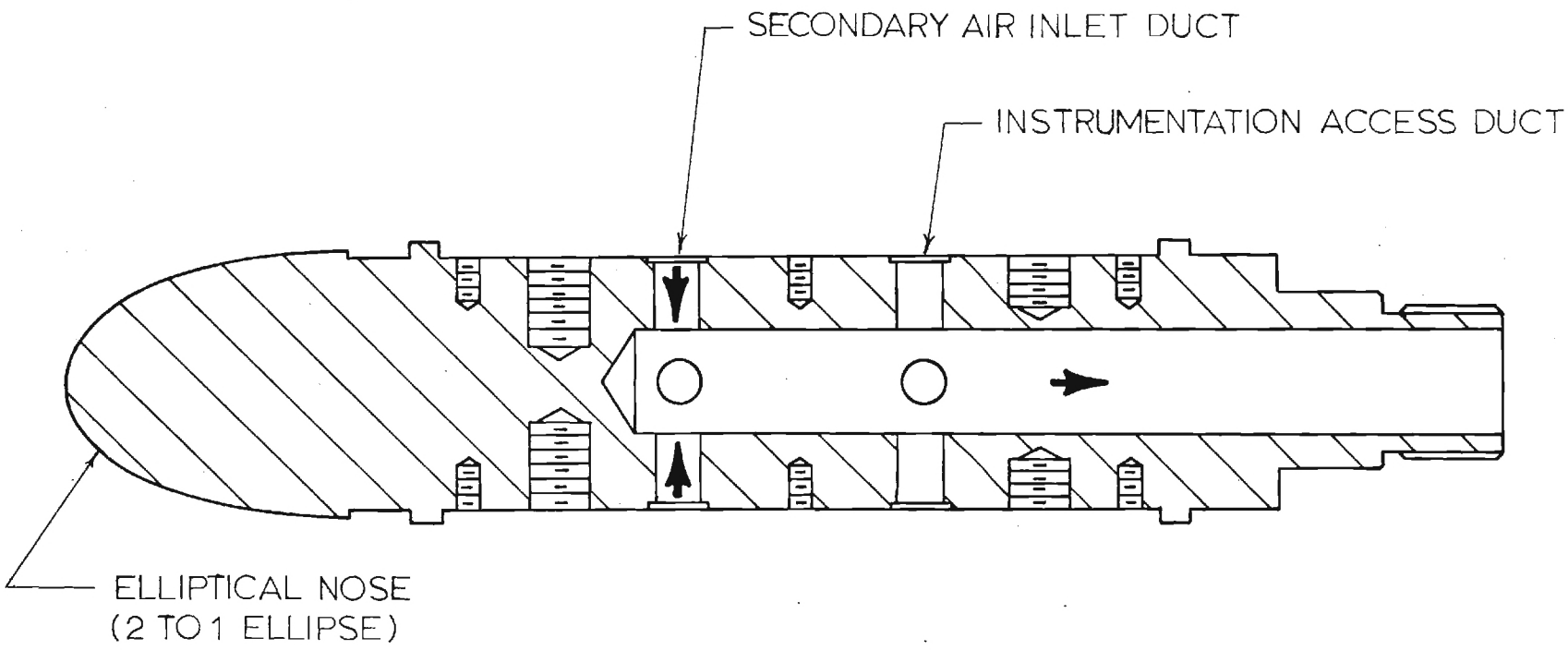

FIGURE 8b. CENTERBODY FORWARD SECTION

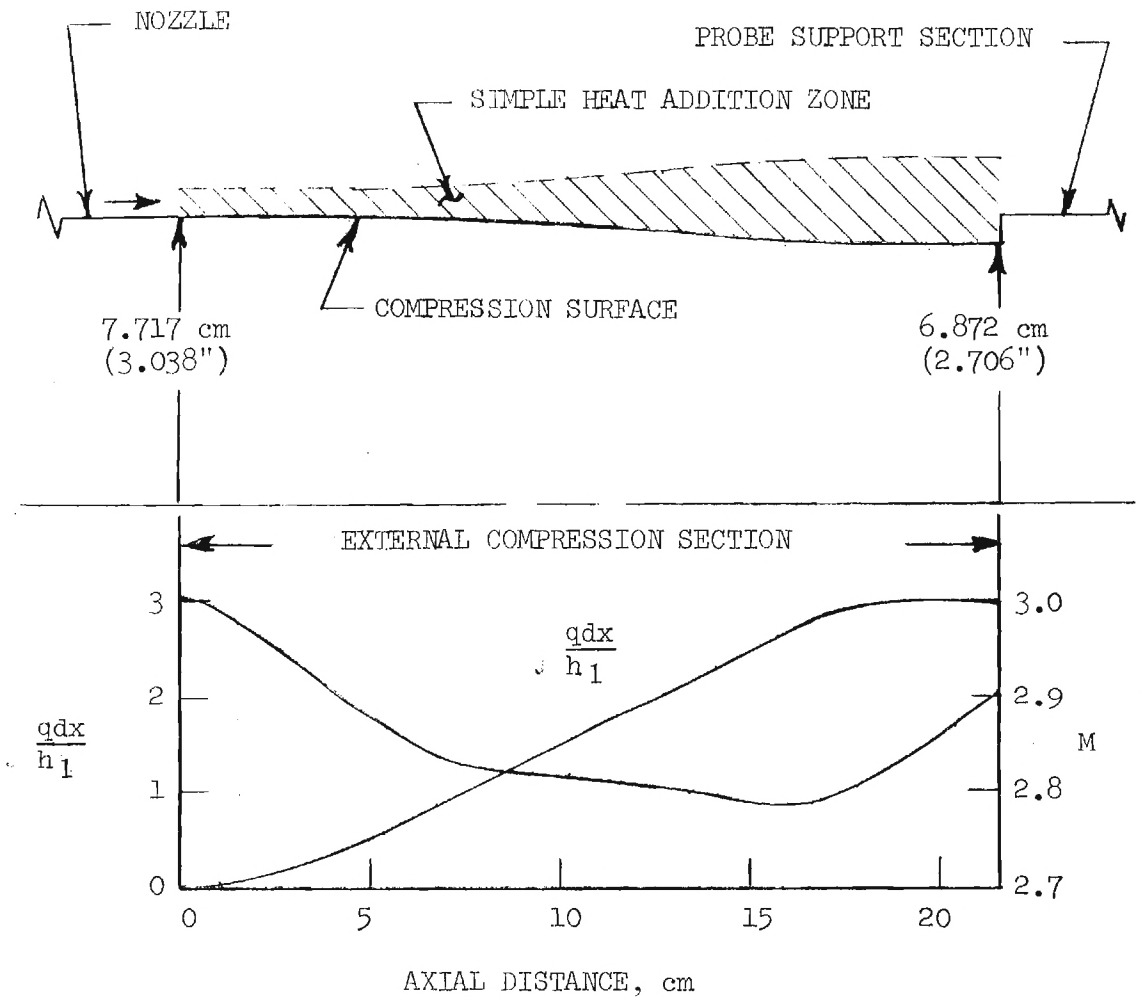

Figure 9. A design of the external compression section and the equivalent cumulative heat release.

constant diameter spacers between the nozzle and the external compression section as indicated in Figure 4. For the configuration shown in Figure 9, the disturbances are initiated one base radius ahead of the base plane. With the three spacers, the disturbances can be moved back in increments of one, two, and three base radii.

The external compression section shown in Figures 7 and 9 has been fabricated but has not been used in tests. Instead, a constant diameter section has been fabricated and used in all tests to date. This configuration has provided basic data without the effects of externally generated disturbances. The next series of tests will use the existing external compression section. Additional external compression sections will then be designed and fabricated for future test series.

A photograph of the test section is shown in Figure 10. This shows the configuration with the constant diameter section downstream of the nozzle. This section is constructed of plexiglas pipe welded to plexiglas flanges. The internal surface is machined and then polished to permit visual monitoring of the base model and probes. All other external compression sections will also be transparent.

Diffuser

The flow is decelerated to subsonic speeds in a 6-inch constant diameter shock diffuser. The total diffuser length downstream of the base near wake is 18 duct diameters or 47 base diameters. Such a long diffuser was considered essential if nearly-complete shock diffusion is to be realized because the far wake velocities must first be accelerated by shear stresses before shock deceleration can be initiated. In contrast, fully developed duct flow can be decelerated in a shock diffuser with a length to diameter ratio of about 10. Consequently in the present design nearly half of the

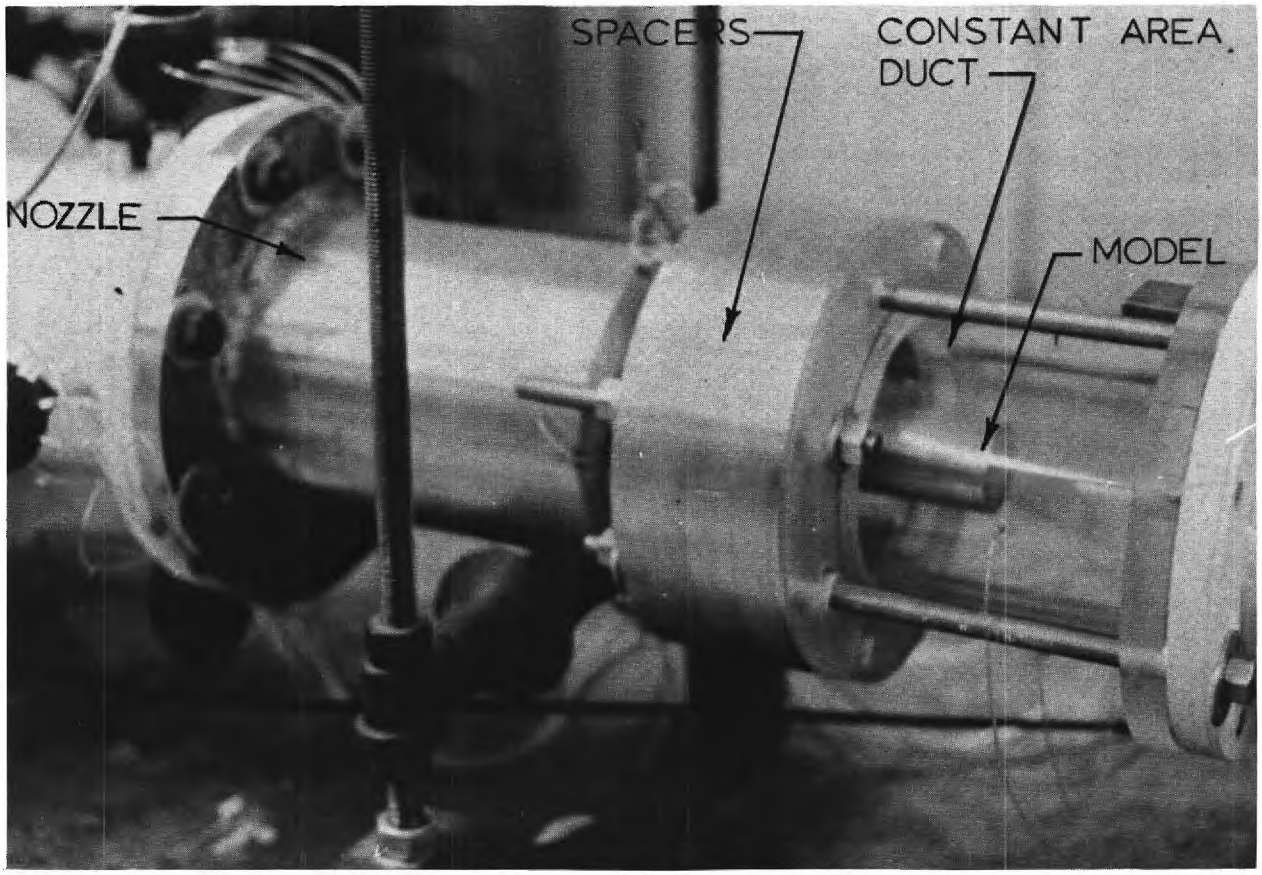

FIGURE 10. TEST SECTION

diffuser length was provided for wake development. It was felt that this would meet the design obejctive of test section stagnation pressures below 100 psia.

Instrumentation

The present test configuration is instrumented with 56 surface static pressure taps; 7 on the base plane, 16 on the cylindrical section of the centerbody, and 33 on the outer ducting from the nozzle exit to the end of the diffuser. Two thermocouples are embeded in the centerbody wall near the base plane and two thermocouples are embeded in the nozzle wall near the exit plane. In addition, a stagnation pressure probe and thermocouple probe are located in the subsonic flow field near the nozzle inlet. Furthermore, the static pressure probe and the pitot probe shown in the photograph of Figure 11 have been used to survey the wake. Both probes are constructed of 0.0625 inch-diameter stainless steel tubing which telescopes into 0.125 and 0.25 inch-diameter tubes for structural support. Long sections of the smaller diameter tubing are used to minimize probe disturbances in the near wake. The 0.0625 inch diameter section of the pitot probe is 3.5 inches long. The four static taps in the static pressure probe are located 4.5 inches from the 0.125 inch diameter tubes. In addition, this 0.0625 inch section of tubing extends 6.5 inches forward of the static taps. This extension threads through a hole in the base plate which provides a secondary support for the probe.

The nozzle-inlet stagnation pressure is measured by a 0-150 psia strain-gage pressure transducer. All other pressures are measured by two 1000 mm Hg, Barocel Electronic Manometers manufactured by Datametric Corporation. These units use highly stable and linear, variable-capacity transducers with

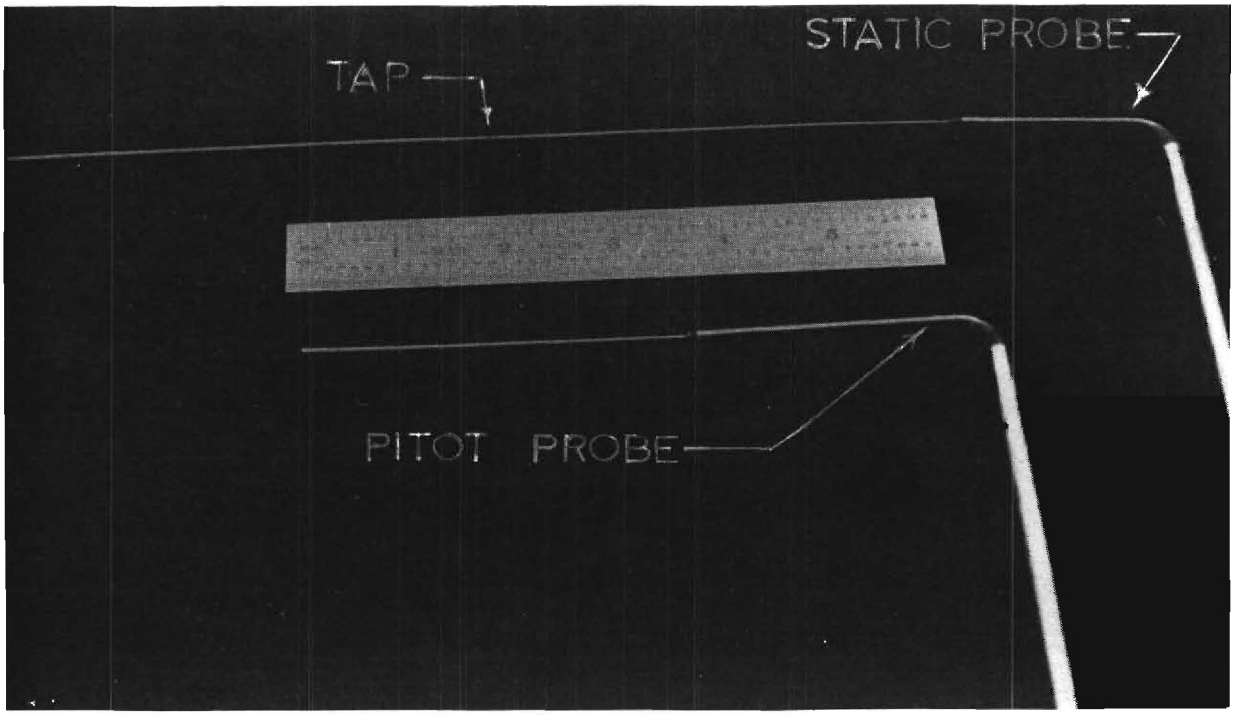

FIGURE 11. STATIC AND PITOT PROBES

automatic ranging output amplification from 1 to 1000. Two 48 channel Scanivalve components are used for rapidly switching the pressures to the two Barocel transducers.

The facility is set up for manual operation during system check-out or for programmed operation, using a computer-based data acquisition system, during the short-duration test runs. The data acquisition system is shown in the photographs of Figure 12. This system uses a Hewlett Packard HP2100A computer with 16K of core storage. The computer is interfaced with a HP2752A teletype for operational control and data output, a high speed tape reader for program inputs, a HP2401C low-level, integrating, digital voltmeter for reading all input voltage data, a 30 channel scanner for connecting the various data channels to the voltmeter, and a 16 contact relay card for actuating the probe drive and scanivalve solenoids. A schematic of the system hook-up is presented in Figure 13.

The use of the high-speed data acquisition both increases the amount and enhances the quality of the data obtained during each short-duration test. During the test the pressure data are normalized by the instantaneous upstream stagnatic pressure to minimize the effects of drifts in test conditions and then stored for later retrieval. Output is generally arranged for a convenient display for rapid assessment of the results. Typical examples of data output are presented in Figure 14. Figures 14a and 14b show the data output for a Reynolds number test consisting of four runs; each run corresponding to a given initial stagnation pressure setting. The normalized surface static pressures are displayed in Figure 14a. The stagnation pressures used to normalize the static pressures are displayed in Figure 14b. The stagnation pressure is measured once for every two static pressure measurements (the static pressure measurements being in the order

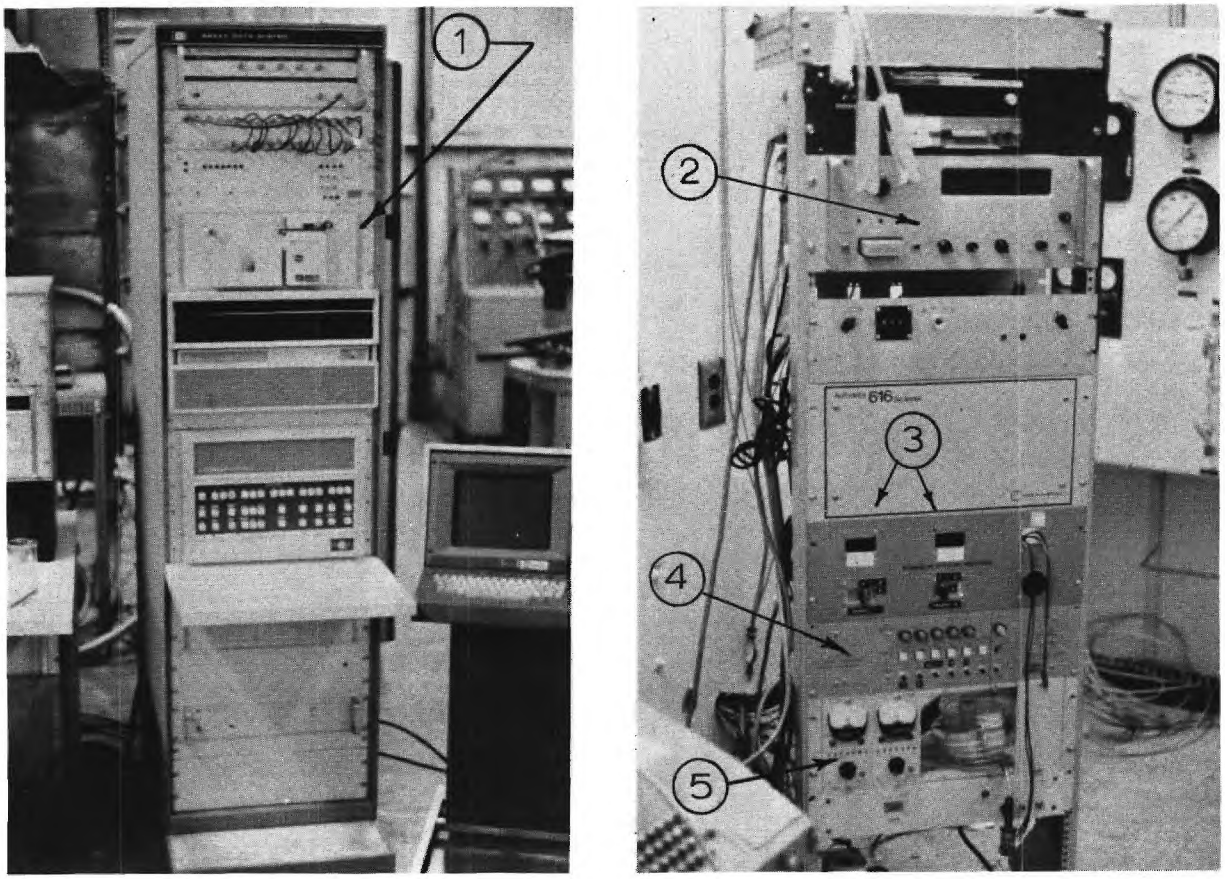

1. COMPUTER
2. INTEGRATING DIGITAL VOLTMETER
3. SCANIVALVE POSITION INDICATORS
4. SCANIVALVE CONTROLLERS
5. BAROCEL SIGNAL CONDITIONERS

FIGURE 12. DATA ACQUISITION SYSTEM

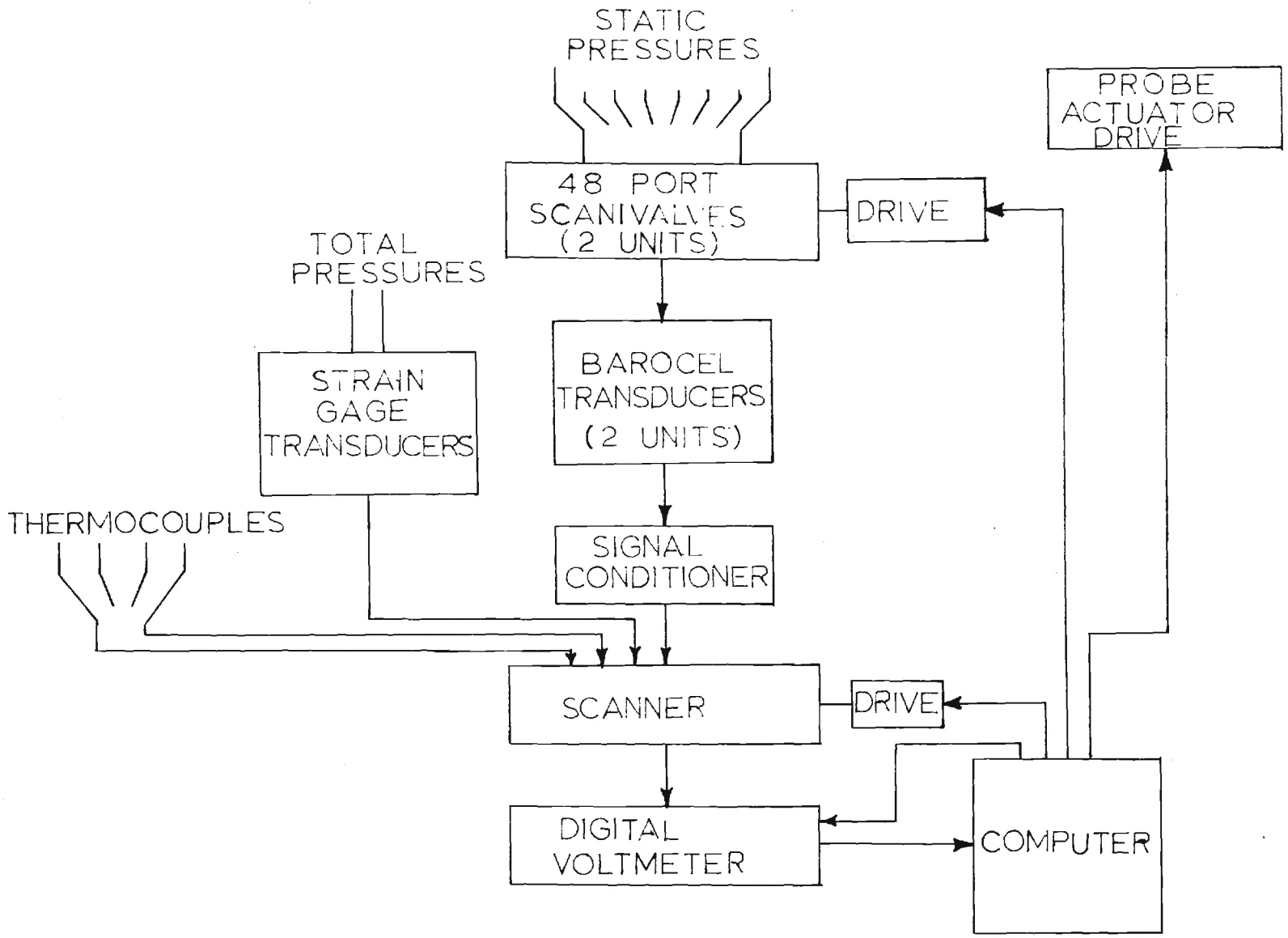

FIGURE 13. SCHEMATIC OF DATA ACQUISITION SYSTEM

J		P(J,1)/P01	P(J,2)/P01	P(J,3)/P01	P(J,4)/P01
1		1.32992E-02	1.32915E-02	1.30072E-02	1.32521E-02
3	BASE	1.37903E-02	1.35137E-02	1.34050E-02	1.37570E-02
5	RADIAL	1.42767E-02	1.42679E-02	1.40845E-02	1.43270E-02
7		1.45475E-02	1.43682E-02	1.41298E-02	1.43070E-02
9		2.61242E-02	2.64831E-02	2.70632E-02	2.69083E-02
11		2.87794E-02	2.87719E-02	2.84723E-02	2.84812E-02
13	CENTER-	2.85193E-02	2.81421E-02	2.81740E-02	2.81560E-02
15	BODY	2.88263E-02	2.89998E-02	2.87053E-02	2.86490E-02
17		2.91365E-02	2.87757E-02	2.88765E-02	2.88203E-02
19	AXIAL	2.75894E-02	2.74729E-02	2.71099E-02	2.69484E-02
21		2.56312E-02	2.56849E-02	2.55302E-02	2.55477E-02
23		2.66332E-02	2.62543E-02	2.63918E-02	2.62267E-02
25		2.52887E-02	2.61599E-02	2.57456E-02	2.57803E-02
27		2.63692E-02	2.60399E-02	2.65201E-02	2.62913E-02
29		3.06047E-02	3.06744E-02	3.06229E-02	3.05510E-02
31		2.88709E-02	2.90268E-02	2.90092E-02	2.91123E-02
33	DUCT	2.83129E-02	2.82852E-02	2.85318E-02	2.84390E-02
35	AXIAL	2.85325E-02	2.86028E-02	2.86760E-02	2.84936E-02
37		2.82694E-02	2.84291E-02	2.83757E-02	2.82592E-02
39		2.88730E-02	2.86782E-02	2.88239E-02	2.86735E-02
41		3.14514E-02	3.15148E-02	3.00285E-02	2.99812E-02
43		2.88381E-02	2.96100E-02	2.93541E-02	2.91002E-02
2		1.29971E-02	1.29989E-02	1.25982E-02	1.28869E-02
4	BASE	1.39166E-02	1.38242E-02	1.37358E-02	1.41507E-02
6	ANGULAR	1.43496E-02	1.43811E-02	1.41501E-02	1.43772E-02
8		1.30478E-02	1.29536E-02	1.26646E-02	1.29157E-02
10	CENTER-	2.76013E-02	2.73038E-02	2.71288E-02	2.70872E-02
12	BODY	2.79283E-02	2.75776E-02	2.74409E-02	2.73983E-02
14	ANGULAR	2.88053E-02	2.86981E-02	2.85719E-02	2.86284E-02
16		2.86883E-02	2.89022E-02	2.88747E-02	2.88093E-02
18	CENTER-	2.61230E-02	2.59226E-02	2.62995E-02	2.62216E-02
20	BODY	2.53756E-02	2.57215E-02	2.55104E-02	2.54298E-02
22	ANGULAR	2.61496E-02	2.63569E-02	2.65111E-02	2.64344E-02
24		2.52683E-02	2.47538E-02	2.48156E-02	2.46908E-02
26	DUCT	3.11640E-02	3.15813E-02	3.11922E-02	3.12312E-02
28	ANGULAR	3.38219E-02	3.30135E-02	3.41046E-02	3.37679E-02
30		3.06933E-02	3.08130E-02	3.06553E-02	3.06149E-02
32		3.12992E-02	3.12363E-02	3.13529E-02	3.12521E-02
34	DUCT	2.68497E-02	2.68300E-02	2.70410E-02	2.69661E-02
36	ANGULAR	2.71806E-02	2.72606E-02	2.72901E-02	2.72726E-02
38		2.83141E-02	2.84337E-02	2.84131E-02	2.83441E-02
40		2.85179E-02	2.83012E-02	2.84797E-02	2.82850E-02
41		3.14514E-02	3.15148E-02	3.00285E-02	2.99812E-02
42	DIFFUSER	3.14647E-02	3.14722E-02	3.01032E-02	3.00628E-02
43		3.00381E-02	2.96100E-02	2.93541E-02	2.91002E-02
44		1.59167E-02	1.58535E-02	1.59010E-02	1.58742E-02

J STATIC PRESSURE TAP INDEX
K RUN INDEX
P(J,K) STATIC PRESSURE ARRAY
P01 STAGNATION PRESSURE

a) SURFACE STATIC PRESSURE DATA

FIGURE 14. TYPICAL DATA OUTPUT

I	P01(1)	P01(2)	P01(3)	P01(4)
1	4066.94	5009.	7531.6	6449.52
2	4072.89	5059.78	7554.17	6416.31
3	4061.2	5009.51	7523.32	6440.12
4	4061.2	5030.2	7492.11	6435.12
5	4048.44	5027.81	7461.27	6423.19
6	4053.67	4999.6	7478.19	6419.43
7	4048.44	5054.65	7454.49	6411.91
8	4032.99	4977.54	7448.85	6406.27
9	4048.44	5030.2	7446.22	6399.39
10	4025.47	4995.84	7426.28	6402.5
11	4040.51	4970.01	7439.45	6381.82
12	4019.82	5025.93	7401.09	6388.1
13	4027.35	4956.35	7419.89	6363.01
14	4010.83	4998.22	7391.68	6372.41
15	4027.35	4995.84	7377.38	6354.25
16	3999.14	4928.14	7375.5	6352.37
17	4017.94	4990.2	7378.52	6341.09
18	4001.02	4966.25	7362.34	6342.97
19	4002.9	4919.23	7352.19	6335.44
20	3995.38	4984.56	7331.51	6331.84
21	3992.02	4932.4	7350.31	6321.64
22	3993.5	4915.47	7328.48	6310.36

K	T0(K)	T1(K)	T2(K)
1	55.621	63.0683	73.4481
2	35.0789	29.6113	63.0767
3	16.2476	.18277	49.0168
4	-3.17978	-26.2115	30.0945

I STAGNATION PRESSURE MEASUREMENT INDEX
K RUN INDEX
P01(K) STAGNATION PRESSURE, mmHG
T0(K) STAGNATION TEMPERATURE, °F
T1(K) CENTERBODY WALL TEMPERATURE, °F
T2(K) NOZZLE WALL TEMPERATURE, °F

b) STAGNATION PRESSURE, STAGNATION TEMPERATURE, AND WALL TEMPERATURE DATA

FIGURE 14. CONTINUED.

X	PROBE P/P01	P(1)/P01	P01	T0	T1
125	1.20870E-02	1.39083E-02	4134.96	48.559	54.7573
150	1.29898E-02	1.39976E-02	4116.56	44.5443	47.2233
175	1.42491E-02	1.40892E-02	4074.77	41.8725	42.7697
200	1.60763E-02	1.40091E-02	4076.65	38.723	36.9166
225	1.78364E-02	1.41203E-02	4065.78	35.5846	31.9523
250	2.00826E-02	1.41778E-02	4023.16	33.3167	26.9243
275	2.24568E-02	1.44184E-02	3988.66	30.5554	21.8232
300	2.46151E-02	1.43269E-02	3979.26	29.6153	19.0076
325	2.63504E-02	1.43240E-02	3966.09	27.3517	16.2476
350	2.88895E-02	1.42834E-02	3977.37	26.4336	14.3784
375	3.04578E-02	1.42279E-02	3978.85	24.5934	10.6236
400	3.13501E-02	1.41866E-02	3969.45	23.6713	8.73781
425	3.27135E-02	1.42843E-02	3935.6	21.3963	5.94666
450	3.39155E-02	1.45098E-02	3915.3	20.4339	3.59342
475	3.37436E-02	1.42542E-02	3922.43	19.6145	1.66698
500	3.41386E-02	1.46271E-02	3856.6	18.1115	.661072
525	3.43559E-02	1.45717E-02	3843.83	16.7533	-1.68127
550	3.43366E-02	1.46520E-02	3822.75	16.2476	-3.17575
575	3.35792E-02	1.44127E-02	3858.48	15.3137	-4.13861
600	3.40000E-02	1.43231E-02	3854.72	14.3784	-6.06879
625	3.41545E-02	1.46822E-02	3808.09	13.0148	-7.94699

PROBE P STATIC PROBE PRESSURE
P(1) A BASE STATIC PRESSURE
X AXIAL DISTANCE FROM BASE, $\times 10^2$ INCHES

c) WAKE AXIAL STATIC PRESSURE SURVEY

FIGURE 14. CONTINUED.

of the tap numbers) and then this stagnation pressure is used to normalize the two static pressures. This sequence is continued until all static pressures are measured. Figure 14b also lists the temperatures which were measured at the beginning of each run. The total test time for the data of Figures 14a and 14b was less than 3 minutes.

Figure 14c displays part of the data taken during the static pressure survey along the axis. The stagnation pressure and a base static pressure are measured each time the probe static pressure is measured. The stagnation pressure is then used to normalize the other two pressures.

CHAPTER III

RESULTS OF FLOW AND DATA EVALUATION TESTS

Preliminary tests were made to evaluate the quality of the flow field, the accuracy and repeatability of test data, and limits of test conditions prior to starting detailed base flow tests. The results of these evaluation studies are presented and discussed in this chapter.

Nozzle Inlet Flow

Velocity distributions along the horizontal and vertical lines through the center of the 8-inch duct upstream of the model support section are shown in Figure 15. The local velocity, u, is normalized by the numerical average of all velocities, $\bar{u}$. The maximum deviation from the average velocity is less than one percent. Since the mean flow Mach number in this section of ducting is only 0.035 the differences between the stagnation pressures of the nozzle inlet streamlines is negligible in comparison with the test-section dynamic head. It may be concluded that the settling chamber, the perforated plate, and the screens and honeycombs in the flow conditioning sections have eliminated the flow non-uniformities created by the large pressure drops through the contral values.

The nozzle inlet stagnation pressure decreases slowly with time after the upstream control valves have been adjusted for a particular pressure setting. A typical variation is illustrated in Figure 16 where the ratios of the stagnation pressure, P_o, to the initial stagnation pressure, P_{o_1}, are plotted against test time. In this case, the stagnation pressure decreases by about four percent in one minute. A cyclic variation, perhaps due to long

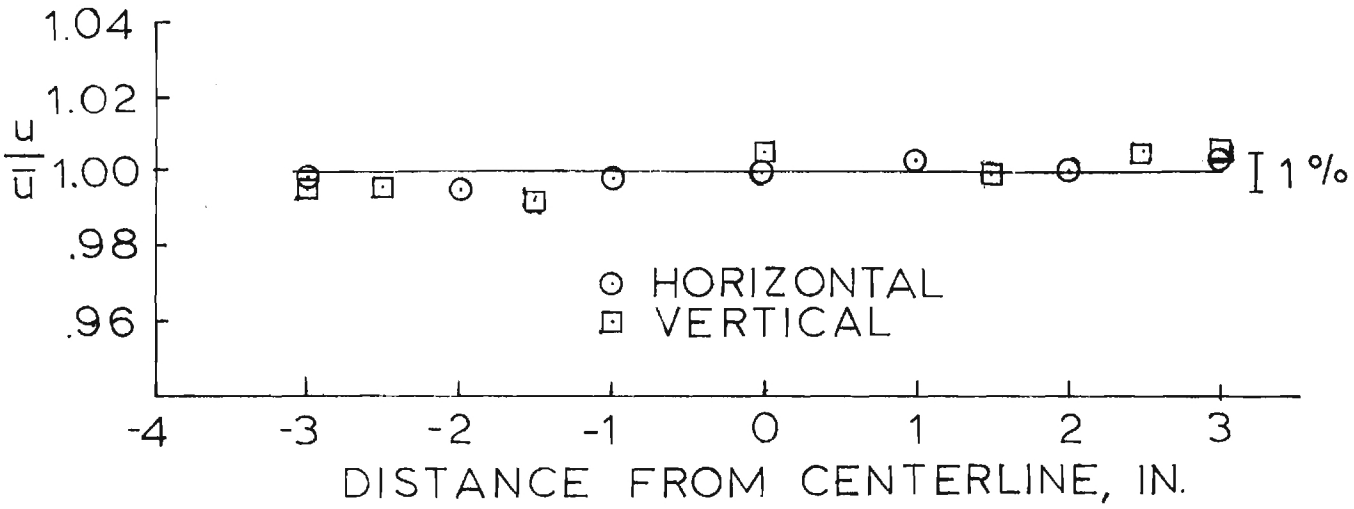

FIGURE 15. VELOCITY DISTRIBUTIONS AT TEST SECTION INLET

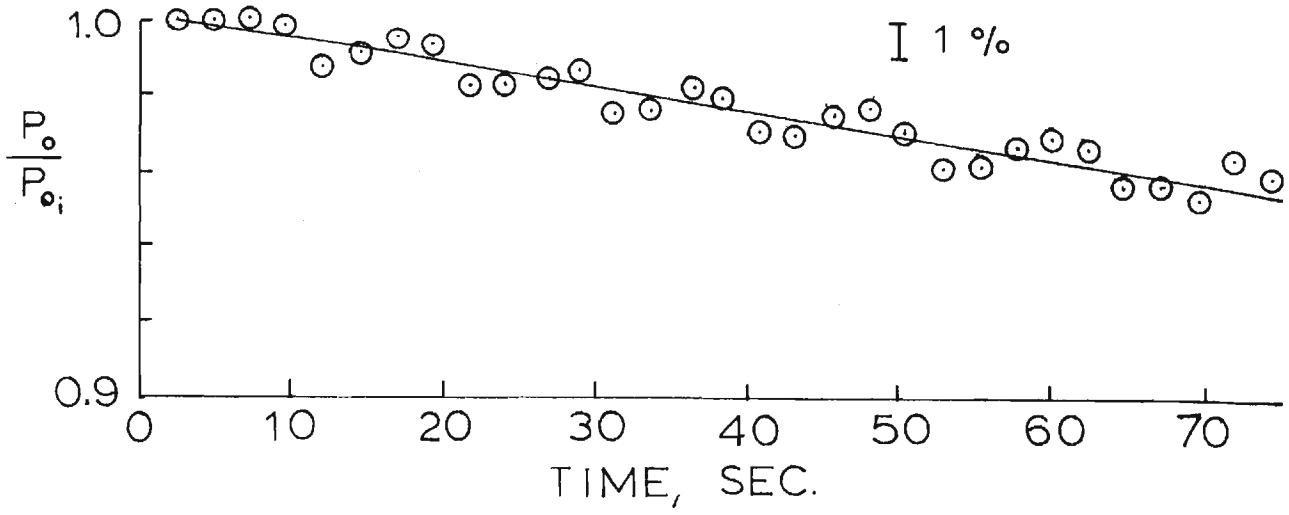

FIGURE 16. VARIATION IN STAGNATION PRESSURE AT TEST SECTION INLET.

period control-value hunting, of approximately 10 seconds duration, is also evident in these results. However, a short period deviation from a linear decay is always less than one percent. In order to minimize the errors due to stagnation pressure variations all other pressures are normalized by stagnation pressures measured periodically during the test. Each pressure is measured within less than one second of the time that its normalizing stagnation pressure is measured. This is an important advantage of the programmed data retrieval system. Consequently, errors due to stagnation pressure variations are believed to be less than one percent (i.e., the maximum deviation from a smooth decay curve).

Diffuser Performance

Pressure distributions along the shock diffuser for four nozzle inlet stagnation pressures are represented in Figure 17 where the local surface pressure, P, is normalized by the upstream stagnation pressure, P_o. For stagnation pressures in excess of 3730 mmHg the shock train begins at more than 30 base diameters downstream of the base plane. The shock pressure rise starts abruptly, as for fully developed pipe flow,[23] and has no effect on the pressures near the base. With the pressure reduced to 3080 mmHg the shock train starts ahead of the base plane, near the nozzle exit. The minimum stagnation pressure with shock deceleration in the diffuser as computed using one-dimensional flow analyses, neglecting surface friction but including base drag, is 3180 mmHg. This is in good agreement with the experimental result. It is of particular interest that the shock train is apparently completed in less than 10 diffuser diameters even though the core of the diffuser flow contains the base wake. This is slightly less (approximately 20 percent) than that reported in Reference 23 on the basis

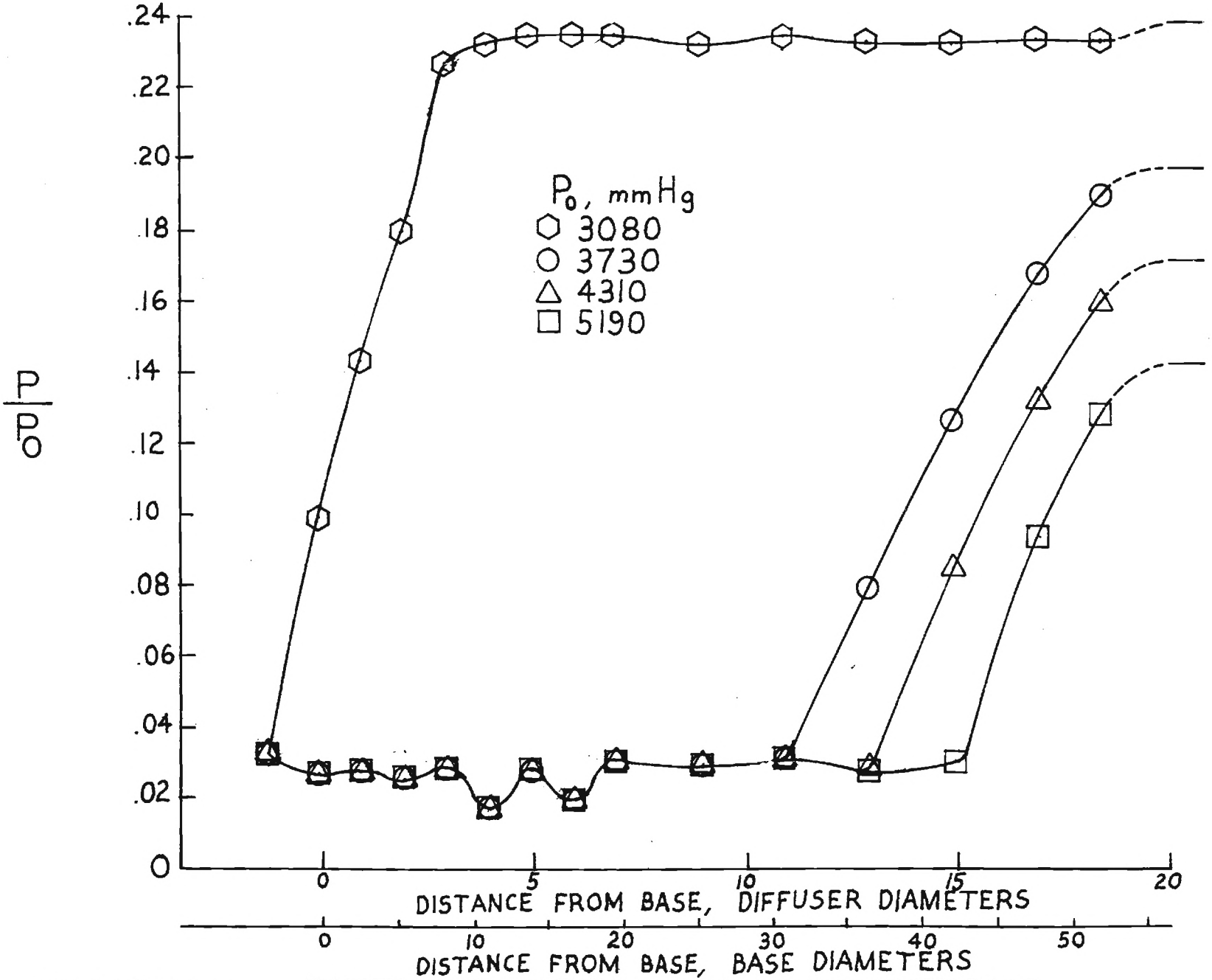

FIGURE 17. DIFFUSER PRESSURE DISTRIBUTIONS

of experiments with a smaller scale, developed pipe flow.

The pressure variations slightly downstream of the base plane are due to the base expansion and wake recompression waves. The proof that these pressure variations do not affect the near wake will be presented in the next chapter.

Test Section Flow

Axial distributions of Mach-numbers along the centerbody from near the nozzle exit to the base plane and along the outer, constant-diameter duct from two inches upstream to two inches downstream of the base plane are shown in Figure 18. The Mach number on the centerbody near the nozzle exit is reasonably close to the design value of 3.02. The Mach number decreases slightly toward the base plane due to the boundary layer growth. Near the base plane the Mach numbers on both the outer ducting and the centerbody are in good agreement with the value of 2.98 computed assuming one-dimensional flow with the flow area corrected for the theoretical values of the boundary-layer displacement thickness. There is also evidence of a slight Mach number increase on the centerbody immediately upstream of the base, due to the expansion at the base shoulder.

The reference Mach number, M_1, on the cylindrical centerbody upstream of the base plane will be taken to be 2.98, corresponding to the one-dimensional flow value, for all subsequent data reduction analyses.

Peripheral distributions of Mach numbers on the centerbody and outer ducting are illustrated in Figure 19. The data points are from one typical run. Each of the mean lines, however, are based on the results of six runs conducted on three days. The maximum deviation of any data point from the mean line is only one percent. Furthermore, the mean value of the Mach

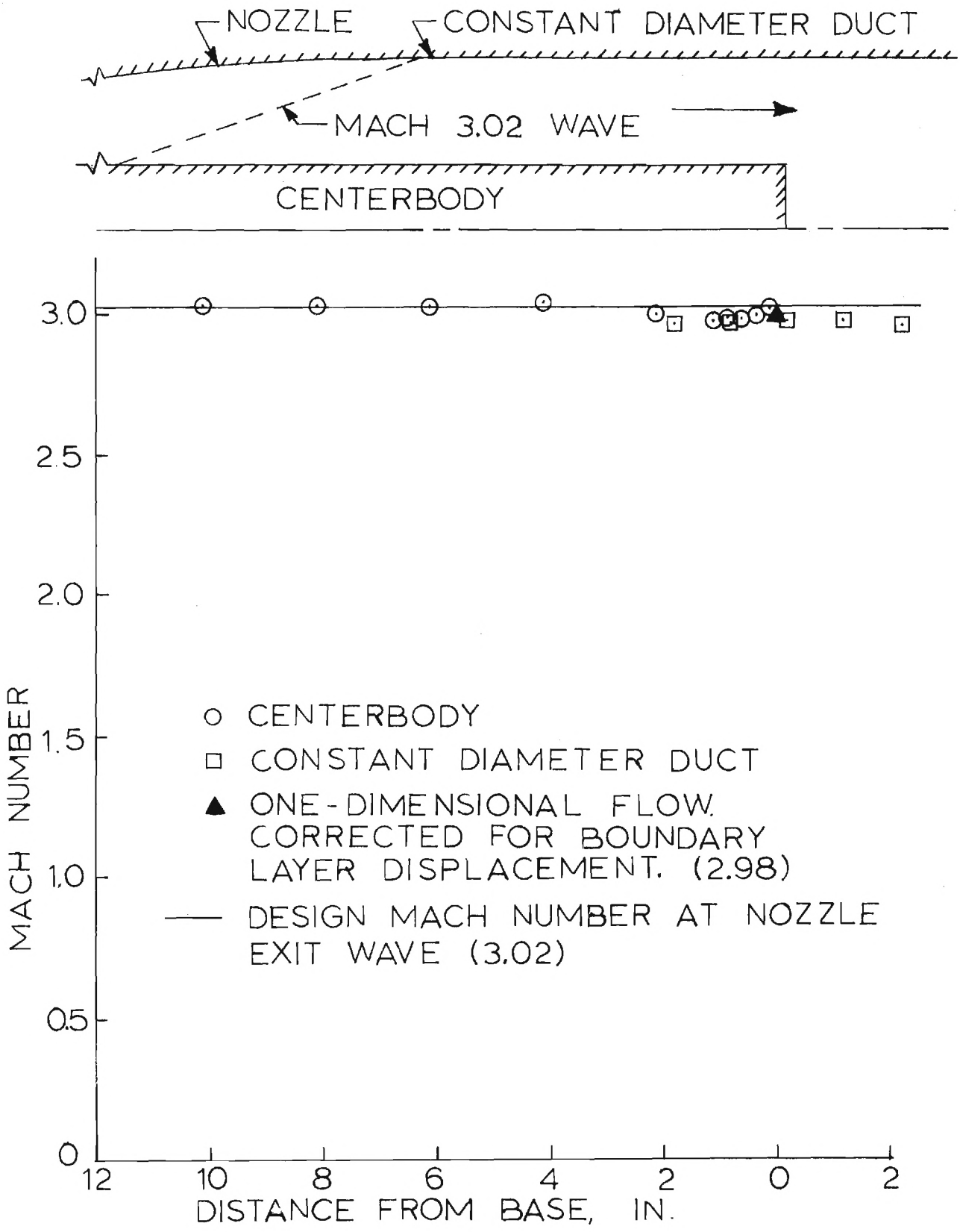

AXIAL MACH NUMBER DISTRIBUTIONS
FIGURE 18.

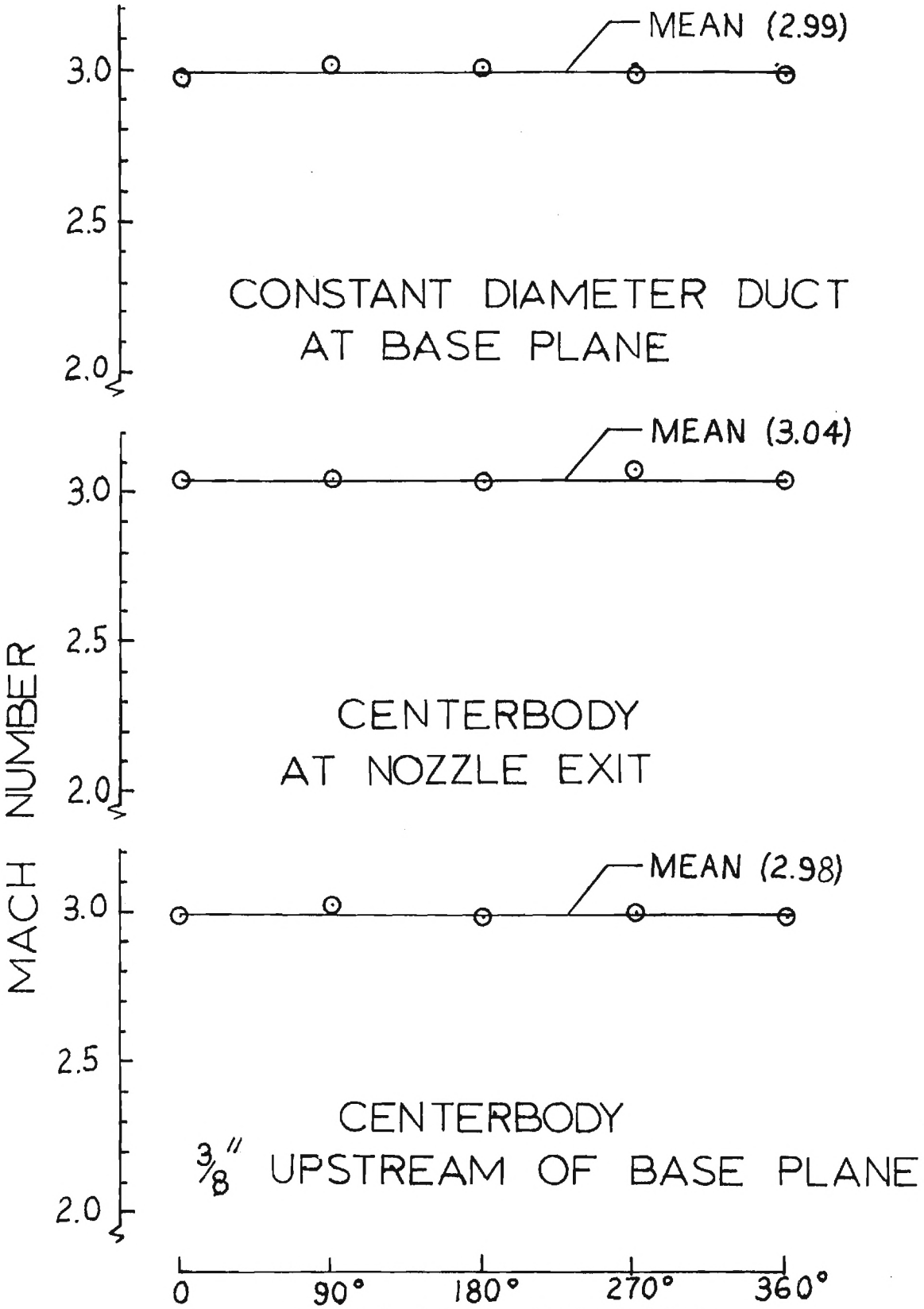

PERIPHERAL MACH NUMBERS

FIGURE 19.

number on the centerbody near the nozzle exit is only 0.5 percent higher than the design value. In addition, the mean values of the Mach number on the centerbody and the outer ducting near the nozzle exit plane are in good agreement with the theoretical, one-dimensional flow value of 2.98.

Ratios of the centerbody surface temperature near the base plane to the freestream stagnation temperature, T_{o_1}, are presented in Figure 20 for two typical runs. For both of these runs, the test period, during which the temperatures were sampled many times, was approximately 100 seconds. For Run 1, the test period started immediately after the upstream flow was stabilized. Consequently, the surface temperature is initially slightly higher than the stagnation temperature. For Run 2, the test period started about 50 seconds after the upstream flow was stabilized. Other data were acquired during this initial 50 seconds. For comparison, the corresponding temperature ratio for an adiabatic wall with a typical flat-plate recovery factor of 0.9 is included on Figure 20. A comparison of this adiabatic wall temperature ratio with the data shows that adiabatic flow is essentially obtained at the end of these two runs. Throughout the entire test periods the ratio of the actual wall temperature to the adiabatic wall temperature is only slightly greater than one. Correspondingly, the effects of heat transfer to the centerbody on the base flow are expected to be small.

Data Accuracy and Repeatability

The pressure transducers are periodically calibrated against accurate dead-weight testers and calibration curves are used in all data retrieval programs. Typical calibration results for the strain-gage transducer and one variable-capacitance Barocel transducer are presented in Figure 21. These results are included to emphasize the quality of the calibration curves

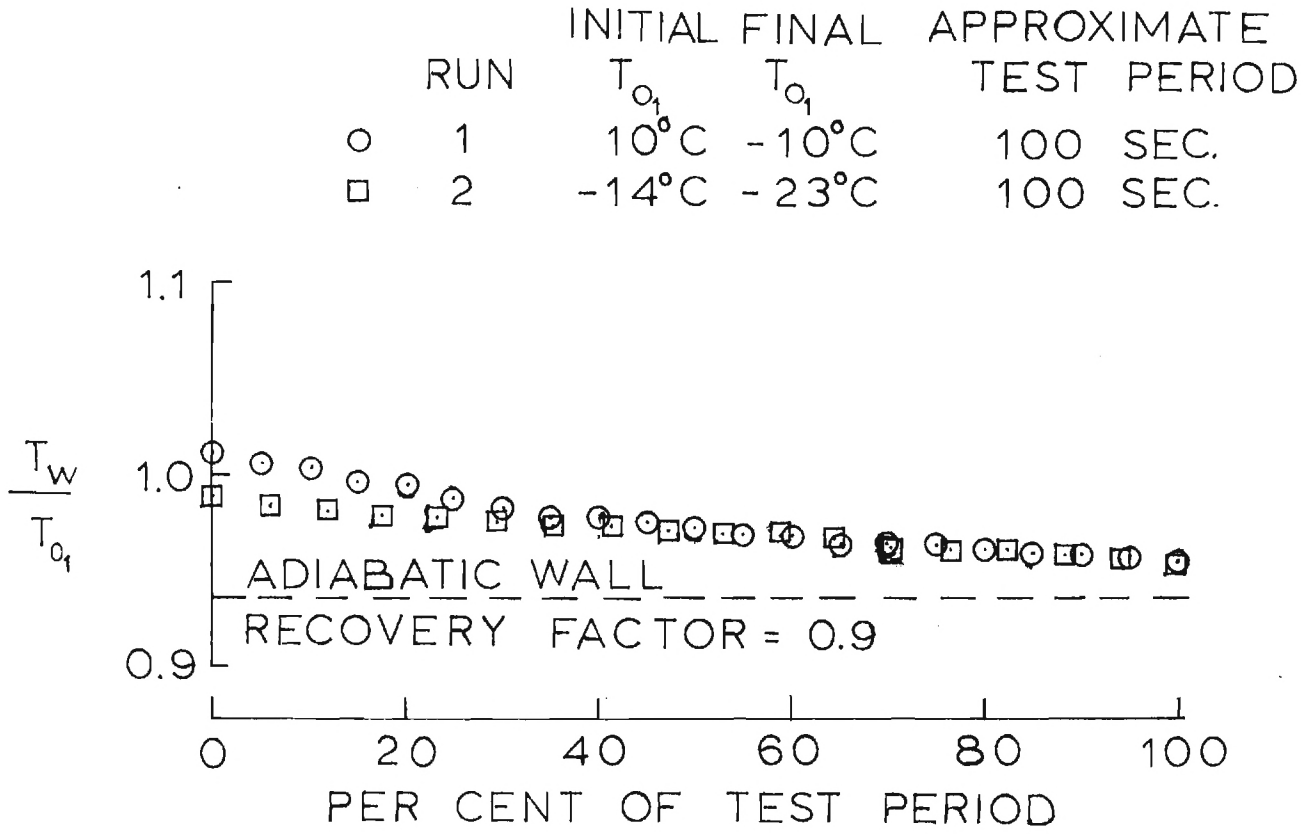

FIGURE 20. TYPICAL VARIATIONS IN THE RATIOS OF CENTERBODY SURFACE TO FREESTREAM STAGNATION TEMPERATURES.

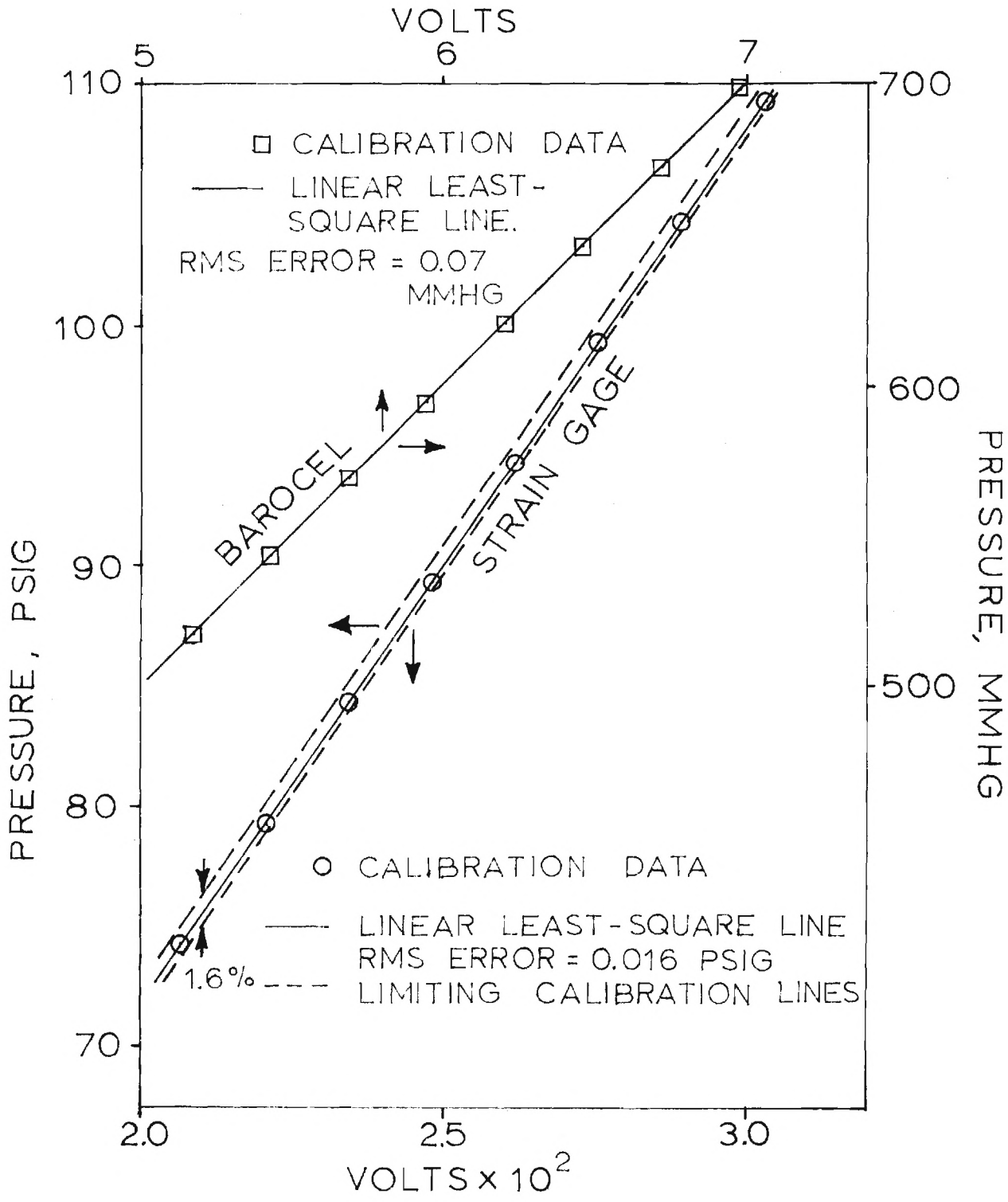

FIGURE 21. CALIBRATION RESULTS FOR PRESSURE TRANSDUCERS

and the expected accuracies of the data. The root-mean-square error of the data deviations from a linear least-square line is negligible in both cases. The only significant source of error is a shift in calibrations with both time and cycling of the pressure loads on the transducers. Calibrating for the cycling effects is impossible for tests of different durations and pressure sampling demands. The dashed lines on Figure 21 show the upper and lower limits of the calibration lines which have been obtained for the strain-gage transducer over a period of four months and with different transducer loading schedules. The total change is only 1.6 percent at the lower pressures. The maximum change for the two Barocel transducers over the same period of time has been only 0.4 percent in the pressure range of interest. Since the Barocel transducers measure the low test-section pressures using an atmospheric reference, this change is amplified to a maximum of no more than three percent of the absolute pressure. However, because calibration curves are periodically obtained for subsequent use in the data retrieval programs, it is believed that all absolute pressures are at least obtained within an accuracy of ± 1 percent, the major source of error being the changes with cycling, which varies from tests to tests.

As previously discussed, variations in the nozzle inlet stagnation pressure also introduce slight errors which are believed to be less than ± 1 percent. The coupling of this error with that of the transducers yields a maximum pressure error of ± 2 percent. This is considered to be a conservative estimate. The effects of pressure lag due to the transducer and line volumes are negligible since minimum pressure scanning rates are established from lag tests of the complete pressure measuring systems.

Figure 22 presents Mach number distributions along the centerbody upstream of the base as obtained in four runs on three days. These typical results are included to illustrate the repeatability of the test data and to support the conclusions concerning the data accuracies. The Mach number variations are a maximum of ± 0.4 percent from the mean. The corresponding pressure variations are ± 1.6 percent. These largest variations occur near the base plane where other measurements have shown that the flow conditions are most sensitive to small changes. Upstream of this region these and other measurements indicate a maximum pressure variation of about ± 1 percent. It is also important to note that variations shown on Figure 22 are apparently random.

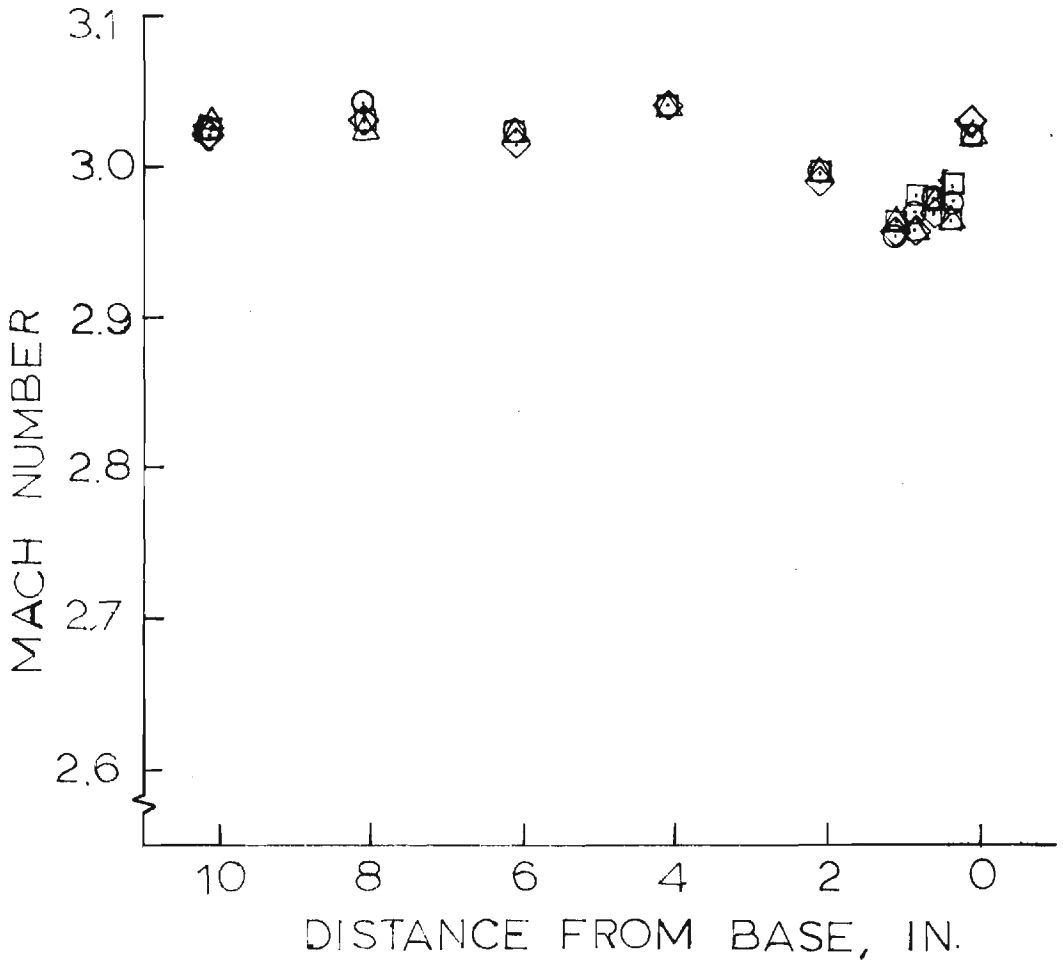

FIGURE 22. COMPARISONS OF RESULTS OF REPEAT TESTS

CHAPTER IV

BASE FLOW RESULTS

To date, all base flow data have been obtained using constant-diameter ducting downstream of the nozzle. Thus, no external disturbances, other than those due to the boundary layer on the centerbody, have been impressed on the near wake. For the tests, the ratio of the boundary layer momentum thickness on the centerbody at the base shoulder, as computed using the theory of Reference 22, to the base radius is 0.0135 for a flow Reynolds number based on the centerbody diameter of 3.8×10^6. The base flow results which have been obtained to date are presented in this Chapter. These results provide the basis for comparisons with existing results as well as with later test results with base flow disturbances.

Distributions of the static and pitot probe pressures along the wake centerline downstream of the base are presented in Figure 23. P_1 and P_{o_1} are the static and stagnation pressure in the free-stream flow immediately ahead of the base plane, P and M are the static pressure and Mach number along the wake centerline, and P_p is the measured pitot probe pressure. All the pressures have been normalized by the stagnation pressure measured during the tests in order to minimize the effects of stagnation pressure drifts.

The rear stagnation point, as determined by the intersection of the pitot and static probe pressures, is located approximately 3 base radii downstream of the base plane. In the reverse flow region nearer the base, the pitot probe measures a probe base pressure which is lower than the local static pressure. The maximum difference between these two pressures

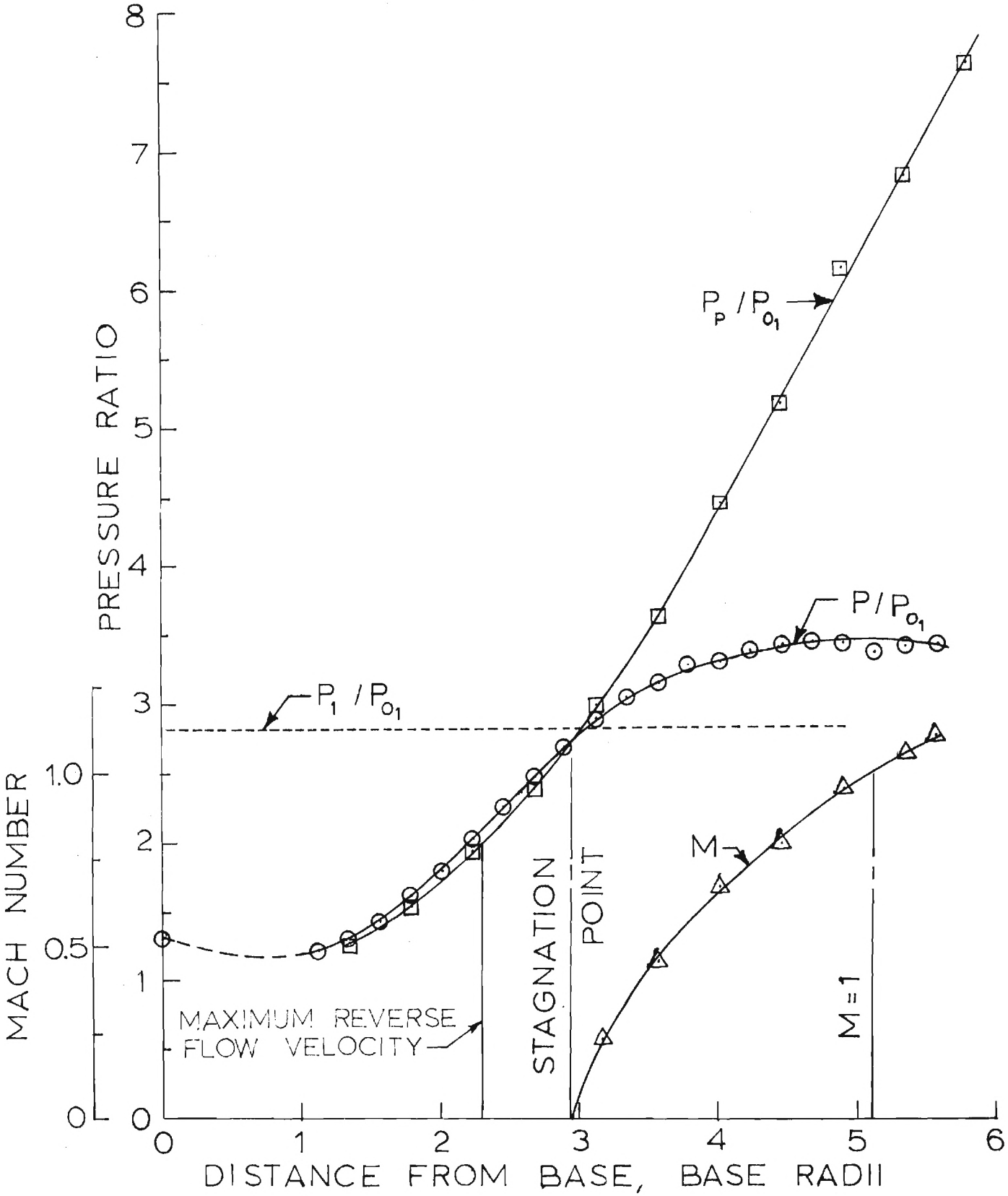

PRESSURE AND MACH NUMBER DISTRIBUTION ALONG WAKE CENTERLINE

FIGURE 23.

occurs at the point where the reverse flow velocity is a maximum. This occurs at approximately 2.3 base radii from the base plane.

The centerline Mach number distribution downstream of the rear stagnation point, as computed from the ratios of the pitot and static probe pressures, is also plotted in Figure 23. The centerline Mach number increases smoothly and becomes sonic at about 5 base radii downstream of the base plane. The wake choking or critical point lies ahead of this sonic condition. Disturbances downstream of this sonic point cannot propogate upstream into the near wake.

The static to stagnation pressure ratio upstream of the base expansion has also been included on Figure 23 for comparison with the centerline static pressure distribution in order to illustrate the overcompression that occurs near the wake neck for axisymmetric base flow. This overcompression is primarily responsible for the base pressures being higher with axisymmetric bodies than with two-dimensional bodies. For the present case, the peak pressure along the wake centerline is 23 percent higher than the upstream pressure.

Figure 24 is included to emphasize that the base pressure is independent of the probe position. P_b is the base static pressure (in this case, P_b is measured at the center of the base) and $\bar{P}_b$ is the numerical average of P_b for all measurements in which the probe was located in the subsonic near wake. The percent variation in the base pressure from the mean base pressure is plotted for each pitot probe location for which the probe is in the subsonic near wake. For the two points with the probe tip nearest the base the 0.125 inch probe shank also projects into the subsonic flow region. However, even the diameter of this shank is less than six percent of the base diameter. The small differences shown on Figure 24 are within the expected data accuracy as previously discussed.

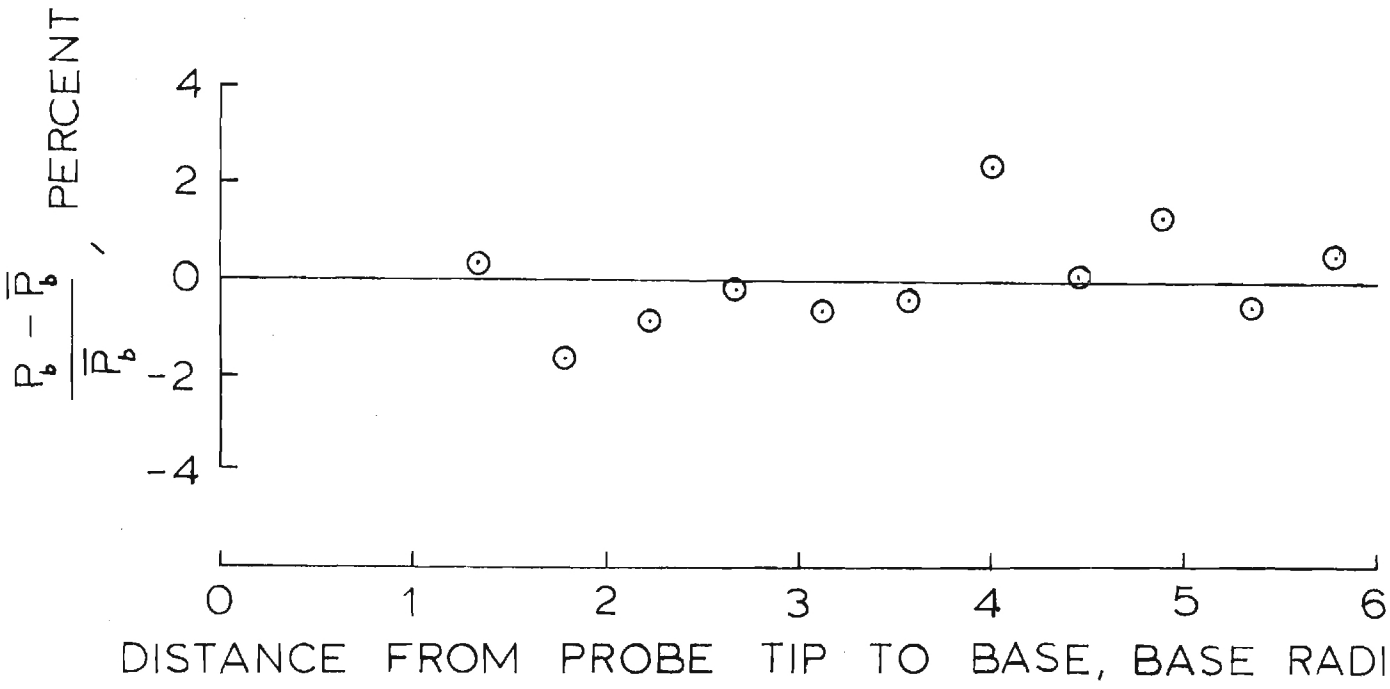

FIGURE 24. VARIATION IN BASE PRESSURE WITH PITOT PROBE POSITION

The Mach number distribution on the outer cylindrical ducting downstream of the base plane is shown in Figure 25. These Mach numbers were computed from the ratios of the surface static pressure and the upstream stagnation pressure. All three spaces (between the nozzle and constant diameter duct) were used for these tests in order to displace the static pressure taps. The Mach number remains constant until the expansion wave from the base shoulder intersects the ducting. This expansion starts at about five base radii downstream of the base plane. At approximately nine base radii downstream, the Mach number decreases sharply as a result of the wake recompression waves which have apparently coalesced into a shock wave. As shown in Figure 23, this recompression, which propagates from the wake boundary, starts at about one base radius downstream of the base. Subsequent reflections of these expansion and compression waves account for the pressure variations farther downstream in the diffuser as shown in Figure 17. However, reflections from the outer cylinder cannot intersect the wake upstream of the sonic point on the wake centerline.

Radial and peripheral base pressure distributions are presented in Figure 26. Again the pressures are normalized by the upstream stagnation pressure. Each data point on Figure 25 represents the mean value for five tests. The five pressures for each point are all within ± 1.5 percent of the mean value, and thus, within the expected limits of accuracy. As shown in the upper part of the figure, the base pressure increases with the radius. From the center to 0.67 base radii the pressure increases by 9 percent. Reid and Hastings[4] reported similar trends for axisymmetric bodies with cylindrical, conical, and parabolic afterbodies at Mach 2.0. However, their radial pressure gradients, which averaged out the peripheral asymmetries by using four radial surveys at 90° intervals, were somewhat

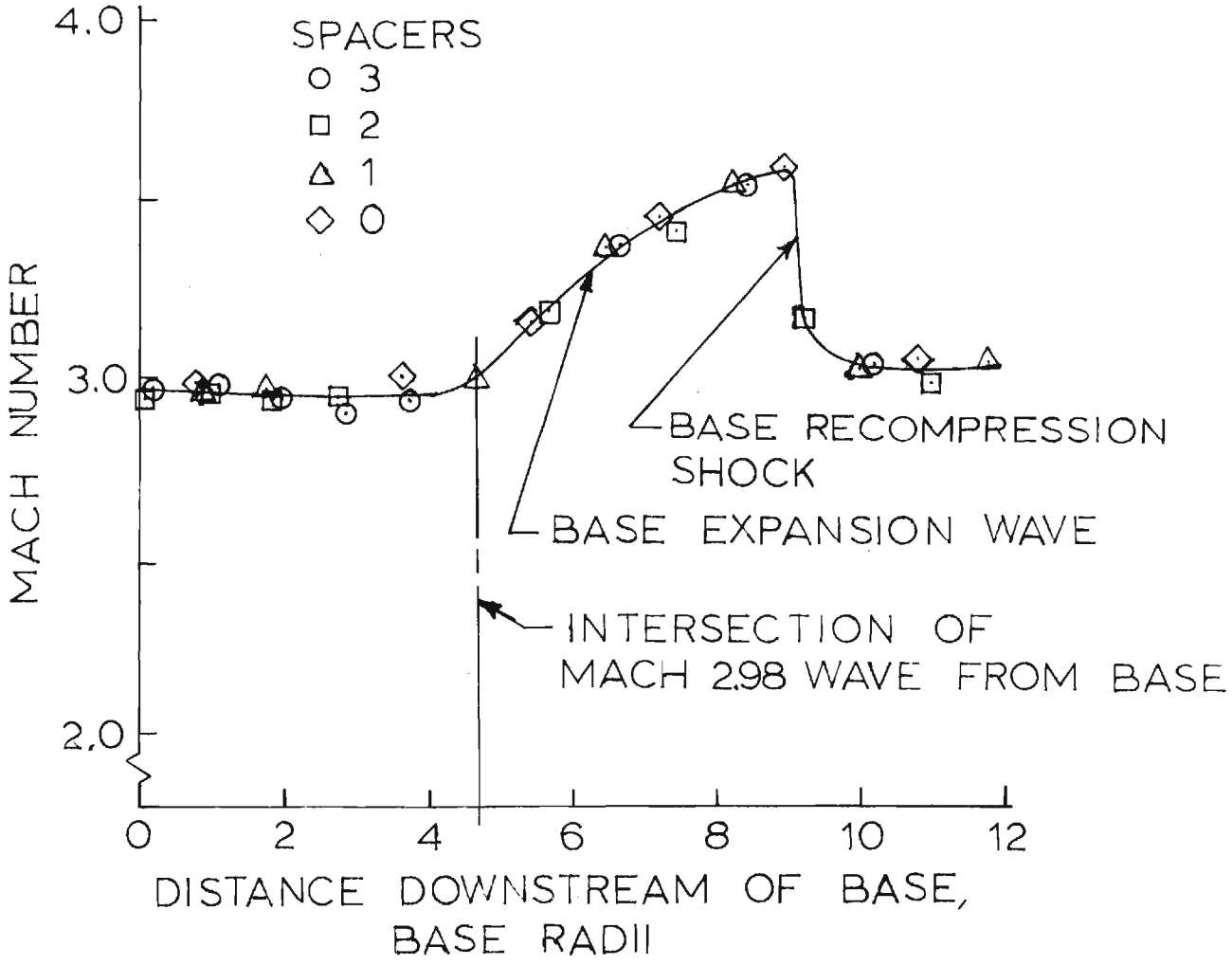

MACH NUMBER DISTRIBUTION ALONG CYLINDERICAL DUCT DOWNSTREAM OF BASE PLANE

FIGURE 25.

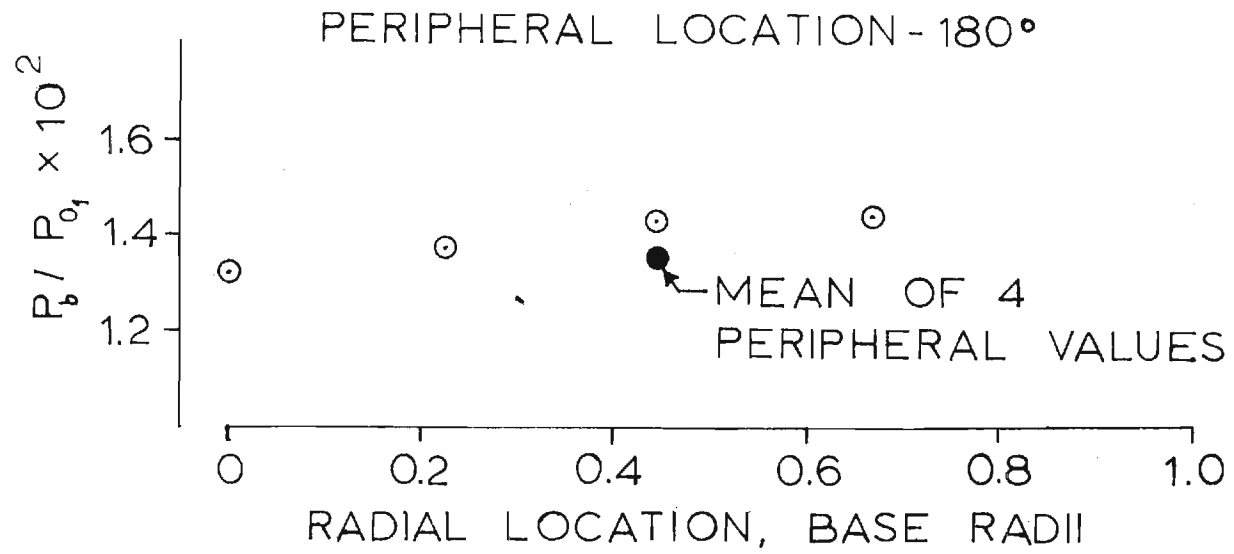

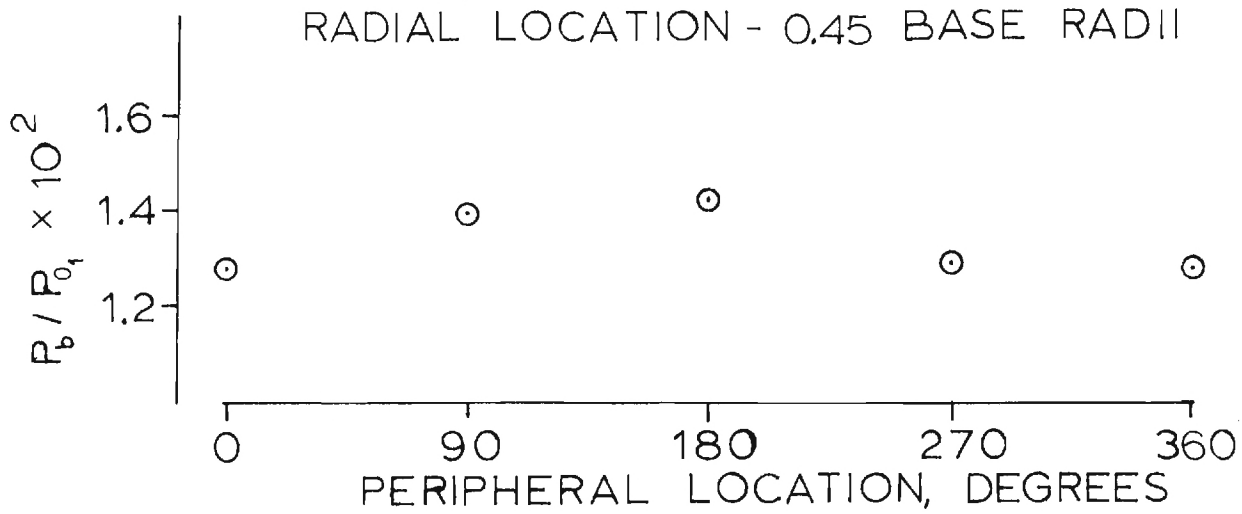

FIGURE 26. BASE PRESSURE DISTRIBUTIONS

smaller than those of Figure 26. Apparently a major portion of the radial pressure increase with the present tests may be attributed to a slight flow asymmetry as shown in the lower part of Figure 26. This figure shows the peripheral variation in the base pressures at 0.45 base radii from the center. To illustrate the effect of the peripheral variations, the mean value of these four peripheral pressures is included as the solid point on the upper figure. Apparently, the average radial pressure gradient is reduced by the peripheral variations.

The numerical average of the base pressure ratios on Figure 26 is $\bar{P}_b | P_{o_1} = 1.357 \times 10^{-2}$. This corresponds to a mean base pressure coefficient of $\bar{C}_{P_b} = -0.083$, based on the average Mach number upstream of the base expansion of $M_1 = 2.98$. This is in good agreement with the results of free-flight and wind-tunnel tests for axisymmetric projectiles of high ineness ratio as summarized by Love[25] and Murthy and Osborn[26].

The Reynolds number was varied over a small range in one test series by varying the upstream stagnation pressure over the range of about 70 to 150 psia. The base pressure results are summarized in the following table. The mean values of the base pressure and pressure coefficient for each test run are based on the numerical average of the seven base pressure measurements. The Reynolds number is based on the diameter of the base. The differences for this small Reynolds number range are within the accuracy of the data.

Run	Re x 10^{-6}	$\bar{P}_b/P_o \times 10^2$	$\bar{C}_{P_b}$
1	2.48	1.368	-0.0824
2	2.70	1.352	-0.0833
3	3.26	1.366	-0.0825
4	4.74	1.366	-0.0825
5	5.19	1.338	-0.0841

REFERENCES

1. Baker, W. T., Davis, T., and Matthews, S., 1951, The John Hopkins' University, Applied Physics Laboratory CM-673.

2. Scanland, T. S., and Hebrank, W. H., 1952, Ballistic Research Laboratories, Memorandum Report No. 596.

3. Townsend, L. H. and Reid, J., 1964, Supersonic Flow, Chemical Processes and Radiative Transfer, p. 135, Macmillan.

4. Davis, L. R., 1968, AIAA, J., 6, 843.

5. Fox, H., Zakkay, V., and Sinha, R., 1966, New York University, NYU-11-66-63.

6. Reeves, B. L. and Lees, L., 1965, AIAA J., 3, 2061.

7. Scott, C. J. and Eckert, E. R. G., 1966, AGARD Conference on Separated Flows, Pt. I, p. 429.

8. Gazley, C. G., Jr., 1956, The RAND Corporation, RM-1892.

9. Wilmarth, W. W., 1957, The RAND Corporation, RM 2078

10. Chu, B. T., 1955, NACA TN 3411.

11. Billig, F. S., 1967, The John Hopkins University, Applied Physics Laboratory, TG912.

12. Strahle, W. C., 1969, Twelfth Symposium (International) on Combustion, p. 1163, The Combustion Institute.

13. Serafini, J. S., Dorsch, R. G., and Fletcher, E. A., 1957, NACA RME 57E15.

14. Crocco, L. and Lees, L., 1952, J. Aerospace Sci, 19, 649.

15. Alber, S. E., 1967, Ph.D. Dissertation, California Institute of Technology.

16. Korst, H. H., Page, R. H., and Childs, M. E., 1955, University of Illinois, ME Technical Note 392-2.

17. Smithy, W. J. H., 1974, Ph.D. Dissertation, Naval Postgraduate School.

18. Horn, N. P., 1974, M.S. Thesis, Nalal Postgraduate School.

19. Smithy, W. J. H. and Fuhs, A. E., 1974, Workshop on Aerodynamics of Base Combustion, Perdue University.

20. Bradshaw, P., 1965, J. Fluid Mech., 22, part 4, 679.

21. Hall, I. M., 1962, Quart. Journ. Mech. and Applied Math, XV, Part 4, 487.

22. Cebeci, T., Smith, A. M. O., and Wang, L. C., 1969, McDonnel Douglas Report No. DAC-67131.

23. Neumann, E. P. and Lustwerk, F., 1949, J. Fluid Mech., 195.

24. Reid, J. and Hastings, R. C., 1959, A. R. C. 21, 707.

25. Love, Eugene S., 1957, NACA TN 3819, (1957).

26. Murthy, S. N. B. and Osborn, J. R., 1973, BRL, C. R. 113.

AFOSR Interim Scientific Report

AFOSR-TR- 77-0602

Experiments and Analysis Related to External Burning for Propulsion

Prepared for

Air Force Office of Scientific Research
Aerospace Sciences Directorate
Bolling Air Force Base, D. C.

by

Douglas H. Neale
James E. Hubbartt
Warren C. Strahle
Walter W. Wilson

School of Aerospace Engineering
Georgia Institute of Technology
Atlanta, Georgia 30332

Approved for public release; distribution unlimited
Grant No. AFOSR 75-2794 March 1977

Unclassified

SECURITY CLASSIFICATION OF THIS PAGE (When Data Entered)

REPORT DOCUMENTATION PAGE		READ INSTRUCTIONS BEFORE COMPLETING FORM
1. REPORT NUMBER AFOSR-TR- 77-0602	2. GOVT ACCESSION NO.	3. RECIPIENT'S CATALOG NUMBER
4. TITLE (and Subtitle) Experiments and Analysis Related to External Burning for Propulsion		5. TYPE OF REPORT & PERIOD COVERED INTERIM Feb. 1976 - Jan. 1977 6. PERFORMING ORG. REPORT NUMBER
7. AUTHOR(s) Douglas H. Neale James E. Hubbartt Warren C. Strahle Walter W. Wilson		8. CONTRACT OR GRANT NUMBER(s) AFOSR-75-2794
9. PERFORMING ORGANIZATION NAME AND ADDRESS Georgia Institute of Technology School of Aerospace Engineering Atlanta, Georgia 30332		10. PROGRAM ELEMENT, PROJECT, TASK AREA & WORK UNIT NUMBERS
11. CONTROLLING OFFICE NAME AND ADDRESS Air Force Office of Scientific Research/NA Bolling Air Force Base, D. C. 20332		12. REPORT DATE March 1977 13. NUMBER OF PAGES 34
14. MONITORING AGENCY NAME & ADDRESS(if different from Controlling Office)		15. SECURITY CLASS. (of this report) Unclassified 15a. DECLASSIFICATION/DOWNGRADING SCHEDULE

16. DISTRIBUTION STATEMENT (of this Report)

Approved for public release; distribution unlimited

17. DISTRIBUTION STATEMENT (of the abstract entered in Block 20, if different from Report)

18. SUPPLEMENTARY NOTES

19. KEY WORDS (Continue on reverse side if necessary and identify by block number)

External burning propulsion
Base flow
Supersonic flow
Wind tunnel

20. ABSTRACT (Continue on reverse side if necessary and identify by block number)

An experimental study of base flow for a 2.25 inch diameter projectile at Mach 3 with and without simulated external burning disturbances is reported. Base pressure and wake structure results from systematic variations in axisymmetric external compression show that substantial base thrust can be produced and that the pressure and length scales of the external compression are imposed on the near wake. Measurements with comparable axisymmetric and asymmetric compression contours show that peripherial gradients reduce the base pressure rise. Furthermore, relatively large changes in the near wake length scales and a slight reduction in

DD FORM 1 JAN 73 1473 EDITION OF 1 NOV 55 IS OBSOLETE

Unclassified

SECURITY CLASSIFICATION OF THIS PAGE (When Data Entered)

the base pressure occur when the solid-blockage effects of discrete radial fuel jets are modeled with pegs mounted near the base of the test projectile.

AFOSR Interim Scientific Report

AFOSR-TR- 77-0602

Experiments and Analysis Related to External Burning for Propulsion

Prepared for

Air Force Office of Scientific Research
Aerospace Sciences Directorate
Bolling Air Force Base, D. C.

by

Douglas H. Neale
James E. Hubbartt
Warren C. Strahle
Walter W. Wilson

School of Aerospace Engineering
Georgia Institute of Technology
Atlanta, Georgia 30332

Approved for public release; distribution unlimited
Grant No. AFOSR 75-2794 March 1977

Abstract

An experimental study of base flows for a 2.25 inch diameter projectile at Mach 3 with and without simulated external burning disturbances is reported. Base pressure and wake structure results from systematic variations in axisymmetric external compression show that substantial base thrust can be produced and that the pressure and length scales of the external compression are imposed on the near wake. Measurements with comparable axisymmetric and asymmetric compression contours show that peripherial gradients reduce the base pressure rise. Furthermore, relatively large changes in the near wake length scales and a slight reduction in the base pressure occur when the solid-blockage effects of discrete radial fuel jets are modeled with pegs mounted near the base of the test projectile.

TABLE OF CONTENTS

I. INTRODUCTION

There are a great number of potential air-to-air, air-to-ground, and ground-to-air weaponry missions that require either a sustain or mild acceleration phase of the missile trajectory or which could benefit from substantial drag reduction during a portion of the trajectory. Furthermore, many of these missions require operation sufficiently low in the atmosphere that airbreathing propulsion, if it is competitive with the rocket, is attractive. Recent concepts of external burning for propulsion appear attractive for these missions because it is possible to make these systems extremely simple, essentially eliminating the requirement for an inlet, combustion chamber and nozzle with an acceptable sacrifice of I_{sp} compared to usual airbreathing systems. The feasibility of this concept, in which the subsonic near-wake transmits high downstream pressure to the base, has been experimentally established. An accurate theory to fully evaluate the potential of external burning has not yet, however, been proven. A major deficiency at the present time is the lack of detailed experimental data reflecting systematic alterations in the external flow field against which the theory can be tested. The present paper describes the results of the first phase of an experimental test program designed to provide proof that an analytical model currently under development will predict the effects on base pressure of many processes which take place during external burning.

II. TEST FACILITY

Flow System

The present base flow test facility was designed to simulate the base flow of a projectile at Mach 3 with a fineness ratio of about 6 and a Reynolds number, based on model diameter, in excess of 3.0×10^6. In addition, the facility design includes provisions for generating and exposing the base flow to disturbances simulating those expected with external burning for propulsion.

Figure 1 schematically shows the test facility flow system. The tunnel is a blow-down type with sufficient storage capacity at 3000 psig for up to 6 minutes of run time per charge depending on the desired test section stagnation pressure. Source air is reduced in pressure to about 350 psig by three parallel, remotely operated regulators with overlapping control ranges. Tunnel flow is accurately set with a hydraulically actuated, remote-controlled globe valve downstream of the main regulators. The flow is then passed through a large diameter plenum equipped with internal baffles and a perforated discharge plate to remove the gross non-uniformities introduced by throttling and turning. Final smoothing and straightening of the flow is achieved with a bell reducer and a combination of three screens and two honeycomb segments.

After the flow has been conditioned, it passes through a model support section, accelerates to Mach 3 in the nozzle and enters the transparent external compression section. This portion of the flow path is shown in more detail in Figure 2. The test section exhausts into a constant area shock diffuser for flow deceleration. An initial segment of the diffuser doubles as a support and guide through which pitot and static pressure probes can be

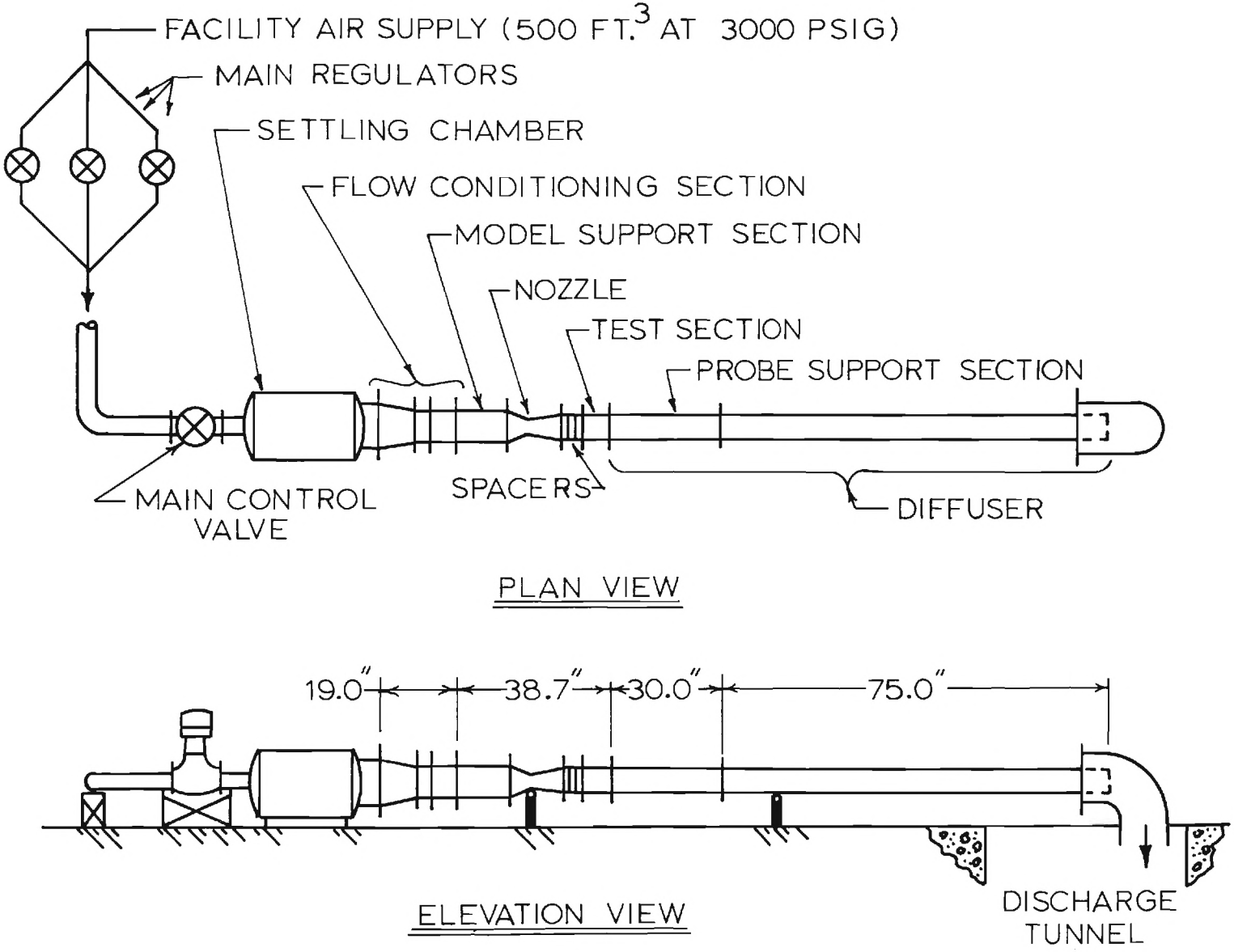

Figure 1. Base Flow Facility Schematic.

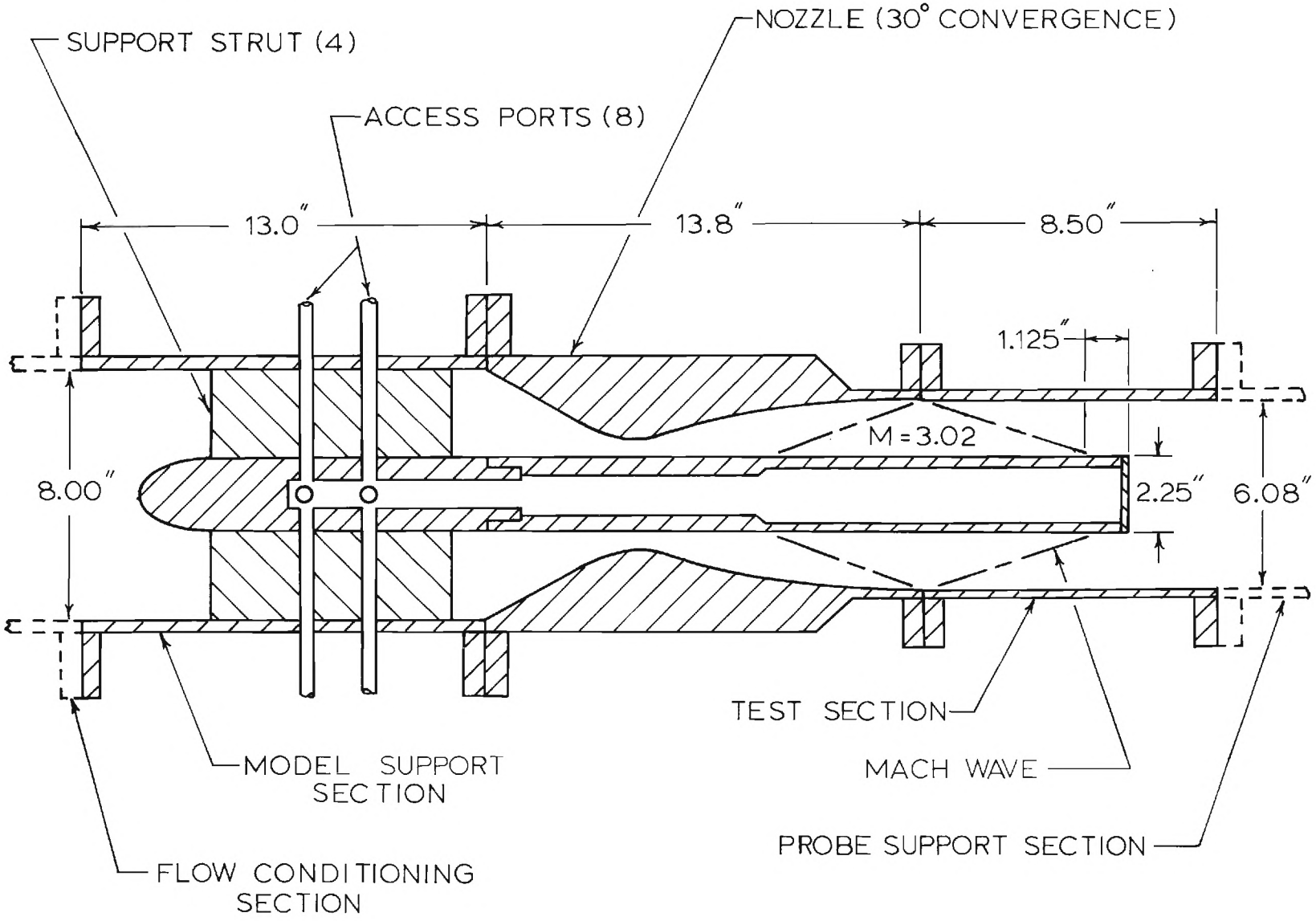

Figure 2. Base Flow Facility Test Section Detail.

introduced to the base flow region. After deceleration, the flow is dumped to atmosphere. Photographs of the base flow test facility are presented in Figure 3.

Instrumentation and Data Acquisition System

The current experimental configuration is instrumented with 56 surface static pressure taps: 7 on the model base, 16 on the model side walls, and 33 on the outer ducting from the nozzle exit to the diffuser discharge. Two thermocouples are bonded to the inner wall of the center-body model just upstream of the base and two additional thermocouples are imbedded in the nozzle wall near the exit plane. Static pressure and temperature data from the model are obtained by threading the respective leads forward through the centerbody bore and out access ports in the model mounting struts.

Total temperature and total pressure of the flow are measured with a thermocouple probe and a pitot probe located in the subsonic flow field just upstream of the model. The wake flow field is surveyed in two steps using separate telescoping pitot and static pressure probes. The wake region is surveyed with the probe traverse unit shown in the photographs of Figure 3. Two stepping motors provide accurate control of axial probe location in a vertical plane passing through the model center.

With the exception of upstream total pressure, measurement of pressures in base flow tests is done with two, 1000 mm Hg maximum pressure differential, variable capacitance type transducers. Each transducer is connected to a 48 port Scanivalve unit for rapid sampling of the pressure array. Upstream total pressure is measured with a strain gage transducer.

The data acquisition system is designed for manual control, used typically during test set-up, or for computer programmed operation employed during actual tests. A Hewlett-Packard 2100A computer with tape input and

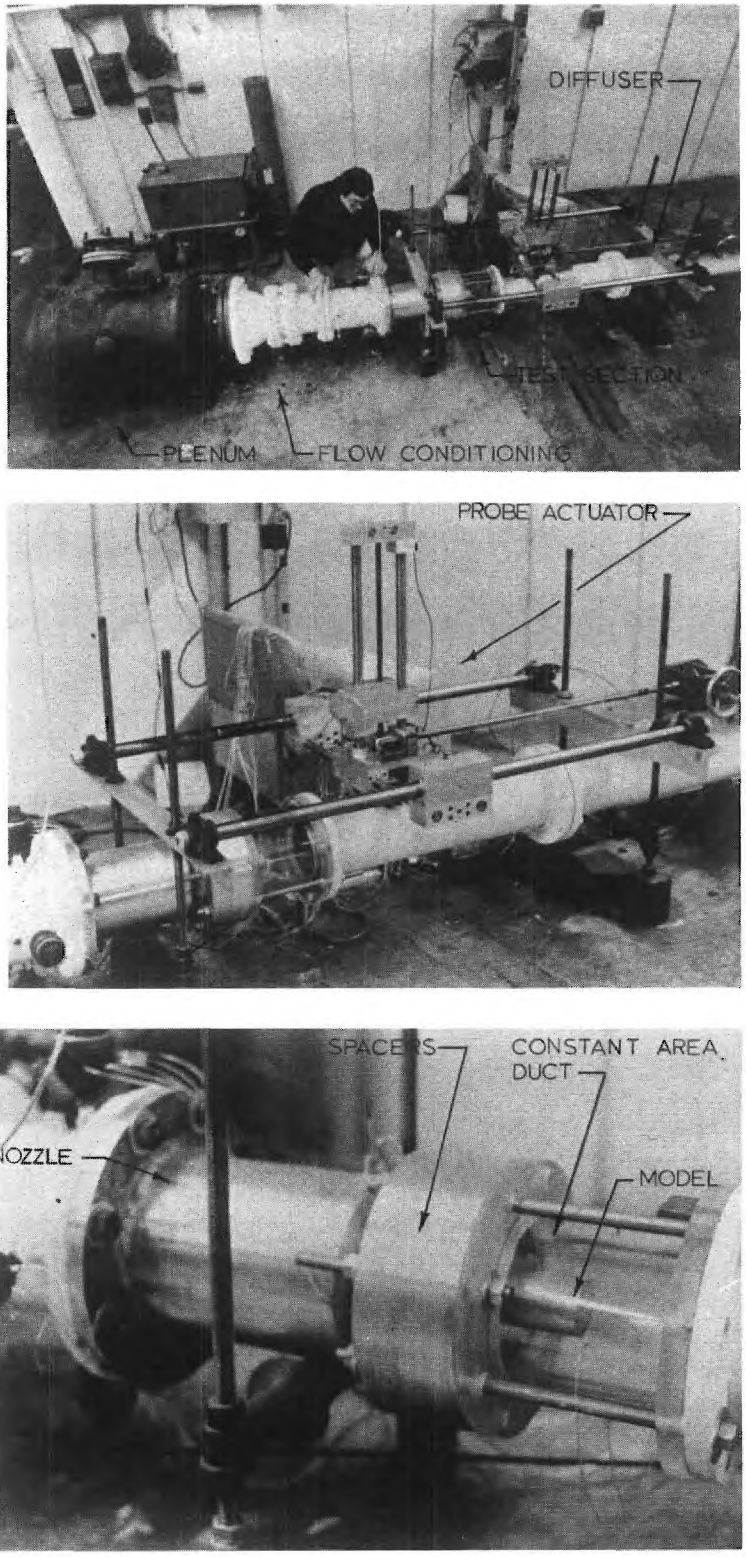

Figure 3. Base Flow Facility.

16K core storage capacity provides for system control, data acquisition, computation of flow parameters and final data output via teletype. Transducer voltage signals are received through a 30 channel scanner with a Hewlett-Packard 2401C low level, integrating digital voltmeter. The traverse stepper motors and scanivalve drivers are computer actuated through a multi-terminal relay card. The complete data system is shown schematically in Figure 4.

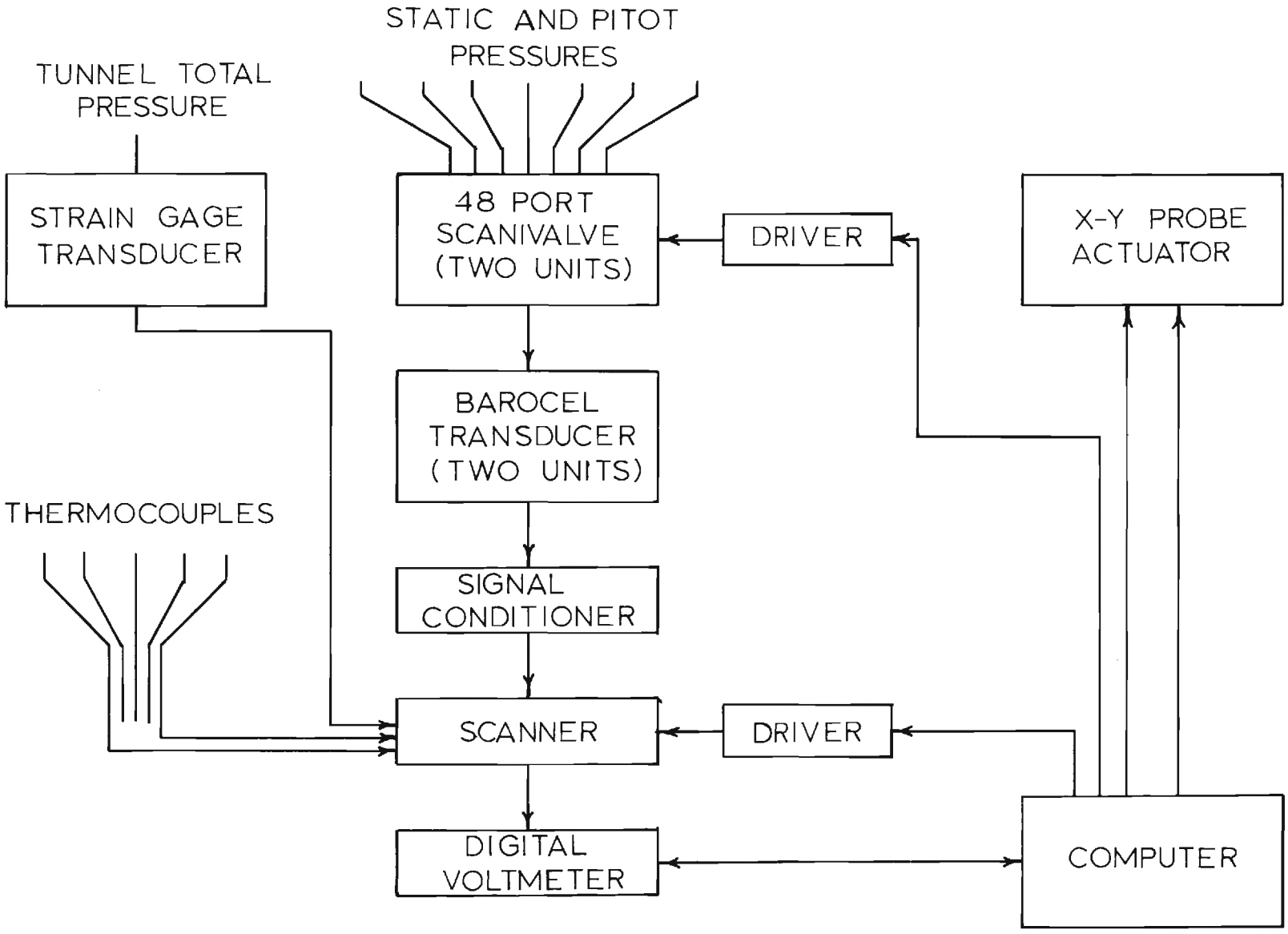

Figure 4. Base Flow Data Acquisition Schematic.

III. EXPERIMENTAL RESULTS

Initial Flow and Measurement Accuracy Evaluation

Before detailed base flow measurements were attempted, tests for flow field uniformity, data accuracy and repeatability and facility operation limits were performed. Calibration of the strain gage and variable capacitance transducers with a standard laboratory dead weight tester showed both devices to be highly linear. All transducers exhibited very slight shifts in calibration with time, on the order of months, and with repeated pressure cycling. Accordingly each transducer was checked periodically with the dead weight tester and current editions of the resulting calibration curves were inserted in the computer data retrieval programs. This procedure insured that absolute pressures were measured within $\pm$ 1% including wake and free stream static pressures that were typically less than 3 psia.

After pressure measurement accuracy was established, the tunnel flow field was evaluated using a constant-area test section duct matched to the nozzle exit diameter. A pitot survey of the flow conditioning section exit plane showed that variations in stagnation pressure among nozzle inlet streamlines was negligible in comparison with test section dynamic head. Flow quality was further verified with test section measurements yielding axial and peripheral Mach number distributions on the model and outer ducting surfaces. Mach numbers computed from test section measurements were found to be in close agreement with design values. As a typical example, the mean Mach number determined from four peripheral measurements on the model surface near the base plane was identical to the value of 2.98 conducted assuming one-dimensional flow corrected for theoretical boundary layer growth. Mean Mach number at this same plane computed from measurements

on the outer duct wall was 2.99. The mean values just described were computed from the results of six separate runs conducted on three days. The maximum deviation of any data point from the mean for this series of tests was found to be less than 1%. These base plane results coupled with similar results at other test section locations confirmed the ability of the apparatus to produce repeatable data.

Further diagnostic testing of the facility revealed minimum upstream stagnation pressures for proper diffuser performance in re-accelerating the subsonic wake to free stream velocities before shocking and discharging to atmosphere. In addition, surface temperature measurements showed that the model surface behaved virtually as an adiabatic wall so that heat transfer to the flow can be considered small. The effects of pressure lag due to transducer and line volumes were evaluated for the system and eliminated by establishing minimum scanning rates. Introduction of the static and pitot probes into the subsonic wake region was observed to have no discernable effect on base pressure. Finally, upstream stagnation pressure was varied over a range of reasonable operating conditions to check the Reynolds number effect on base pressure. For Reynolds numbers based on model diameter and free stream Mach number from 2.48×10^6 to 5.19×10^6 the differences in ratio of base pressure to upstream stagnation pressure were less than the stated accuracy of the data.

Zero External Disturbance Studies

An initial series of detailed wake measurements were performed using a constant-diameter test section to simulate base flow with no external disturbances other than those due to centerbody and outer duct boundary layers. The theoretical boundary layer momentum thickness on the model at the base plane was 1.2% of the model radius for a nominal test Reynolds number, based on centerbody diameter, of 2.7×10^6. Computation of the outer duct boundary layer at the nozzle exit showed similarly small characteristic dimensions.

Figures 5 and 6 present typical test measurements conducted in the near wake region. Figure 5 shows pitot and static pressure distributions along the model centerline downstream of the base. The corresponding centerline Mach number aft of the rear stagnation point is also displayed. P_1 and Po_1 denote the static and stagnation pressures in the free stream immediately ahead of the base plane. P and P_p are the probe-measured static and pitot pressures and M is the calculated Mach number. All pressures have been normalized by Po_1 measured almost simultaneously to minimize the effects of stagnation pressure drifts.

The rear stagnation point, determined from the intersection of the pitot and static pressure curves, is also specified in Figure 5. In addition, Figure 5 shows the smooth centerline flow acceleration from stagnation through sonic velocity. Finally, the ratio of static to stagnation pressure upstream of the base, P_1/Po_1, is included for comparison with the centerline static pressure distribution to illustrate the over-compression that occurs near the wake neck for axisymmetric base flow. This over-compression is primarily responsible for the higher base pressures demonstrated by axisymmetric bodies when compared with equivalent two-dimensional bodies.

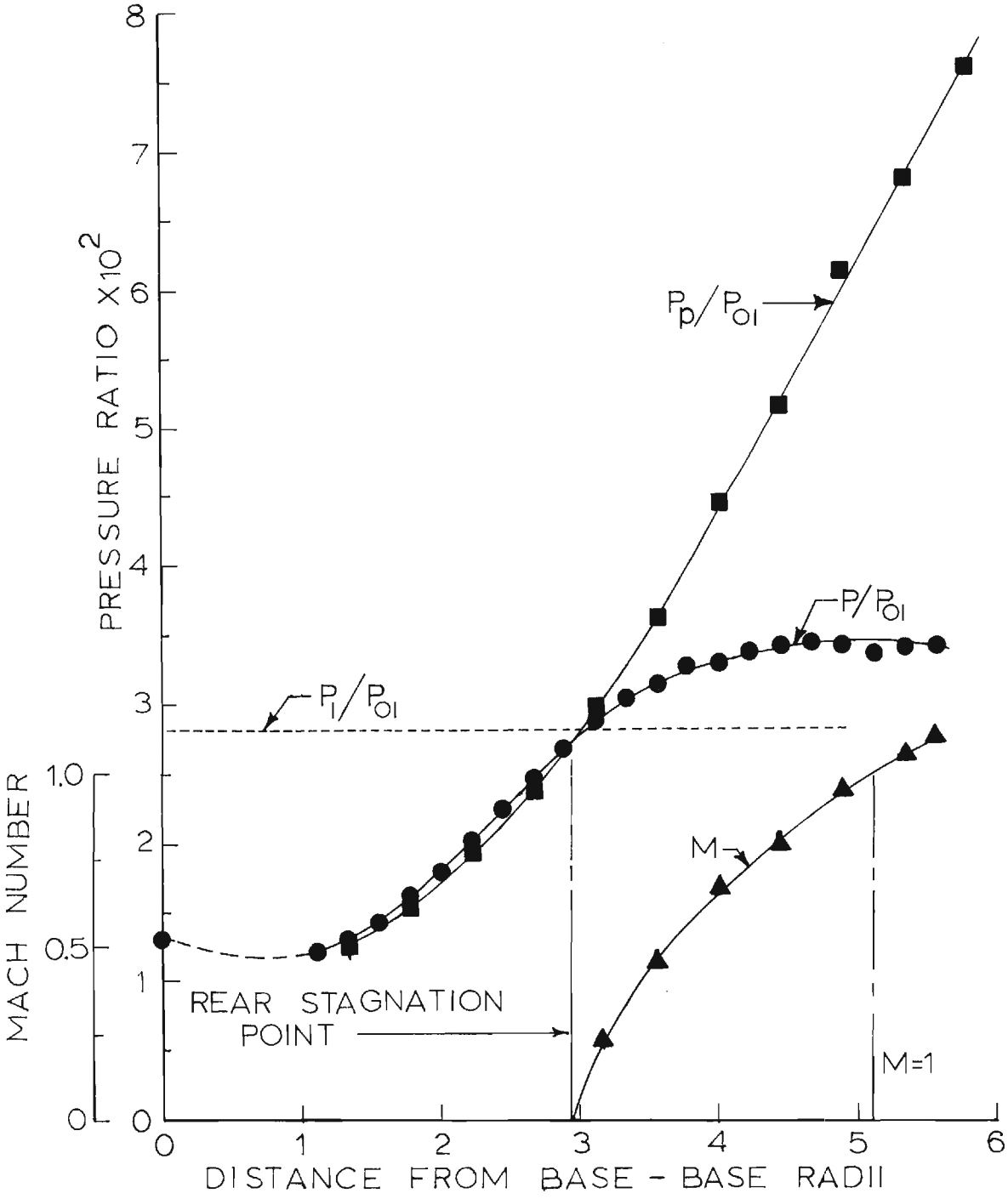

Figure 5. Near Wake Centerline Pressure and Mach Number Distributions - Constant Area Test Section (Zero External Compression).

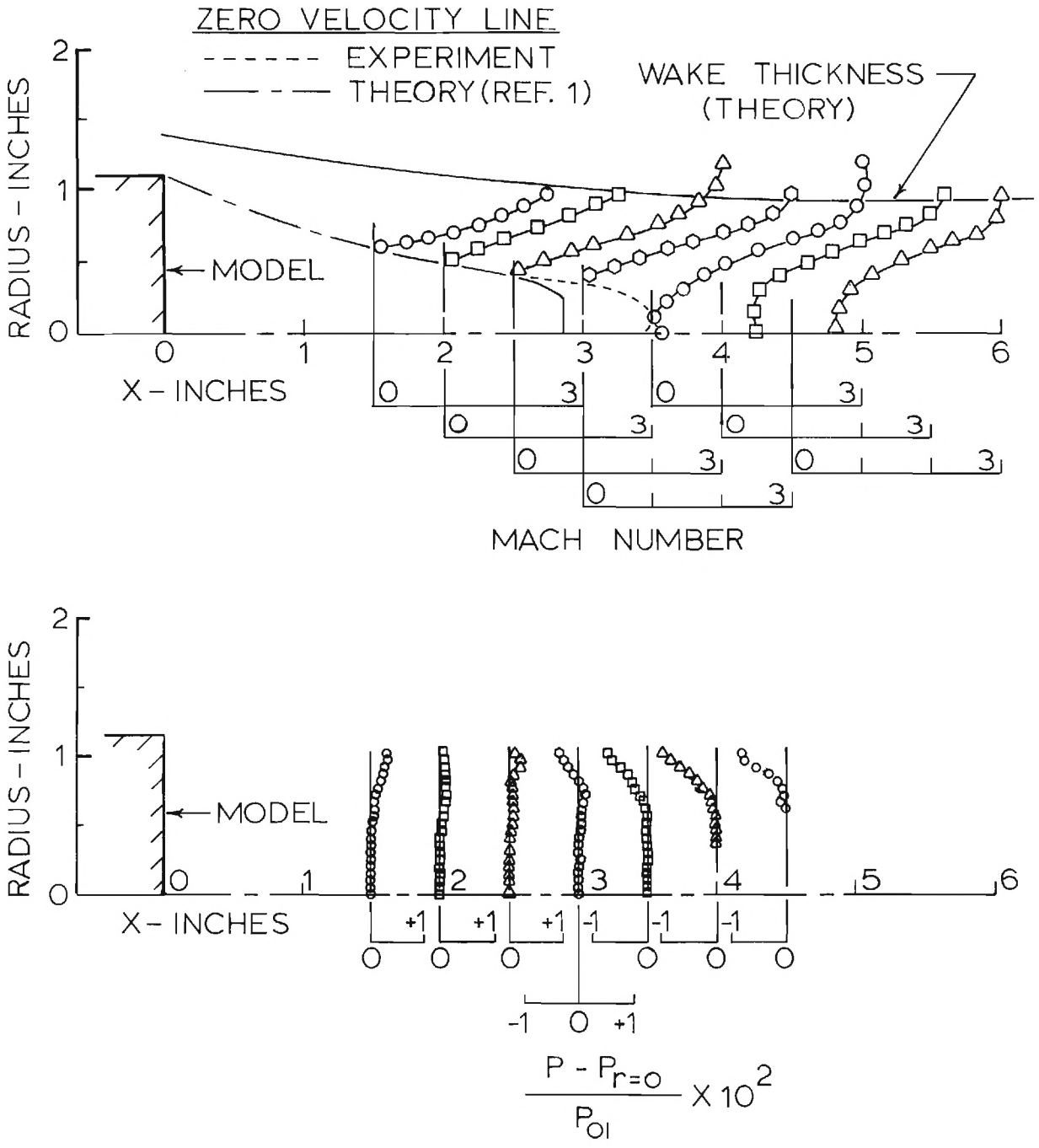

Figure 6. Near Wake Radial Mach Number and Static Pressure Distributions - Constant Area Test Section (Zero External Compression).

Figure 6. presents typical results from wake pitot and static pressure surveys in a vertical plane through the model centerline. Flow development in the wake outside of the recirculation region is shown by means of Mach number profiles in the upper portion of the figure. The experimental data is compared with a prediction of wake thickness and zero-velocity line position from a theory developed by Mehta and Strahle (Ref. 1). The theory is an integral method for solution of the fully turbulent, adiabatic near-wake field behind axisymmetric bluff base bodies in supersonic flow. Figure 6 shows excellent agreement between this theory and the experimentally determined wake thickness. The zero velocity line also matches well with experiment upstream of the theoretically predicted rear stagnation point.

The radial surveys reveal a slight assymmetry in the base flow which may suggest a minor redefinition of the rear stagnation point location. It was found that, in the vertical plane, the true wake centerline is displaced upwards such that a zero velocity point persists in the Mach number profile back to approximately 3.5 inches from the base. This represents a 0.2 inch axial shift in rear stagnation point from that determined by model centerline measurements. The true wake centerline offset at 3.5 inches from the base is 0.075 inches.

Radial static pressure surveys in the base flow region are shown in the lower portion of Figure 6. The variation from centerline pressure with increasing radius is consistent with streamline curvature as the flow initially converges toward and then turns back parallel with the axis. It should be noted that radial static pressure variations in the inner, lower velocity region of the shear flow are small when compared with the axial gradients.

Figures 7 and 8 compare the theory of Mehta and Strahle with the present experimental centerline results for static pressures in the near wake and for flow acceleration aft of the rear stagnation point (RSP). The slightly higher experimental base pressure in Figure 7 can be attributed to a small compression field

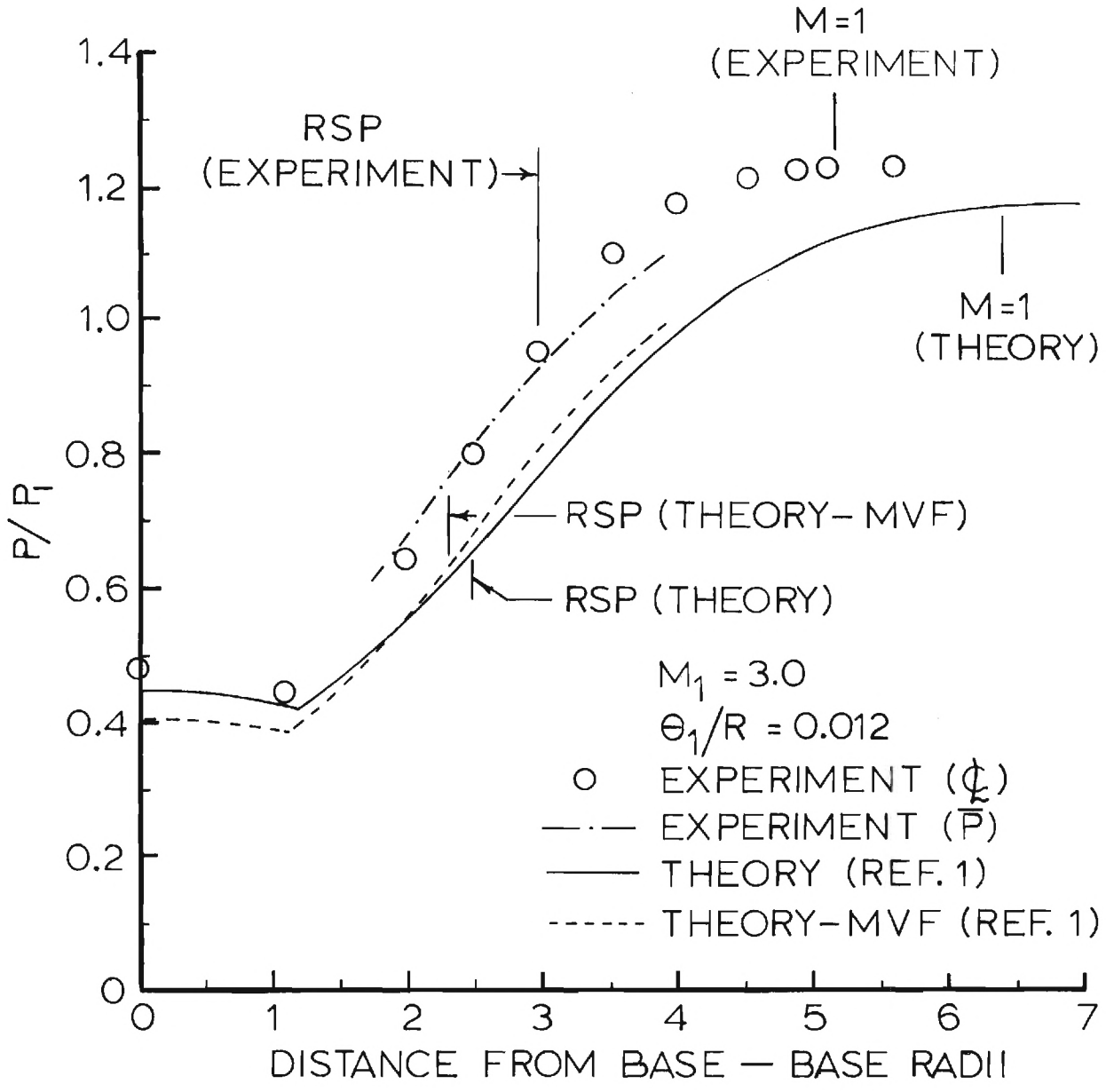

Figure 7. Comparison of Experimental Near Wake Centerline Static Pressure Distribution with Theoretical Prediction - Constant Area Test Section (Zero External Compression).

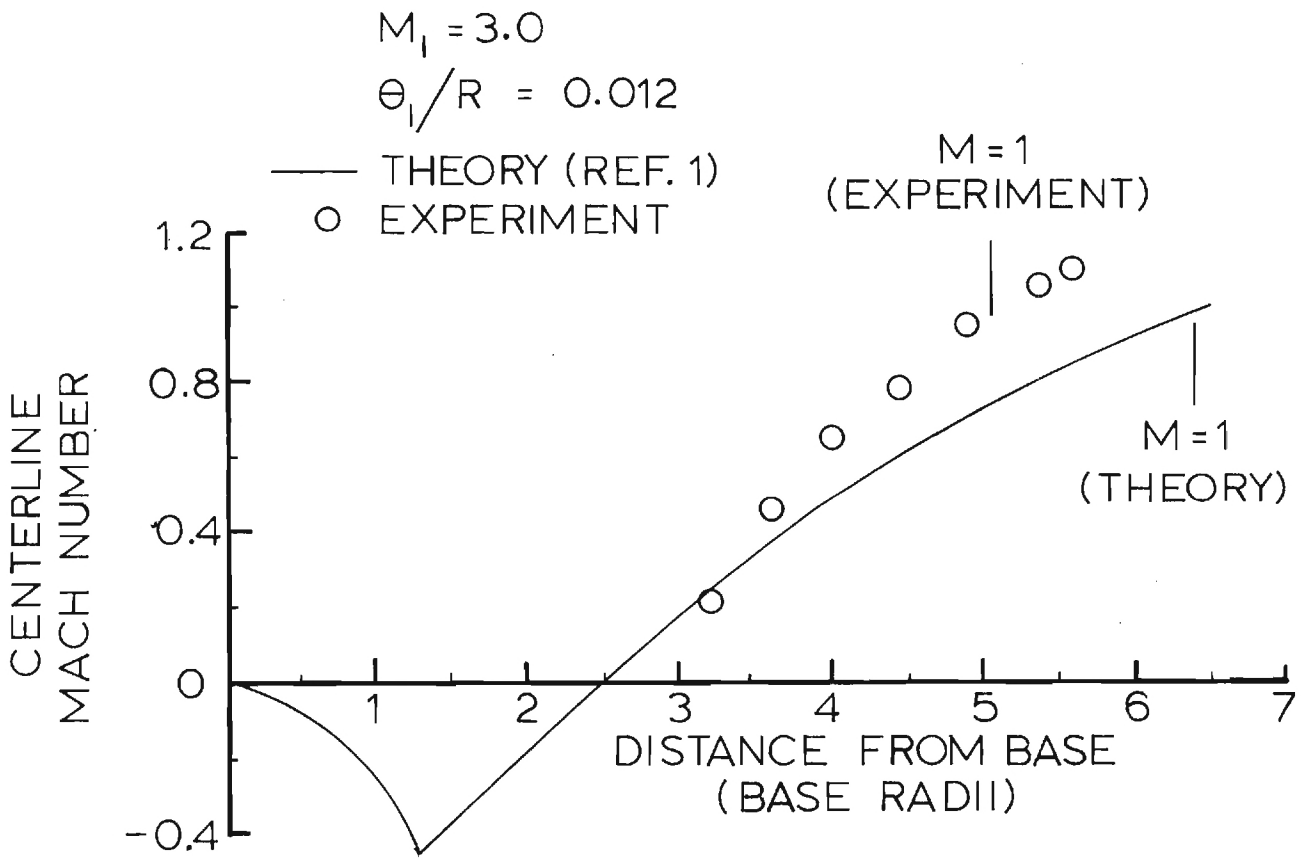

Figure 8. Comparison of Experimental Near Wake Centerline Mach Number Distribution with Theoretical Prediction - Constant Area Test Section (Zero External Compression).

initiated by the presence of a boundary layer on the outer duct. Both the experimental centerline static pressure data and a curve of the area-weighted mean static pressure, $\bar{P}$, have been included on the figure to show the small but significant effect of radial pressure gradients in the shear layer. The centerline static pressure distribution is predicted using two forms of the theory of Mehta and Strahle. The basic theory employs a standard compressible eddy viscosity model in the shear regions. Mehta and Strahle found, however, that a modified viscosity form (MVF) of the theory using an empirical initial free stream Mach number correction to the local eddy viscosity model yielded better correlation of experimental and theoretical results over a wider range of Mach numbers. In general, the analytical and experimental wake development shown in Figures 7 and 8 agree well.

Figure 9 compares similar solutions for incompressible axisymmetric wakes (Ref. 2) with two experimental velocity profiles. The experimental data radial coordinates are transformed to the incompressible form using a Stewartson-type transformation. These similar profiles and a set of nearly indistinguishable cosine profiles were both employed in the integral theory of Mehta and Strahle using a Stewartson-type transformation to account for compressibility. The experimental velocity profiles are in reasonably good agreement with the analytical representations. It is apparent that excellent agreement over the major portion of the profile would be obtained if the centerlines of the experimental data were shifted slightly so as to match experimental and analytical velocity gradients at the half-velocity point.

External Disturbance Studies

After completion of the base flow studies in an undisturbed free stream, the test facility was modified for simulation of external compression with burning. Replacement of the original constant area test section with a series of converging ducts provided free stream compression fields focused on the centerbody near

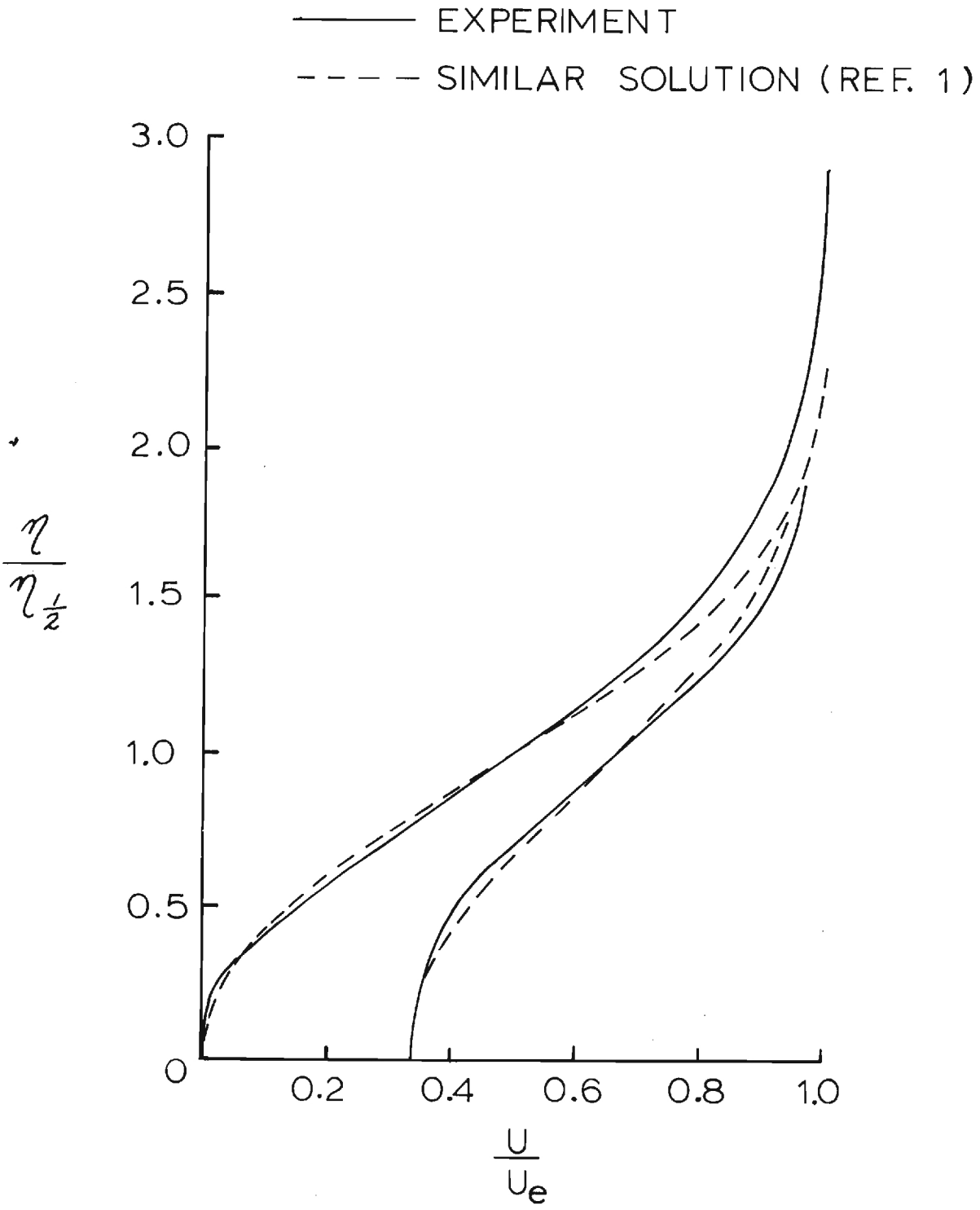

Figure 9. Comparison of Experimental and Similar Solution Velocity Profiles - Constant Area Test Section (Zero External Compression).

wake. The initial contour (Compression Section I) was designed to impose a pressure field on the wake that would approximately eliminate base drag. An axisymmetric heat released model was then constructed to duplicate the initial contour. Two subsequent alternate test section contours were then designed to simulate an identical total heat addition at varying release rates. A fourth test section was constructed using six symmetrically located half bodies of revolution attached to the inner wall of a cylindrical duct. The axial area distribution of this section was identical to that of the second axisymmetric compression section and was included to study the effects of equivalent heat addition in discrete plumes.

A series of five spacer rings were constructed to allow axial translation of the external disturbance ducts relative to the model. The inside diameter of the rings match the exit diameter of the nozzle and are inserted between the nozzle exhaust and the compression section inlet. Use of the spacers provides for translation of the external disturbance in increments of one base radius.

Finally, an alternate base plate was fabricated for modeling the solid body blockage of discrete radial fuel jets exhausting near the base. The jets were simulated with six solid cylindrical pegs fixed on the model perimeter to allow study of blockage effects without the complication of actual mass injection.

Axisymmetric Disturbance Test Results.

The design and performance of each axisymmetric compression duct are shown respectively in Figures 10 and 11. Figure 10 tabulates the axial distribution of design radius, Mach number and static pressure. Boundary layer growth has been accounted for in the Mach number and static pressure values. The design pressures are plotted in Figure 11 and are shown to be in good agreement with typical static pressure measurements on the duct surface.

The test configuration for external compression is shown in Figure 12 along with resulting base pressure measurements. The initial, mild contour (Compression section I) performed as designed by approximately eliminating base drag. A weak optimum axial location is shown for this case when the compression has been dis-

	COMPRESSION SECTION								
	I			II			III		
X IN.	R IN.	M	$P/P_{O_1} \times 10^2$	R IN.	M	$P/P_{O_1} \times 10^2$	R IN.	M	$P/P_{O_1} \times 10^2$
0	2.989	2.980	2.805	2.989	2.980	2.805	2.989	2.980	2.805
0.5	2.986	2.944	2.962	2.985	2.923	3.057	2.977	2.795	3.713
1	2.977	2.909	3.122	2.968	2.834	3.499	2.925	2.599	5.019
1.5	2.963	2.873	3.297	2.936	2.763	3.869	2.848	2.503	5.826
2	2.942	2.837	3.483	2.893	2.713	4.210	2.765	2.498	5.871
2.5	2.916	2.799	3.690	2.845	2.680	4.429	2.692	2.581	5.161
3	2.886	2.793	3.724	2.793	2.663	4.547	2.646	2.725	4.133
3.5	2.858	2.787	3.759	2.742	2.662	4.554	2.627	2.836	3.488
4	2.827	2.779	3.805	2.695	2.679	4.436	2.624	2.892	3.204
4.5	2.798	2.773	3.840	2.654	2.713	4.210	2.629	2.925	3.048
5	2.769	2.766	3.881	2.624	2.760	3.917	2.639	2.945	2.957
5.5	2.739	2.758	3.929	2.605	2.820	3.574			
6	2.710	2.749	3.984	2.600	2.883	3.248	2.666	2.965	2.869
6.5	2.681	2.749	3.984						
7	2.656	2.768	3.870	2.614	2.943	2.966	2.698	2.974	2.831
7.5	2.636	2.798	3.696						
8	2.625	2.829	3.525	2.644	2.965	2.869	2.733	2.977	2.818
8.5	2.621	2.867	3.328	2.662	2.969	2.852	2.751	2.977	2.818

Figure 10. Tabulation of Radius, Mach Number and Static Pressure Distributions for External Compression Test Section Ducts.

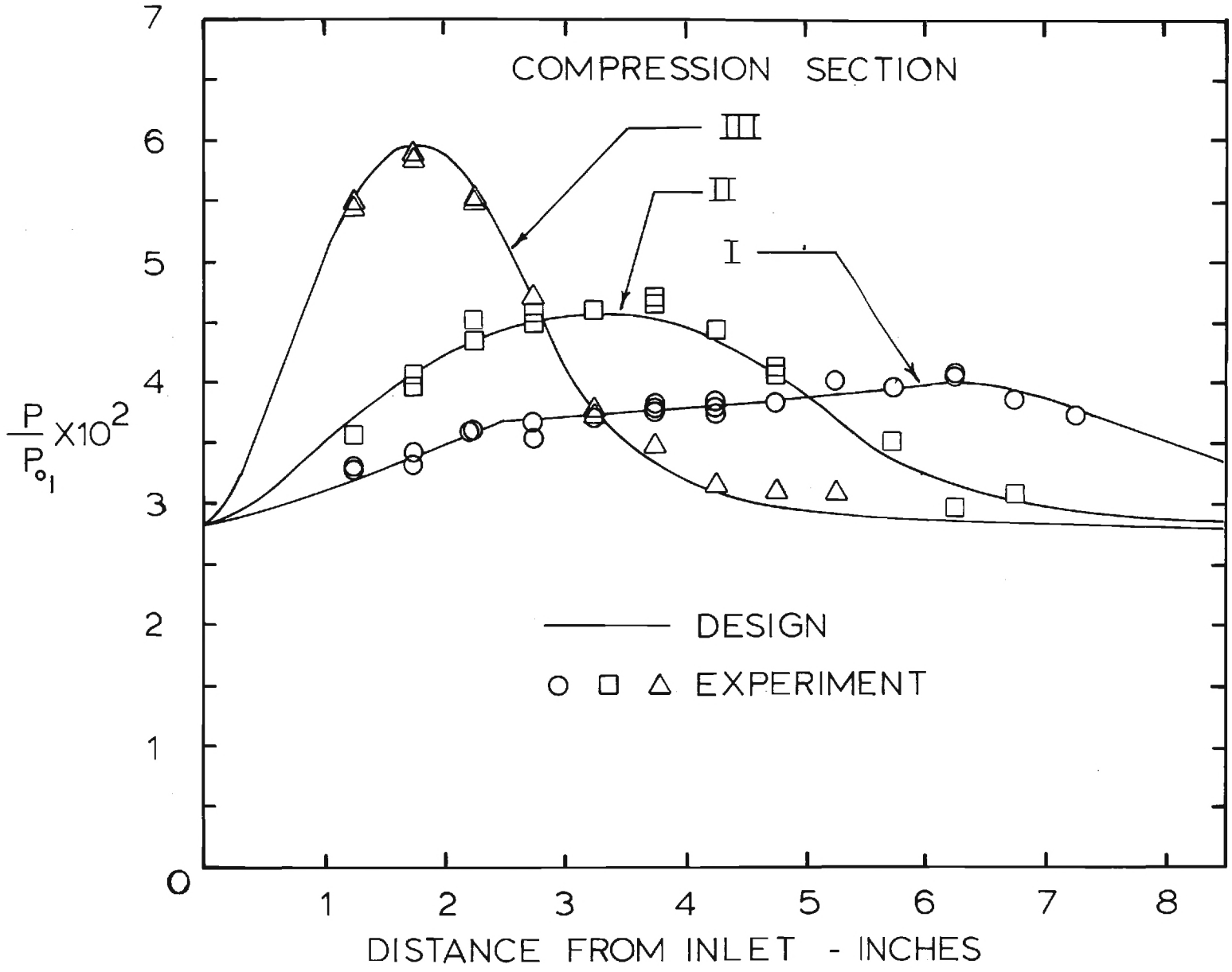

Figure 11. Comparison of External Compression Test Section Design and Performance.

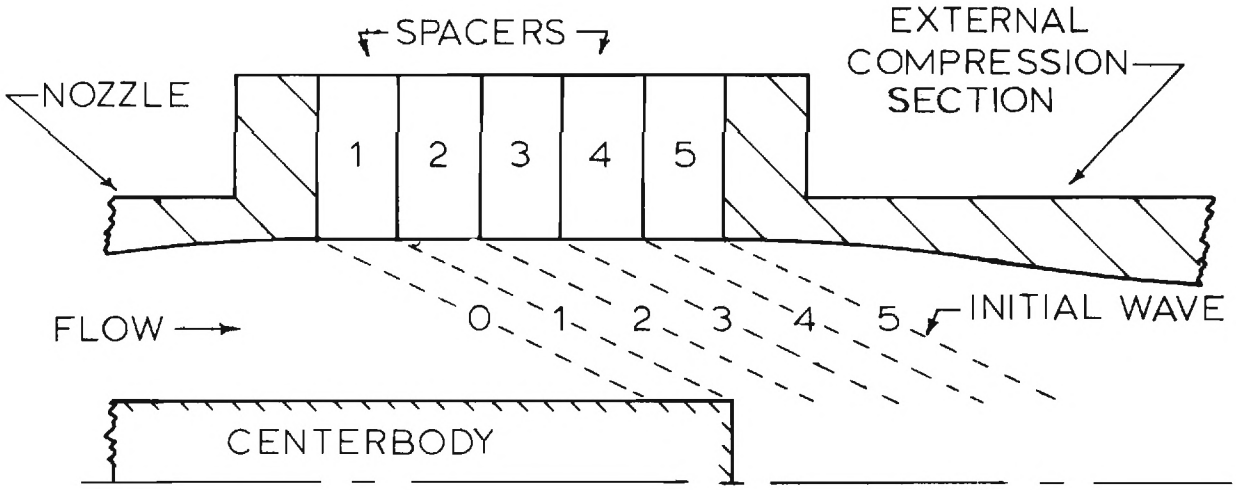

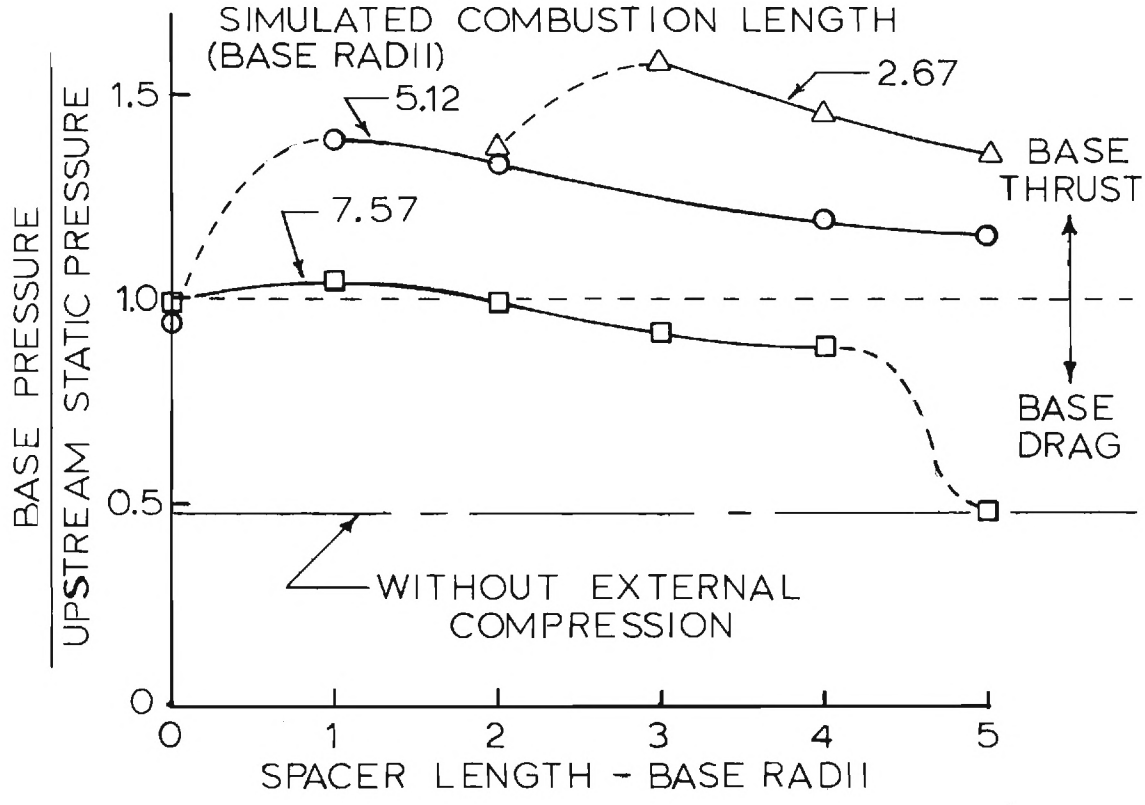

Figure 12. Effects of External Compression Strength and Location on Base Pressure.

placed downstream by one base radius. Base pressure falls slightly with the insertion of additional spacers up to a total of four. Base pressure, however, returns sharply to the value measured with a constant area duct when the fifth spacer is introduced. For this case, the initial compression wave intersects the wake downstream of the sonic point and can no longer influence the base region.

Translation of the two alternate axisymmetric disturbance sections verified the base flow trends shown with the original compression duct. As the compression severity increases, the optimum location of each duct moves downstream and the corresponding maximum base pressure rises. The rearward shift in optimum location probably results from the steepening of compression waves due to coalescence. Finally, Figure 12 shows that the third, most severe compression-rate duct yields an elevation in the base pressure sufficient to completely neutralize drag on a well designed projectile for which base and wave drag are typically comparable.

The systematic variation of disturbance position and strength revealed two additional characteristic lengths inherent in base flows with external compression. As shown in Figure 13, the wake length scales vary directly with location of the compression surfaces. Thus, movement of the disturbance field downstream tends to lengthen the distances from the base to the rear stagnation and sonic velocity points. Conversely, as the compression strength increases by decreasing the compression length for a fixed location, the wake length decreases.

Figure 14 further illustrates the direct relation of wake length to disturbance location for the initial, relatively mild compression surface. For those cases in which the compression field tends to elevate base pressure, the normalized centerline static pressure distributions clearly reflect disturbance loca-

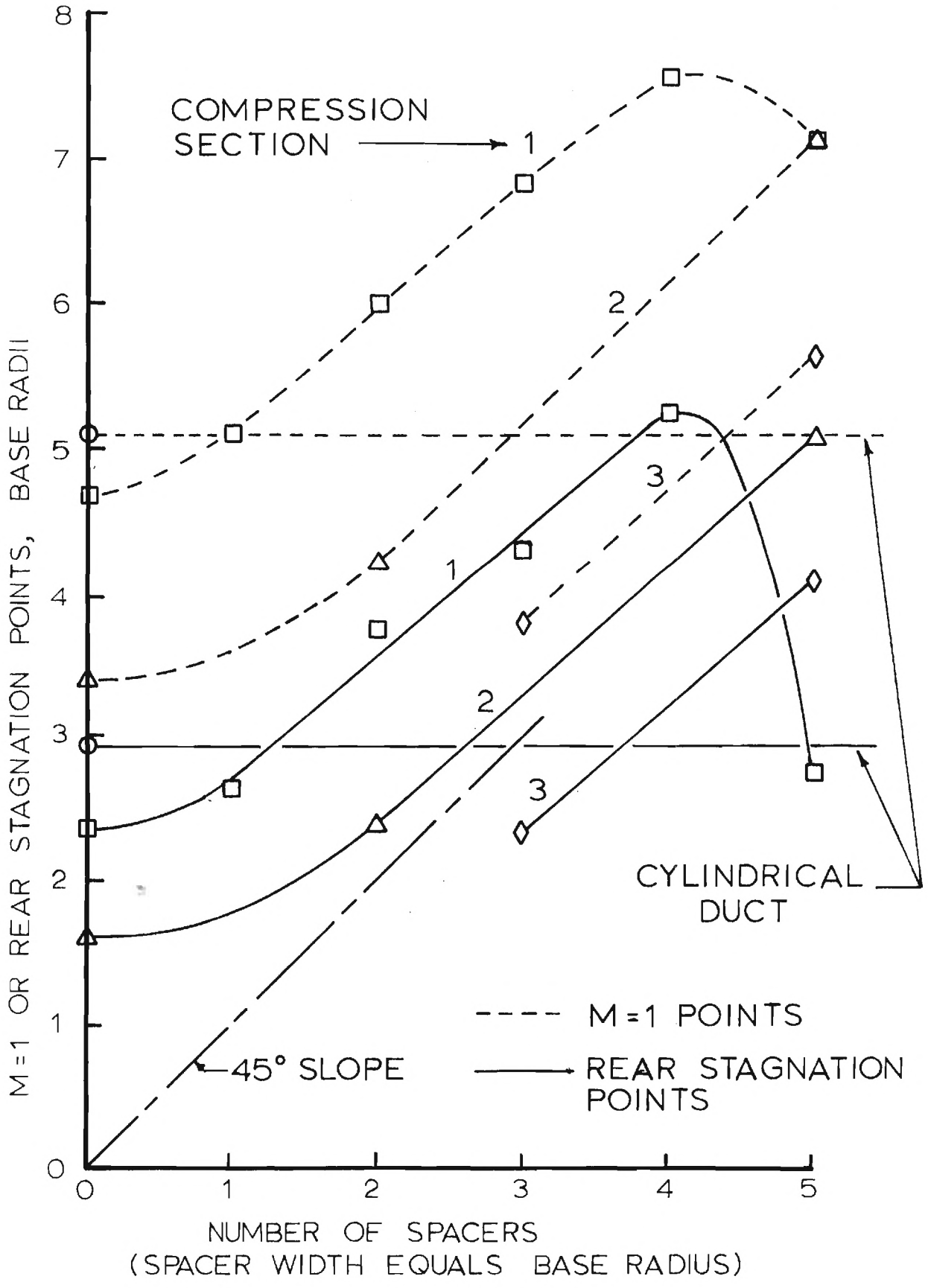

Figure 13. Effects of External Compression Strength and Location on Near Wake Length Scales.

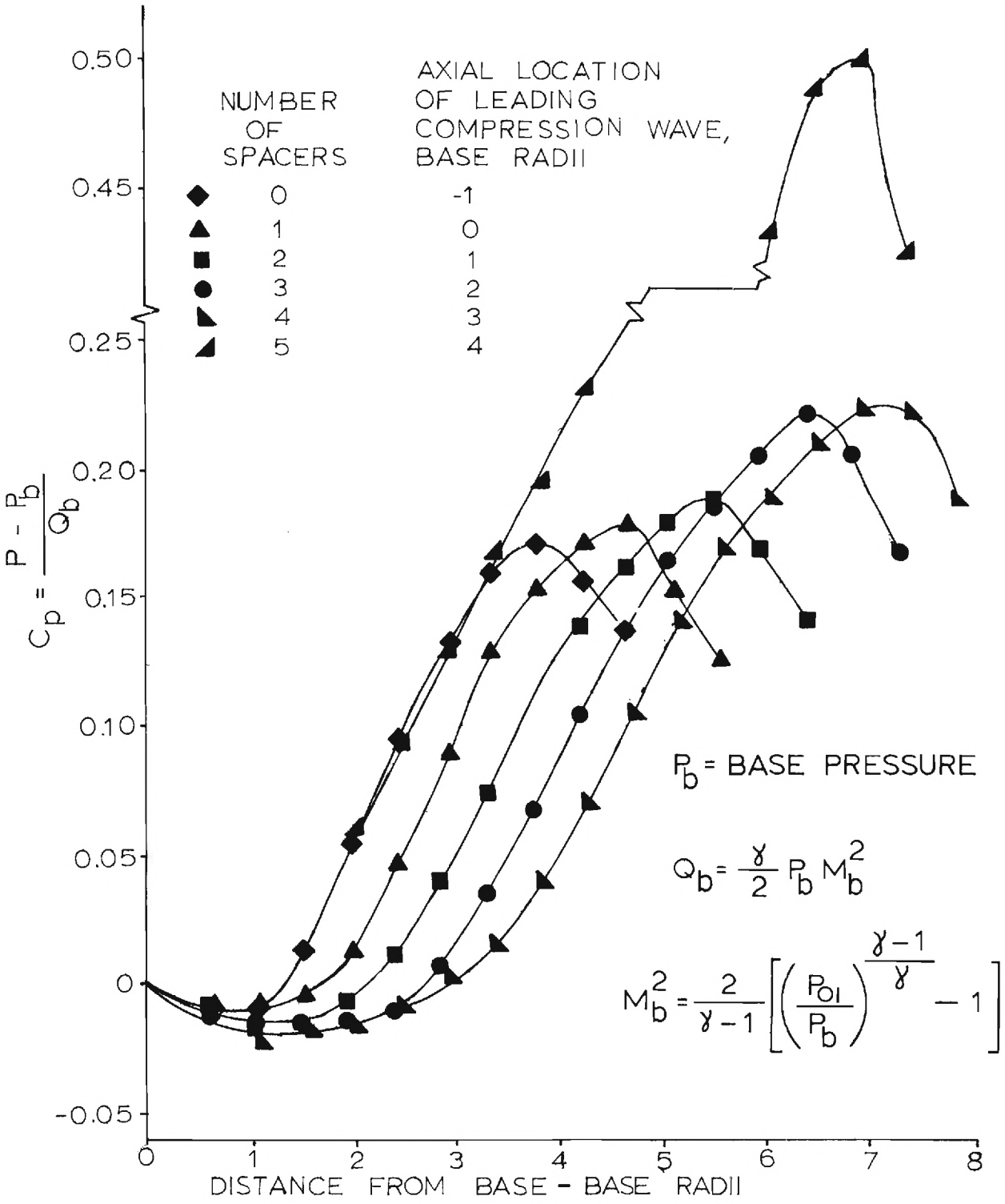

Figure 14. Effects of External Compression Location on Centerline Pressure Distribution - Compression Section I.

tion. The trend terminates abruptly, however, for the five-spacer case when base pressure reverts to the no-compression value.

Radial and axial measurements of Mach number and static pressure in the wake for the initial compression section with no spacers are shown in Figure 15. Comparison of the Mach number profiles for this case with those presented in Figure 6 for the cylindrical duct illustrates a slightly fuller and shortened recirculation region reflecting the elevated base pressure. As in Figure 6, the static pressure profiles in Figure 15 indicate the effects of flow curvature. In general, the radial pressure variation magnitudes are larger for the compression case resulting from the increased severity of turning associated with the shorter wake.

Discrete Disturbance Test Results.

In actual practice,external burning to influence base pressure would most likely take place in discrete plumes originating from radial fuel injection nozzles located near the projectile base. As mentioned previously, a fourth test section employing six half bodies of revolution was fabricated to compare the effects of discrete and equivalent axisymmetric disturbances. The axial area distribution of this fourth section was identical to that of the second compression duct (II).

Figure 16 schematically shows the fourth compression section along with base pressure test results for various axial duct locations. A significant reduction in base pressure from the axisymmetric case is seen at any given duct position. Figure 17 compares centerline static pressure and Mach number distributions for the axisymmetric and discrete distrubance ducts with two spacers. It is clear that, in addition to reducing base pressures, use of discrete disturbances has moved the rear stagnation point forward and has midly increased the peak centerline static pressure.

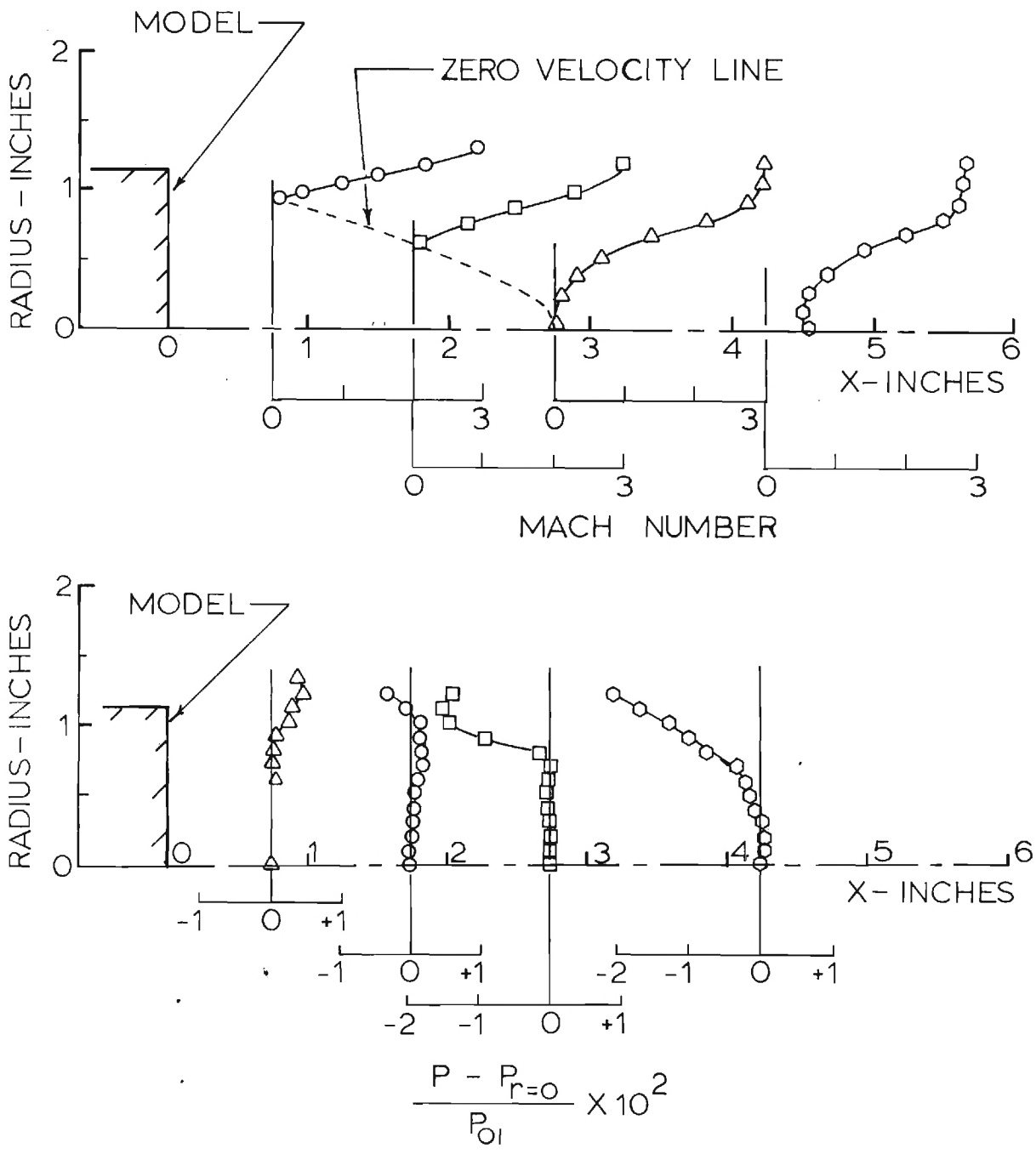

Figure 15. Near Wake Radial Mach Number and Static Pressure Distributions - Compression Section I, Zero Spacers.

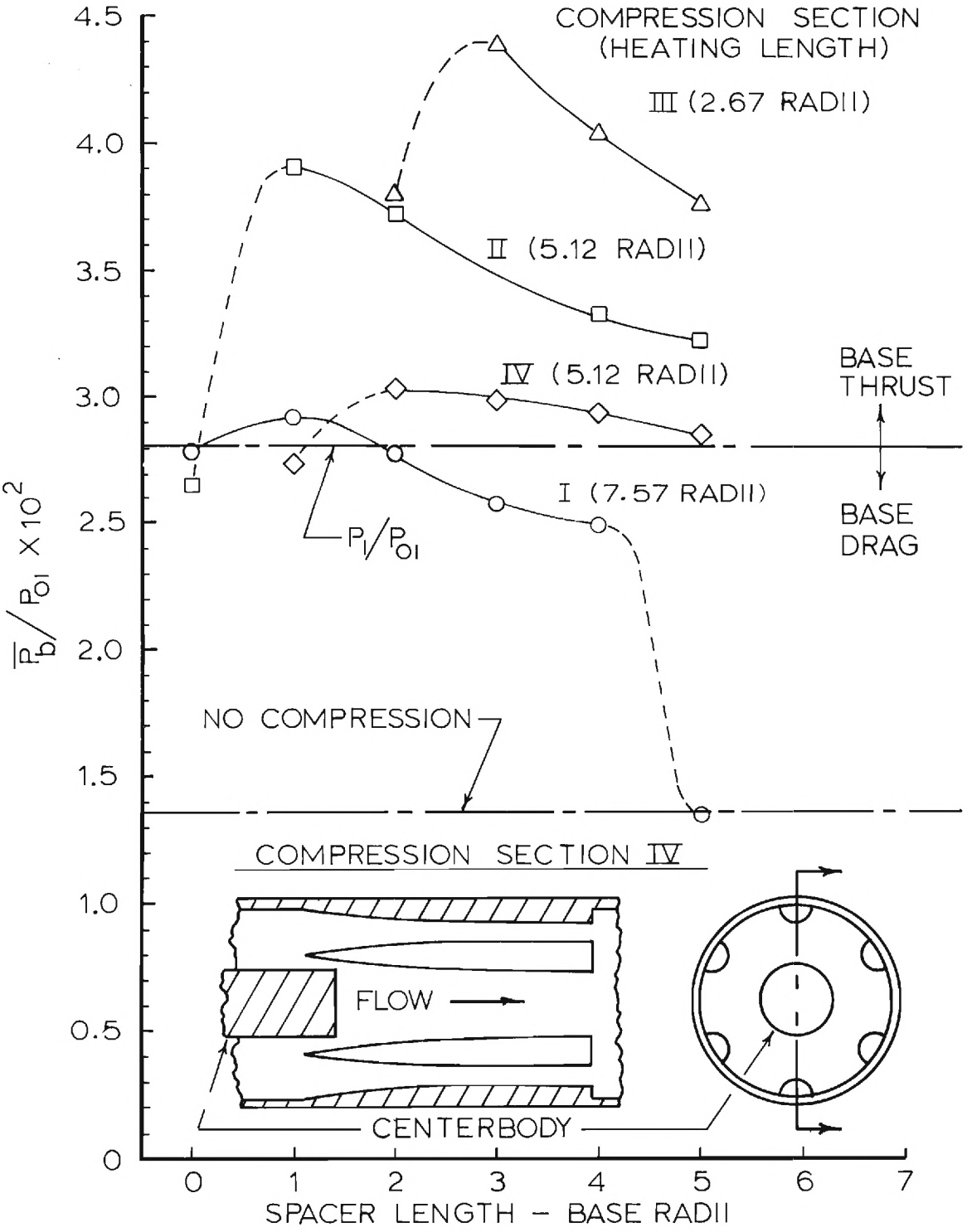

Figure 16. Comparison of Base Pressures for Axisymmetric and Equivalent Discrete Compression Sections (II and IV).

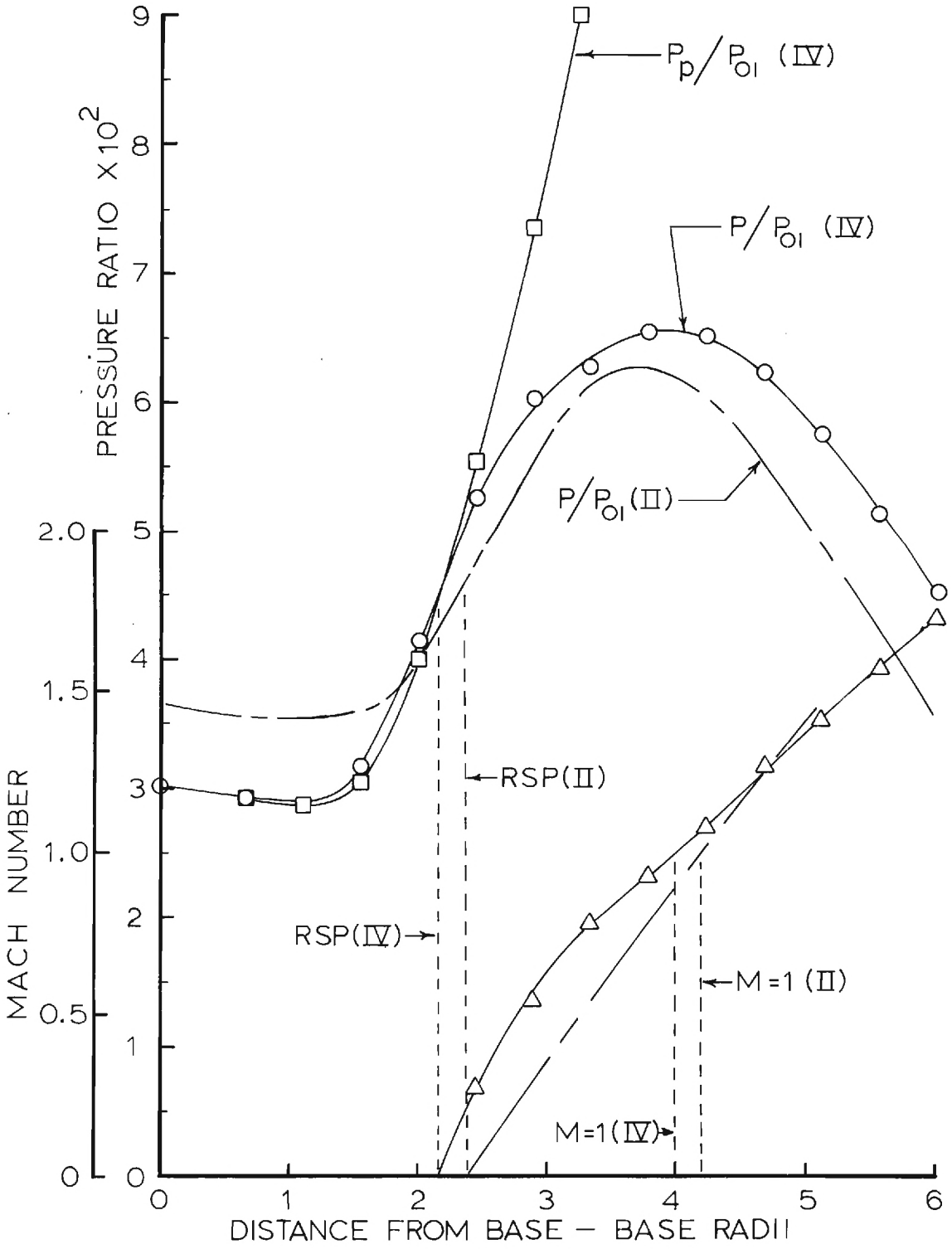

Figure 17. Comparison of Near Wake Centerline Pressure and Mach Number Distributions for Axisymmetric and Equivalent Discrete Compression Sections (II and IV).

It is believed that an explanation for the somewhat deteriorated performance just described may be found in a secondary vorticity field created by the discrete disturbance contours. Static pressure measurements along the duct and centerbody surfaces between half-bodies revealed considerably higher values than for the axisymmetric compression section (II). These higher wall pressures are due to coalescence of waves from adjacent contours and indicate the existence of strong peripheral pressure gradients in the free stream. Zones of higher pressure existing between half-bodies alternate with regions of lower pressure directly over the bodies and create the potential for streamwise secondary vorticity in the wake shear flow. The resulting increased mixing most certainly influences wake development by thickening and energizing the shear layer such as to increase its ability to oppose recompression. Since the maximum static pressure for the axisymmetric and discrete compression cases is nearly the same, base pressure for the discrete disturbance case must adjust downward to accommodate the increased pressure rise. It should be noted, however, that even though base pressure is lower for the discrete disturbance case, the base drag has still been neutralized.

To conclude the test program of simulating external burning disturbances without actual mass injection, the solid blockage of radial fuel jets exhausting near the base was modeled. For these tests an alternate base unit with six cylindrical pegs attached to the perimeter was substituted for the original base plate. The peg base is shown in Figure 18. The pegs were scaled to represent the solid body blockage associated with jets in crossflow excluding entrainment. Dimensions were based on the gaseous jet penetration analysis of Reference 3 assuming complete elimination of projectile drag with practical values of specific impulse and jet nozzle pressure ratio. Tests with the peg base model were conducted with the constant area (no compression) test section.

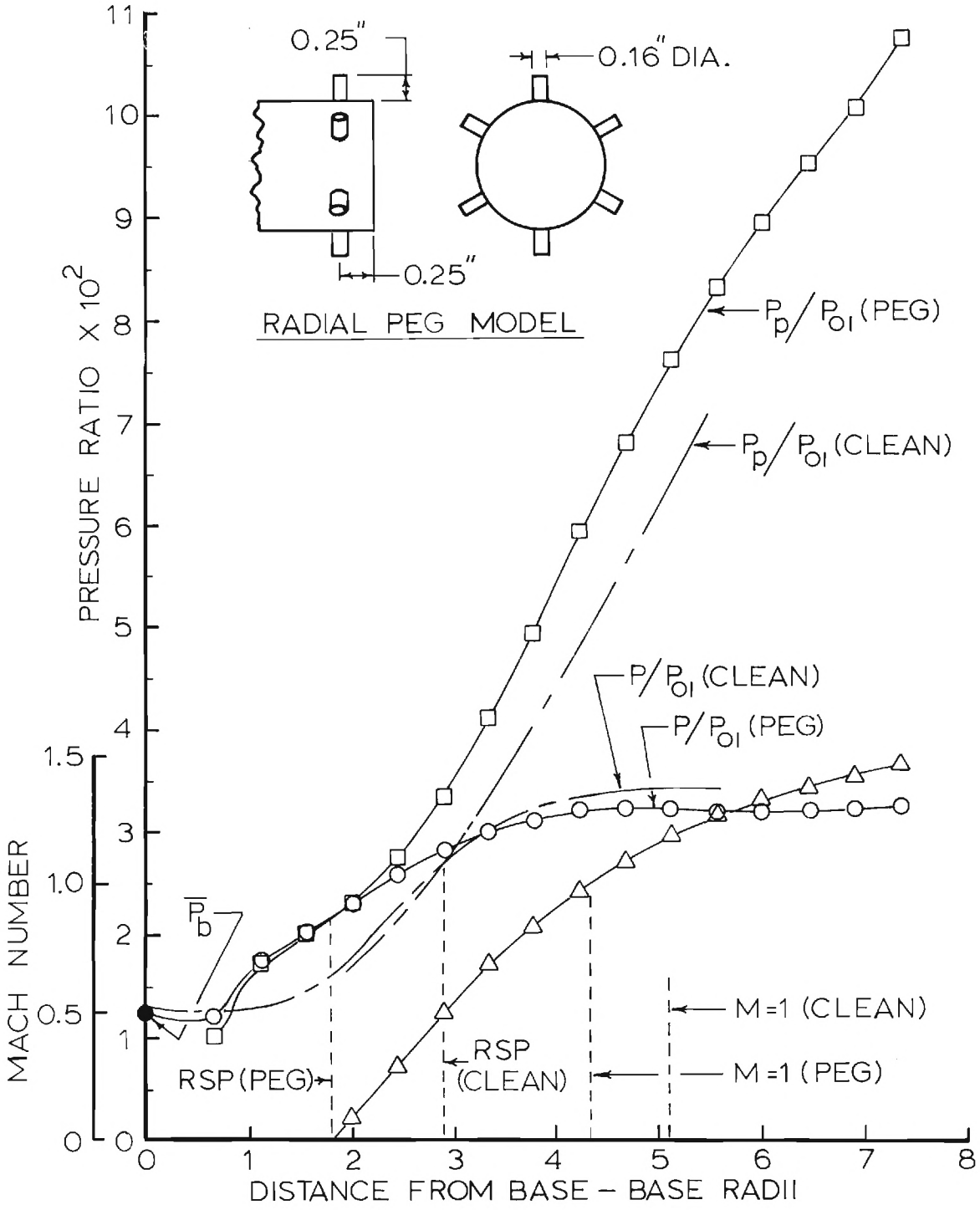

Figure 18. Comparison of Near Wake Centerline Pressure and Mach Number Distributions for Clean Base and Peg Base (Simulated Discrete Radial Jet Blockage).

Figure 18 presents the centerline pressure and Mach number distributions from the peg base tests. Results from the "clean" base tests are also provided to show changes in the wake structure. It is apparent that the presence of the pegs has significantly shortened the wake. Also, the base pressure, determined from a simple average of seven taps, is about 8% lower than the clean base configuration value of $\bar{P}_B/P_{o_1} = 1.36 \times 10^{-2}$. The reduction in the base pressure and the change in the base flow structure is thought to be primarily a result of increased mixing due to streamwise secondary vorticity generated by the pegs.

SUMMARY

The present experimental simulated external burning program has shown that substantial base thrust can be obtained by imposing axisymmetric or asymmetric compressions on the turbulent near-wake region of a projectile in supersonic flight. Systematic variations in disturbance strength and axial position reveal that the length scales of these compressions are reflected in the wake structure. As expected, base pressure rises and the near-wake shortens with increasing compression severity for any particular axial disturbance location. Downstream translation of a given disturbance acts to lengthen the wake and yields a mild optimum base pressure for that disturbance. The present tests demonstrate a case in which base pressure elevation is sufficient to completely neutralize base and forebody drag on a well designed projectile.

In actual practice, external burning will probably take place in discrete plumes originating from radial injection of fuel in the vicinity of the base plane. Tests simulating this configuration showed that base pressure elevation is significantly reduced for discrete externally generated disturbances when compared with the equivalent axisymmetric compression. The loss in base thrust is apparently related to streamwise vorticity created in and above the shear layer by the non-uniform external compression field. The present tests demonstrated, however, that base pressure had still been boosted sufficiently to eliminate base drag.

Finally, modeling of the solid body blockage effects of discrete radial fuel jets near the base showed relatively large changes in the near-wake length scales. Despite the alteration in wake structure, base pressure was only slightly lower than for a "clean" projectile with no radial jet modeling.

BIBLIOGRAPHY

Ref. 1. Mehta, G. K., and Strahle, W. C., "A Theory of the Supersonic Turbulent Axisymmetric Near Wake Behind Bluff-Base Bodies," to be published as AIAA Journal Synoptic.

Ref. 2. Kubota, T., Reeves, B. L., and Buss, H., "A Family of Similar Solutions for Axisymmetric Incompressible Wakes," AIAA Journal, 2, August 1964, pp. 1493-1495.

Ref. 3. Billig, F. S., Orth, R. C., and Lasky, M., "A Unified Analysis of Gaseous Jet Penetration," AIAA Journal, 9, June, 1971, pp. 1048-1058.

AFOSR Final Scientific Report

AFOSR-TR-77- 1291

Experiments Related to External Burning for Propulsion

Prepared for

Air Force Office of Scientific Research
Aerospace Sciences Directorate
Bolling Air Force Base, D. C.

by

Warren C. Strahle
James E. Hubbartt
Douglas H. Neale
Danny J. Huval

School of Aerospace Engineering
Georgia Institute of Technology
Atlanta, Georgia 30332

Approved for public release; distribution unlimited
Grant No. AFOSR 75-2794 October 1977

REPORT DOCUMENTATION PAGE

READ INSTRUCTIONS BEFORE COMPLETING FORM

1. REPORT NUMBER: AFOSR-TR-77- 1291
2. GOVT ACCESSION NO.:
3. RECIPIENT'S CATALOG NUMBER:

4. TITLE (and Subtitle): EXPERIMENTS RELATED TO EXTERNAL BURNING FOR PROPULSION

5. TYPE OF REPORT & PERIOD COVERED: FINAL FEB. 1977-SEPT. 1977

6. PERFORMING ORG. REPORT NUMBER:

7. AUTHOR(s): Warren C. Strahle, Douglas H. Neale, James E. Hubbartt, Danny J. Huval

8. CONTRACT OR GRANT NUMBER(s): AFOSR-75-2794

9. PERFORMING ORGANIZATION NAME AND ADDRESS
Georgia Institute of Technology
School of Aerospace Engineering
Atlanta, Ga. 30332

10. PROGRAM ELEMENT, PROJECT, TASK AREA & WORK UNIT NUMBERS:

11. CONTROLLING OFFICE NAME AND ADDRESS
Air Force Office of Scientific Research/NA
Bolling Air Force Base, D.C. 20332

12. REPORT DATE: October 1977

13. NUMBER OF PAGES: 17

14. MONITORING AGENCY NAME & ADDRESS (if different from Controlling Office):

15. SECURITY CLASS. (of this report): Unclassified.

15a. DECLASSIFICATION/DOWNGRADING SCHEDULE:

16. DISTRIBUTION STATEMENT (of this Report)

Approved for public release; distribution unlimited

17. DISTRIBUTION STATEMENT (of the abstract entered in Block 20, if different from Report)

18. SUPPLEMENTARY NOTES

19. KEY WORDS (Continue on reverse side if necessary and identify by block number)

External Burning Propulsion
Base Flow
Supersonic Flow
Wind Tunnel

20. ABSTRACT (Continue on reverse side if necessary and identify by block number)

An experimental study of base flows for a 2.25 inch diameter projectile at Mach 3 with cold air injection is reported. Upstream radial jet injection and base injection are used. The work is a continuation of a systematic study of many of the flow field features of external burning. It is shown that radial jet injection alters the wake structure, shortens the wake, and reduces the base pressure. In addition, the advantage of base injection using porous base bleed diminish with injection rate and external compression.

AFOSR Final Scientific Report

AFOSR-TR-77- 1291

Experiments Related to External Burning for Propulsion

Prepared for

Air Force Office of Scientific Research
Aerospace Sciences Directorate
Bolling Air Force Base, D. C.

by

Warren C. Strahle
James E. Hubbartt
Douglas H. Neale
Danny J. Huval

School of Aerospace Engineering
Georgia Institute of Technology
Atlanta, Georgia 30332

Approved for public release; distribution unlimited
Grant No. AFOSR 75-2794 October 1977

Abstract

An experimental study of base flows for a 2.25 inch diameter projectile at Mach 3 with cold air injection is reported. Upstream radial jet injection and base injection are used. The work is a continuation of a systematic study of many of the flow field features of external burning. It is shown that radial jet injection alters the wake structure, shortens the wake, and reduces the base pressure. In addition, the advantage of base injection using porous base bleed diminish with injection rate and external compression.

TABLE OF CONTENTS

I. INTRODUCTION

In prior work[1]-[3] with the present facility, tests with axisymmetric and discrete compression surfaces, tests with upstream pegs simulating frontal-area blockage of fuel introduced by lateral injection, and analysis of the adiabatic near wake have been reported. At the conclusion of this work, the following facts had been established: a) the base pressure can be raised, by focusing compression waves on the near wake, to levels that provide net thrust on a well designed projectile, b) the length scales of the compression surfaces are imposed on the near wake - a weak optimum is obtained with the compression beginning immediately downstream of the base plane, c) base pressure elevation is significantly reduced with discrete surfaces as opposed to an equivalent axisymmetric surface, d) upstream-radial pegs cause a slight reduction in base pressure and a relatively large shortening of the wake structure, and e) an integral analysis[4] agrees reasonably well with experiments for no compression and axisymmetric compression.

Continuing tests have studied cold air injection with radial jets just upstream of the base plane and porous base bleed. This present report describes this continuing work built upon the above foundation.

II. RESULTS

All tests were conducted at a free stream Mach number, upstream of the base plane, of $M_1 = 2.98$. The base diameter was 2.25 inches and the nominal test Reynolds based on the base diameter was 2.7×10^6. The boundary layer momentum thickness at the base plane was computed to be 1.2 percent of the base radius. Details of the test facility are reported in Ref. (1), (2), and (3).

Radial Jet Injection

Cold air was injected through six orifices drilled into the hollow forebody at 60^o intervals around the periphery 0.22 base radii upstream of the base plane. The sonic exit flow discharged normal to the freestream. Two orifice diameters were tested to independently vary injection rate and pressure ratio. Jet penetration height at the Mach disk, computed by the theory of Ref. (5), increased with injection rate from about 0.2 to 0.3 base radii.

The base to free stream static pressure ratio (P_b/P_1) and the jet to free stream stagnation pressure ratio (P_{o_J}/P_{o_1}) are plotted against the injection parameter (the ratio of the jet flow rate to the free stream flow rate through an area equal to the base area) in Figure 1. Results are shown for no compression and for axisymmetric compression with compression section II[(2)] which produces a net base thrust. The important point is that the base pressure decreases with cold air injection as a result of the competing effects of vortex generation, flow displacement,

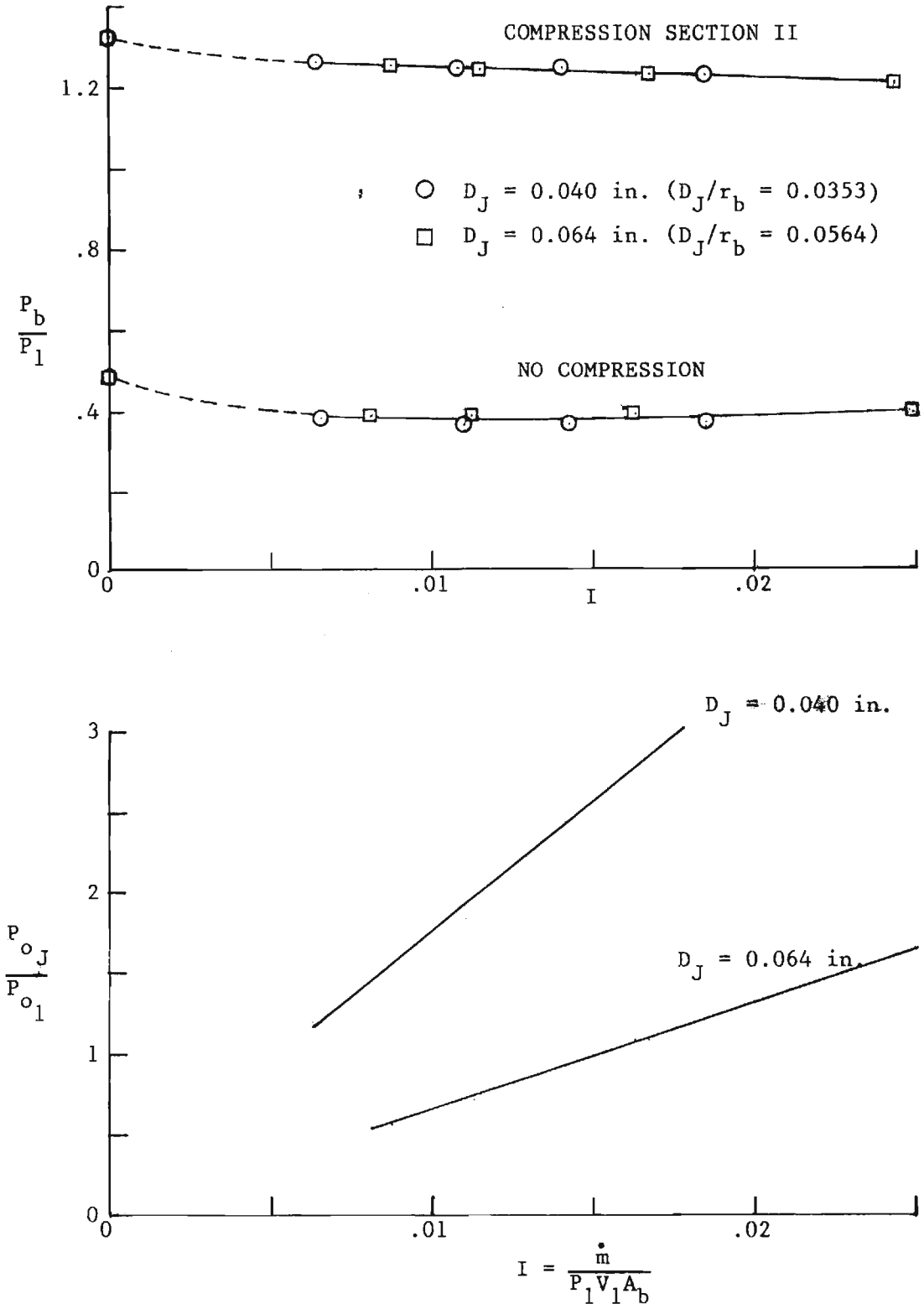

Figure 1. Base Pressure and Jet Nozzle Pressure Ratios for Cold-Air Radial Injection

elevation of the upstream body pressure by the shock system, and a degradation in total pressure by the shock system. This decrease is essentially independent of orifice diameter and reaches a maximum of over 10 percent of the free stream static pressure for both no compression and axisymmetric compression.

The static pressures immediately ahead and behind a radial jet, as important for penetration analysis[5], are presented in Figure 2. For comparison, the static pressure ahead of a radial peg, designed to simulate the frontal area blockage of the radial jet[2], is also shown. (The pressure downstream of the radial peg was not measured.) The upstream pressure for the radial peg is essentially that for two-dimensional, shock-induced boundary layer separation. The additional effect of mass entrainment significantly lowers the upstream pressure for the radial jet. The additive effects of blockage and mass entrainment result in a reducing downstream pressure with increasing injection rate.

Typical pressure and Mach number distributions along the centerline of the near wake with radial injection are compared with those for the clean base in Figure 3. Injection significantly alters the wake structure and causes a large reduction in the wake length scales. The wake changes indicate increased mixing with injection. Figure 4 shows a comparison of wake centerline results with radial injection and with radial pegs designed to simulate the frontal area blockage of the radial jets.[2]. The wake length scales and the base pressures with the radial peg model are reduced relative to those for the clean base[2]. The radial jets cause an additional reduction in the base pressure and, as seen in

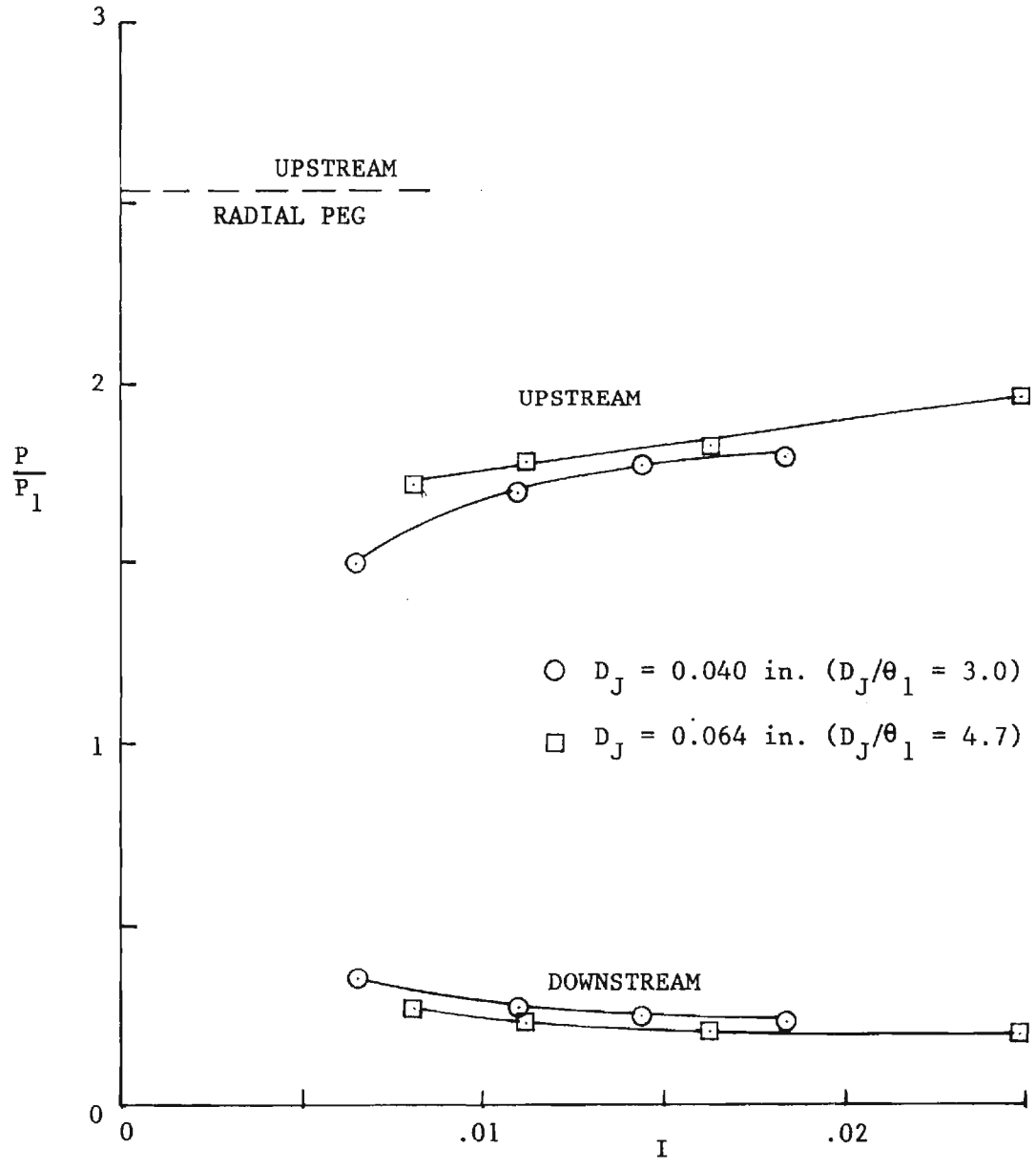

Figure 2. Surface pressures upstream and downstream of a radial jet.

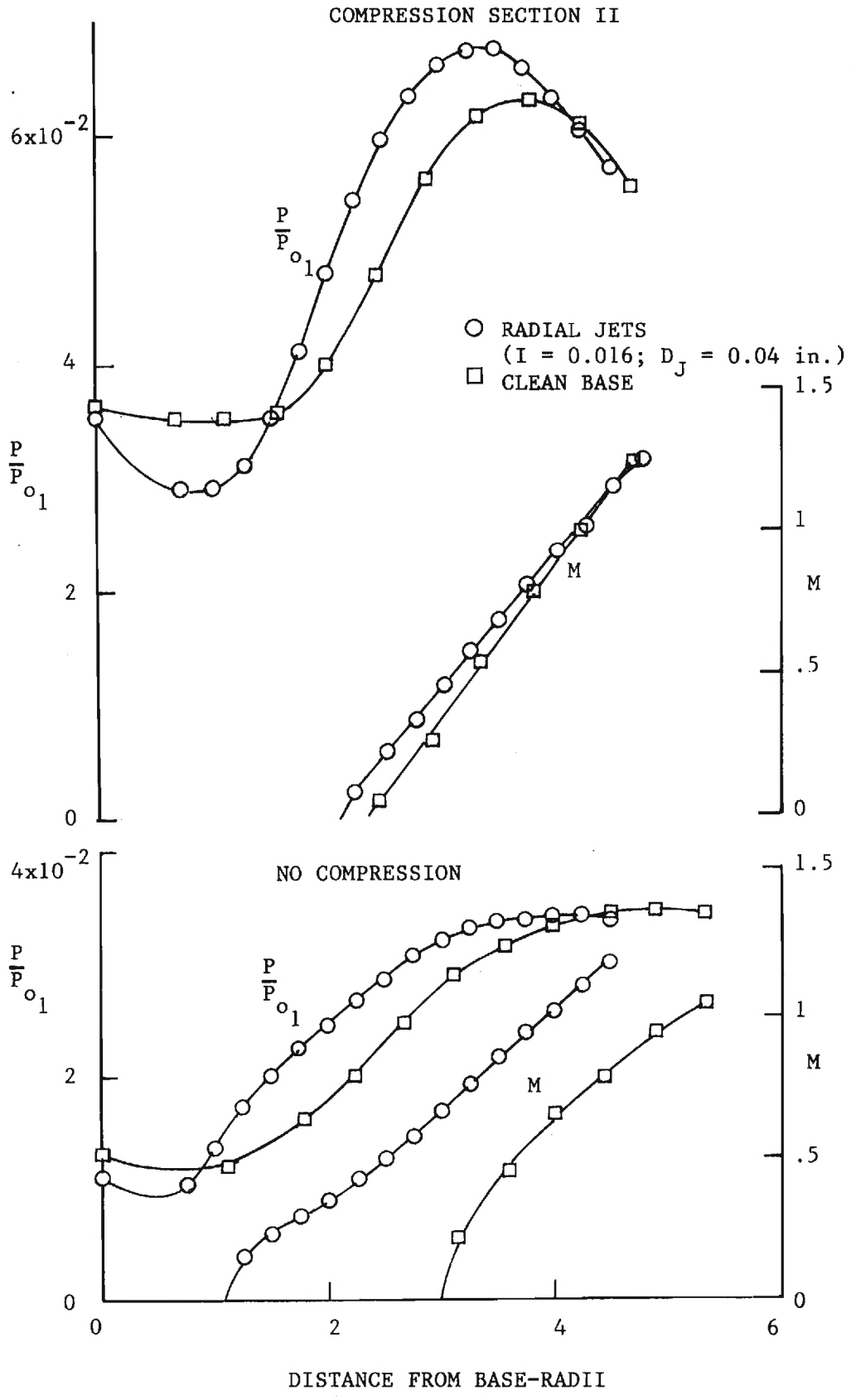

Figure 3. Near Wake Centerline Static Pressure and Mach Number Distributions with and without Radial Injection.

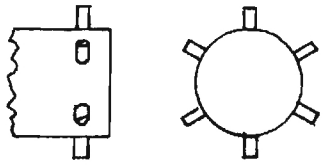

RADIAL PEG MODEL

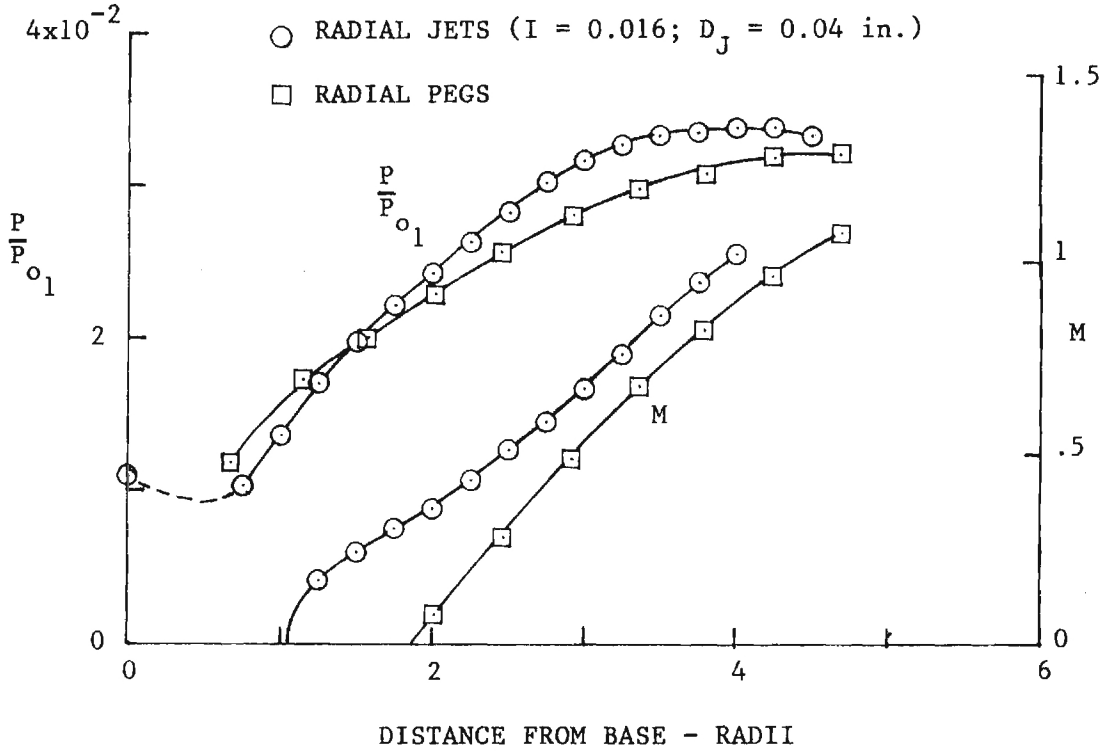

Figure 4. Comparison of Centerline Pressure Mach Number Distributions for Radial Jets and Radial Pegs.

Figure 4, they further shorten the wake even though the injected flow displaces the free stream downstream of the injection point. It is felt that slight flow asymmetries can account for some of the differences in Figure 4 in the low velocity region. However, the important point is that the effects of discrete jet injection is needed in the modelling of the near wake for a real external combustion system.

Near wake Mach number profiles behind a jet and midway between two jets are compared in Figure 5. This comparison demonstrates that the core of the jet does penetrate the near-wake shear layer. The line of maximum velocity difference is indicated on the figure. It seems doubtful, however, that the penetration with this shortened wake is deep enough to significantly alter the temperatures in the regions of flow reversal, and, hence, alter the base pressure by decreased stagnation pressures, if the injected flow is combustible.

Porous Base Bleed

The base injection tests were made with cold air bleed through porous sintered metal. The bore of the cylindrical base model was plugged at the base plane with a 1/16 inch thick sintered metal disk (see the sketch in Figure 6). The base pressures were measured with five flush static pressure taps located in the disk (one at the center and four equally spaced around the periphery at a radius of 0.5 inches). Since these pressure taps were immersed in the injected flow discharging from the porous plug, calibration tests were first made to relate the measured base pressure to an "effective" base pressure, P_{be}. For these calibration tests the sintered metal disc was mounted in a constant diameter tube.

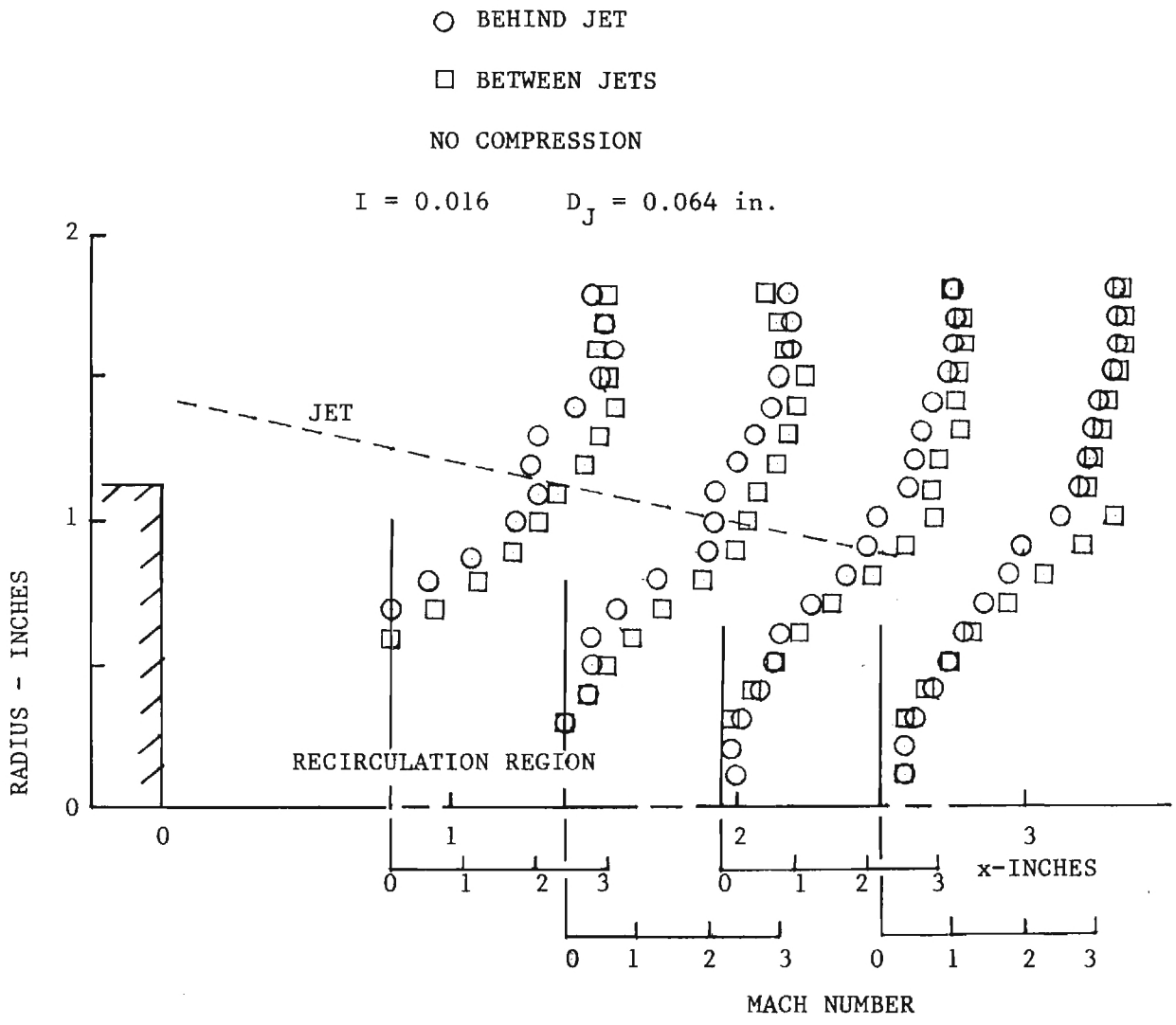

Figure 5. Near Wake Mach Number Profiles With Radial Injection.

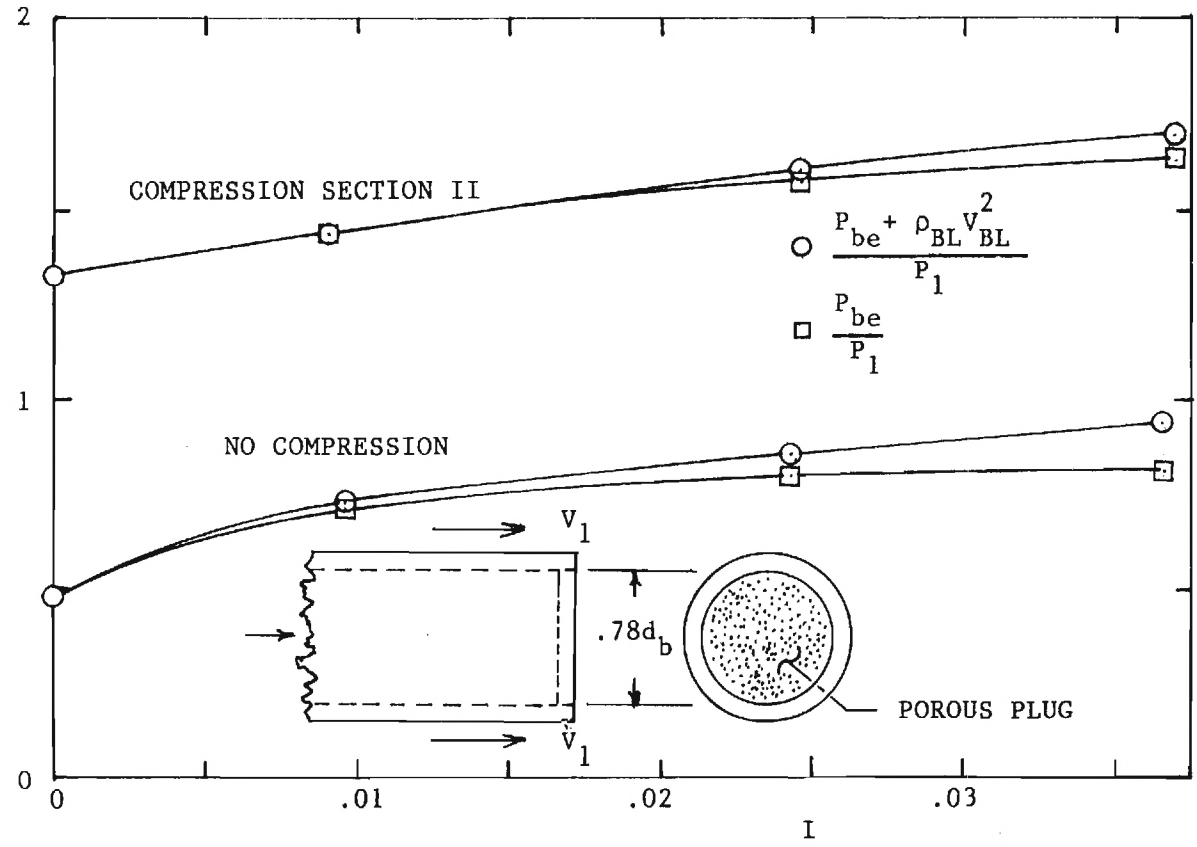

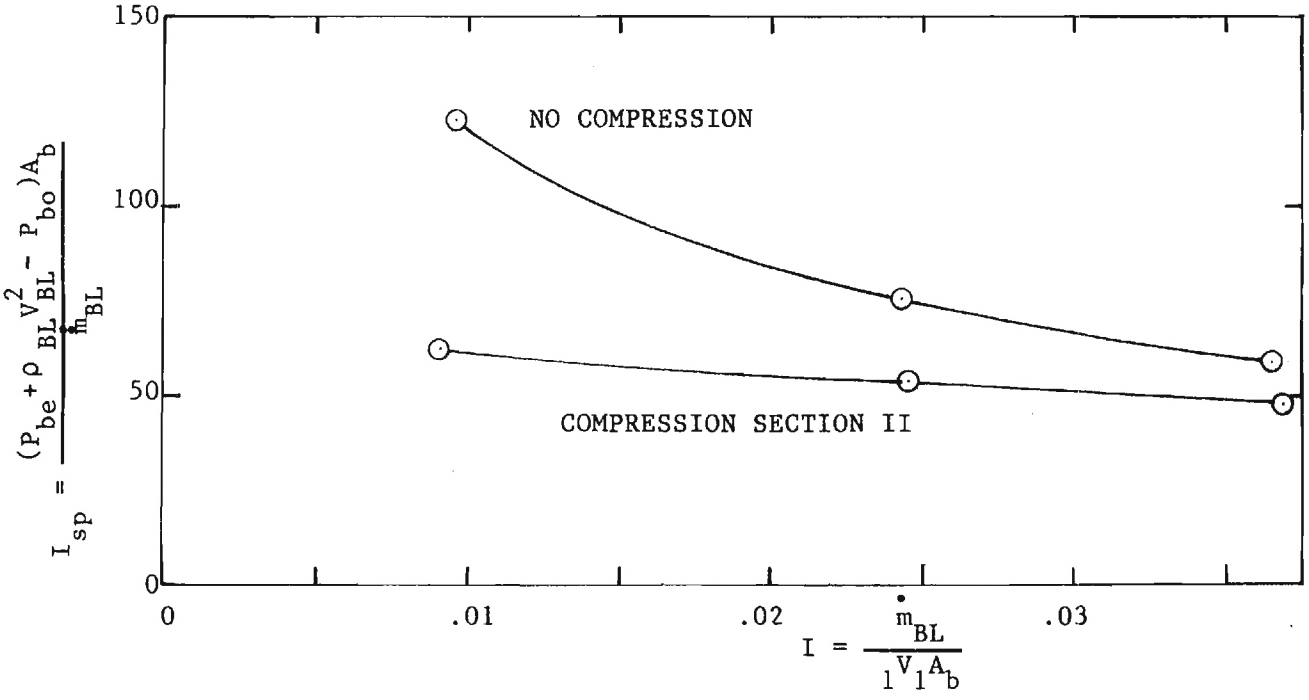

Figure 6. Base Forces and Base Thrust Specific Impulse with Base Injection.

Flow through the tube was metered and the base pressures on the porous plug and the mixed-flow static pressure or effective base pressure was measured downstream. This effective base pressure was then correlated with the measured base pressure and flow rate.

Figure 6 presents the results of the base force data with base bleed. The upper part of this figure shows the effect of the mass injection rate on both the effective base pressure and the net base force per unit area (i.e., the impulse function per unit area or the sum of the effective base pressure and momentum flow rate). Results are shown for no compression and for compression with compression section II which produces base thrust without base injection. At the higher flow rates the bleed flow momentum is significant. In addition, at the highest flow rate, base drag is essentially eliminated for the case of no compression while for the case of compression the elevation in base force is sufficient to completely neutralize drag of a well designed projectile. The rate of increase in the net base force with injection rate decreases with increasing injection rate. Furthermore, compression reduces the rate of increase in the net force with injection rate. These trends are emphasized in the lower part of Figure 6 which shows the specific impulse, I_{SP}, based on the increase in net base force due to injection. P_{bo} is the base pressure for the clean base configuration. The specific impulse decreases with the injection parameter and with compression. The initial rise in base pressure with injection parameter for no compression agrees well with the results of Bowman and Clayden for $M_1 = 2.99$.[6] However, their results, using base nozzle injection, showed a peak base pressure at $I \approx 0.005$.

Static pressure and Mach number distributions along the centerline of the near wake with no compression are shown in Figure 7 for no injection and two values of the injection rate. For the lower injection rate, I = 0.01, the recirculation bubble extends from one to four base radii downstream of the base plane. For the higher injection rate, I = 0.037, the recirculation bubble has been blown off. The primary effect of injection noted here other than the increase in base pressure, is to increase the near-wake length and, correspondingly, reduce the adverse pressure gradients. The simultaneous increase in length and decrease in pressure gradient indicate relatively large reductions in shear stresses acting on the flow along the axis.

The effect of compression on the near-wake centerline pressure and Mach number distributions is illustrated in Figure 8. The control enforced by the compression waves shortens the near wake. Mass addition with compression results in a slight lengthening of the wake and a substantial reduction in the peak over-pressure. Downstream of this peak the flow accelerates rapidly under the favorable pressure gradient due to expansion waves focused on the wake.

Near-wake static pressure and Mach number profiles are shown in Figure 9 for no compression and I = 0.010. A uniform central core of bleed flow fills the base area upstream of the recirculation bubble. The corner expansion is evident in the outer portion of the shear layer. Downstream of the recirculation bubble a developed shear flow is established and the radial pressure gradients are indicative of the recompression curvature. In the plane near the center of the recirculation bubble the radial pressure gradients are small.

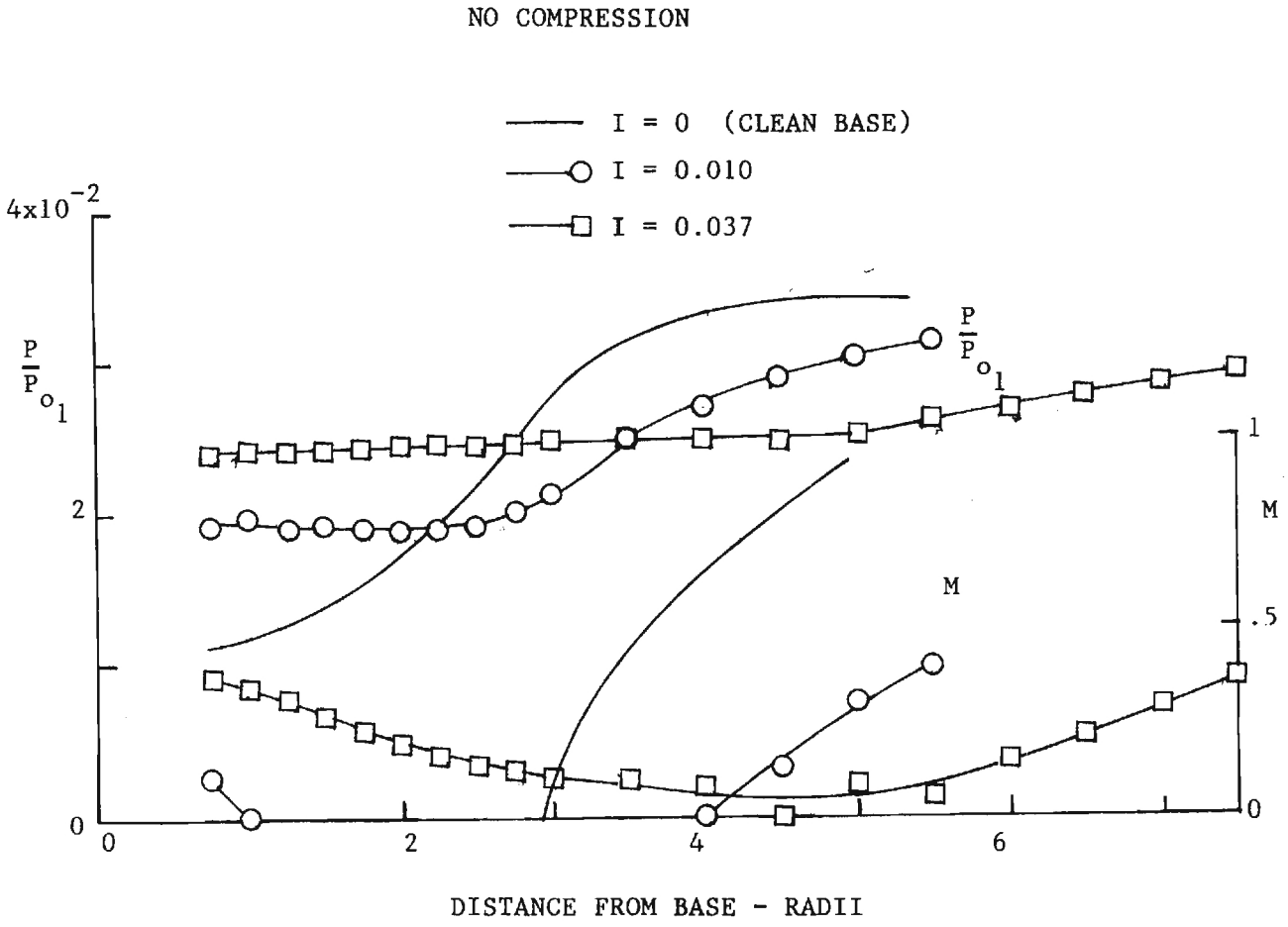

Figure 7. Near Wake Centerline Static Pressure and Mach Number Distributions with and without Base Injection.

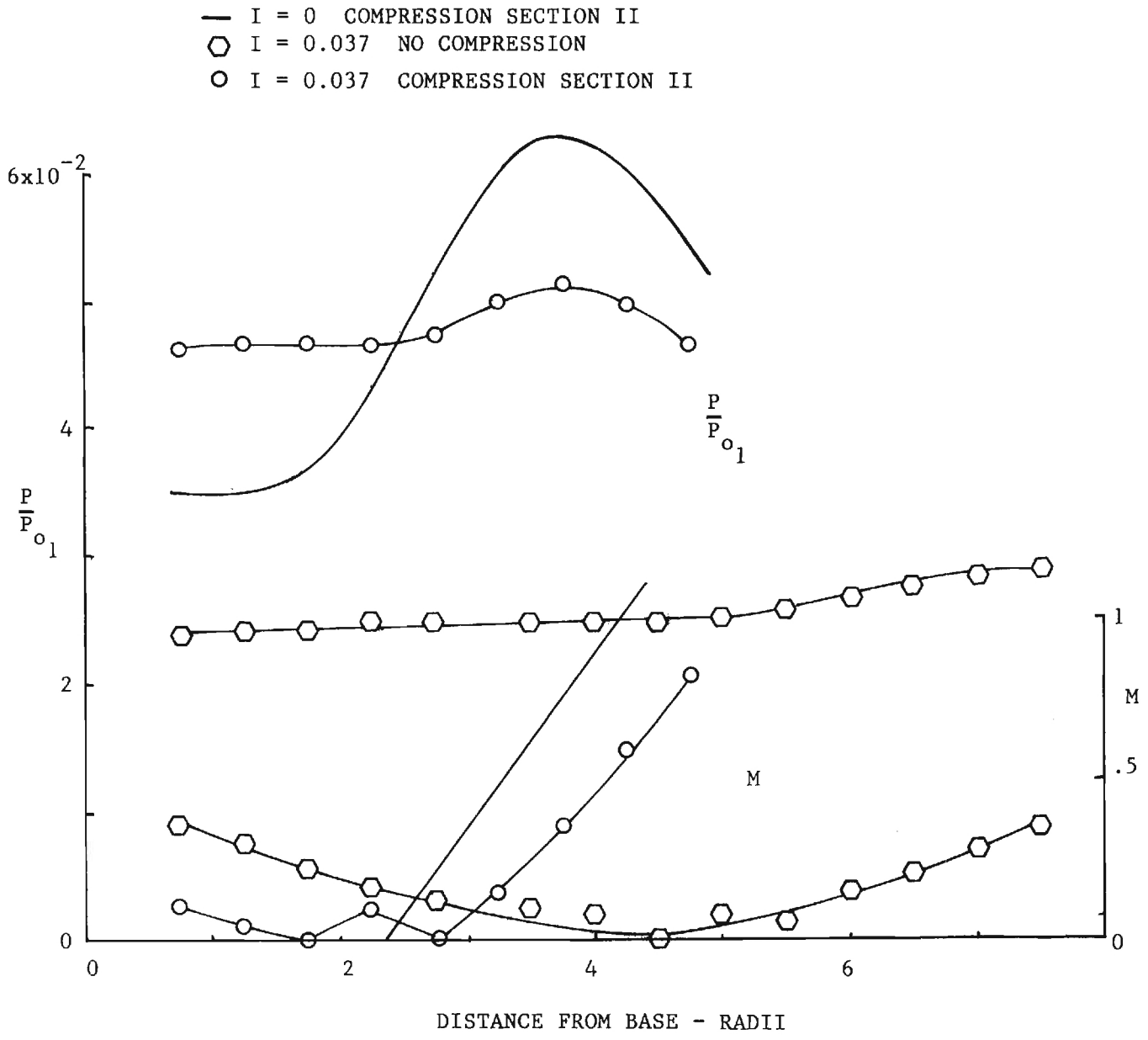

Figure 8. Effects of Compression on Base Centerline Static Pressure And Mach Number Distributions.

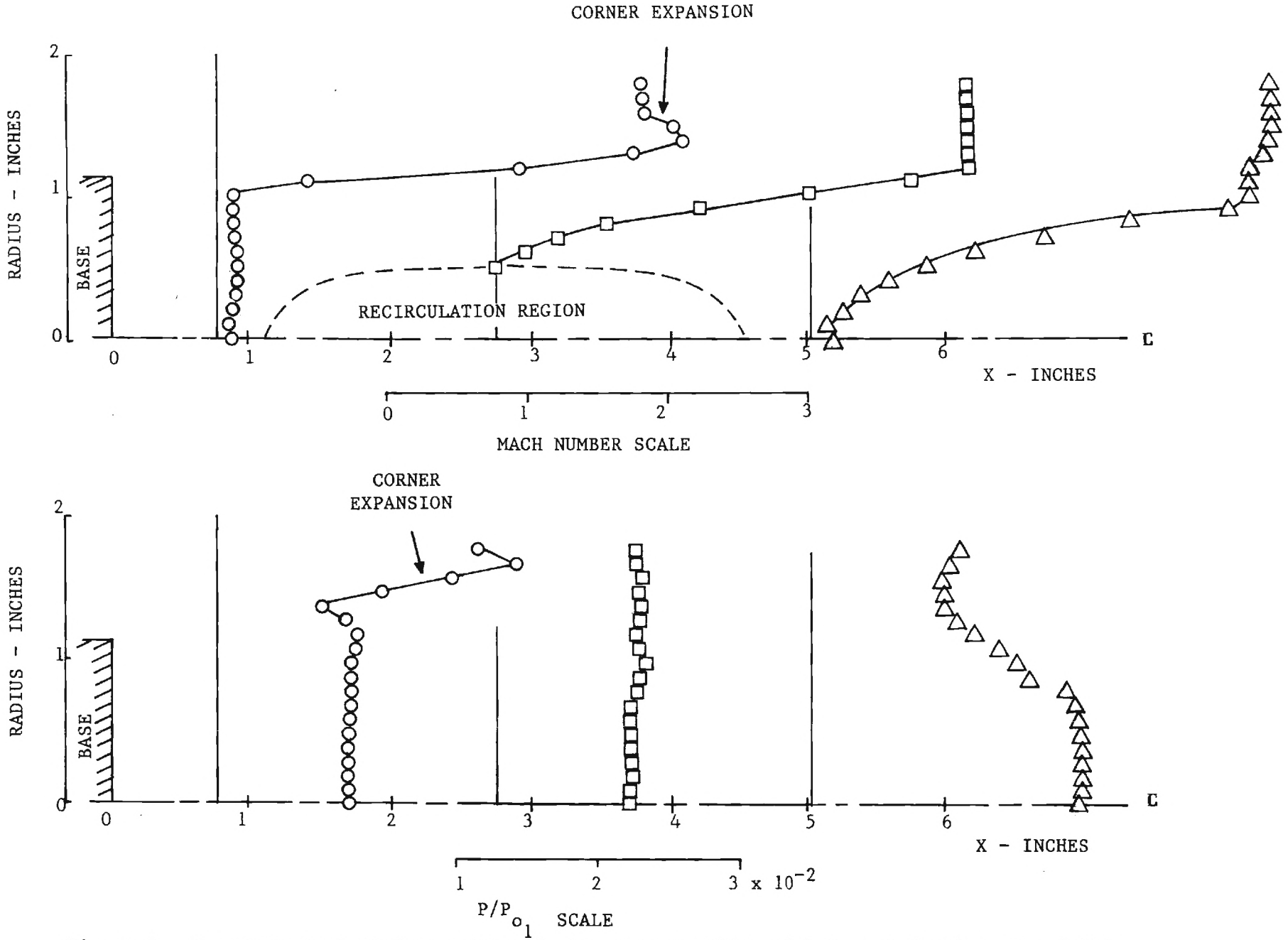

Figure 9. Near Wake Mach Number and Static Pressure Profiles with Base Injection I = 0.010.

III. CONCLUSIONS

Cold air, radial injection tests have shown that discrete jet injection immediately ahead of the base plane significantly alters the wake structure, reduces the wake length scales, and lowers the base pressure. The effects of discrete jet injection must, therefore, be incorporated in a realistic analytical model of the near wake for a real external combustion system. This is exclusive of the degradations due to asymmetric compression as encountered in earlier tests.

Cold air, base injection tests have shown that for porous base bleed and no compression the base force per unit area increases continuously with injection rate to approximately the free stream pressure when the recirculation bubble has been blown off. However, the gain in base force due to base injection decreases with increasing injection rate. Furthermore for a given base injection rate, compression lowers the base force elevation due to injection. Base injection causes large increases in the wake length scales with no compression and slight increases with compression.

REFERENCES

1. Hubbartt, J.E., Strahle, W.C., Neale, D.H., and Wilson, W.W., "Experiments and Analysis Related to External Burning for Propulsion," AFOSR-TR-76-0563, March, 1976.

2. Neale, D.H., Hubbartt, J.E., Strahle, W.C., and Wilson, W.W., "Experiments and Analysis Related to External Burning for Propulsion," AFOSR-TR-77-0602, March, 1977.

3. Neale, D.H., Hubbartt, J.E., Strahle, W.C., and Wilson, W.W., "Effects of External Compression on an Axisymmetric Turbulent Near Wake," AIAA Paper 77-925, Orlando, Florida, July, 1977.

4. Mehta, G.K., and Strahle, W.C., "A Theory of the Supersonic Turbulent Axisymmetric Near Wake Behind Bluff-Base Bodies," AIAA Journal, Vol. 15, August, 1977, pp. 1059-1060.

5. Billig, F.S., Orth, R.C., and Lasky, M., "A Unified Analysis of Gaseous Jet Penetration," AIAA Journal, Vol. 9, June, 1971, pp. 1048-1058.

6. Bowman, J.E., and Clayden, W.A., "Cylindrical Afterbodies in Supersonic Flow with Gas Injection," AIAA Journal, Vol. 5, August, 1967, pp. 1524 1525.